DRYING SHRINKAGE OF SELF-COMPACTING CONCRETE INCORPORATING FLY ASH

J. M.A. ABDALHMID

Ph.D

UNIVERSITY OF BRADFORD

2019

In the Name of God

The Most Gracious and the Most Merciful

ABSTRACT

Drying shrinkage of self-compacting concrete incorporating fly ash

JAMILA M. A. ABDALHMID

University of Bradford, UK, 2019

Keywords: Self-compacting concrete, Drying shrinkage, Fly ash, Prediction, Artificial neural networks.

The present research is conducted to investigate long term (more than two years) free and confined drying shrinkage magnitude and behaviour of self-compacting concrete (SCC) and compare with normal concrete (NC). For all SCCs mixes, Portland cement was replaced with 0-60% of fly ash (FA), fine and coarse aggregates were kept constant at 890 kg/m3 and 780 kg/m3, respectively. Two different water binder ratios of 0.44 and 0.33 were examined for both SCCs and NCs. Fresh properties of SCCs such as filling ability, passing ability, viscosity and resistance to segregation and hardened properties such as compressive and flexural strengths, water absorption and density of SCCs and NCs were also determined. Experimental results of free drying shrinkage obtained from this study together with collected comprehensive database from different sources available in the literature were compared to five existing models, namely the ACI 209R-92 model, BSEN-92 model, ACI 209R-92 (Huo) model, B3 model, and GL2000 model. To assess the quality of predictive models, the influence of various parameters (compressive strength, cement content, water content and relative humidity) on the drying shrinkage strain are studied. An artificial neural network models

(ANNM) for prediction of drying shrinkage strains of SCC was developed using the same data used in the existing models. Two ANNM sets namely ANNM1 and ANNM2 with different numbers of hidden layer neurones were constructed. Comparison between the results given by the ANNM1 model and the results obtained by the five existing predicted models were presented.

The results showed that, using up to 60% of FA as cement replacement can produce SCC with a compressive strength as high as 30 MPa and low drying shrinkage strain. SCCs long-term drying shrinkage from 356 to 1000 days was higher than NCs. Concrete filled elliptical tubes (CFET) with self-compacting concrete containing FA up to 60% are recommended for use in construction in order to prevent confined drying strain.

ACI 209R-92 model provided a better prediction of drying shrinkage compared with the other four models. However, a very high predictability with high accuracy was achieved with the ANNM1 model with a mean of 1.004. Moreover, by using ANNM models, it is easy to insert any of factors effecting drying shrinkage to the input parameters to predict drying shrinkage strain of SCC.

DECLARATION

I declare that this thesis is the result of my own work except where references have been made to the work related to others. This thesis has not been submitted anywhere for the application of another degree, diploma, or other qualification.

LIST OF PUBLICATIONS

During this research, a number of papers have been published which are based on the work carried out in this thesis as listed below:

1. Jamila M. Abdalhmid; A.F. Ashour and T. Sheehan ‘Long-term drying shrinkage of self-compacting concrete: Experimental and analytical investigations’ Construction and Building Materials 202 (2019) 825–837.
2. J. Abdalhmid; M.Mahgub; A.F. Ashour; D. Lam; and T. Sheehan “Prediction of drying shrinkage and compressive strength of self-compacting concrete using artificial neural networks” International Conference of Annual Cement and Concrete Science Conference (34th: 2014: Sheffield, Uk).
3. Jamila Abdalhmid; Ashraf Ashour and Therese Sheehan ‘Long-term drying shrinkage study of self-compacting concrete incorporating fly ash’ in the Faculty of Engineering and Informatics, 2nd Annual Innovative Engineering Research Conference, AIERC 18, held at University of Bradford 17 October 2018.
4. El-Khoja, A.; Ashour, A.; Abdalhmid, J.; Dai, X.; Khan, A. (2018), 'Prediction of Rubberised Concrete Strength by Using Artificial Neural Networks ' World Academy of Science, Engineering and Technology, International Science Index 143, International Journal of Civil, Environmental, Structural, Construction and Architectural Engineering, 12(11), 1068 - 1073.

5. Amal El-khoja, Ashraf Ashour, Jamila Abdalhmid, X. Dai and Amir Khan, 4th prize (the best paper) titled ‘Using Artificial Neural Networks to Predict the Compressive Strength of Rubberised Concrete’ in the Faculty of Engineering and Informatics, 2nd Annual Innovative Engineering Research Conference, AIERC 18, held at University of Bradford 17 October 2018.

DEDICATION

To my husband and kids for their endless support and patience during study years, without them, I would not have been able to study and succeed

ACKNOWLEDGMENTS

This thesis would not exist at all without the generous financial support of my beloved country, Libya represented by the Ministry of Higher Education and gave me this opportunity. I wish for my country Libya peace and progress.

My special appreciation and thanks go to my supervisors Prof. Ashraf Ashour and Dr. Therese Sheehan for their support, encouragement and for allowing me to grow as a researcher.

My deeply thanks to Prof. Ashour for his great support, help and patience throughout my difficult time and critical circumstances during my study.

My thanks go to the member's laboratory for taking time out from their busy schedule to help me. I would like to particularly thank Steve Robinson and Ian Mackay for their expert help during the experimental investigation.

Special thanks to my family for their endless support and patience during study years. Words cannot express how grateful I am to my beloved husband and children for all of the sacrifices that they have made on my behalf, especially during the final stage of the study.

In addition, I extend my warm thanks to my mother, brothers and sisters. Your constant prayer for me was what sustained me this far.

I would also like to express my appreciation to all my friends, especially my office members who supported me to strive towards my goal.

Finally, my heartfelt thanks go to my sister Dr. Rabia, who passed away during last stage of my study for her support and encouragement.

TABLE OF CONTENTS

ABSTRACT II

DECLARATION IV

LIST OF PUBLICATIONS V

DEDICATION VII

ACKNOWLEDGMENTS VIII

TABLE OF CONTENTS IX

LIST OF FIGURES XVI

LIST OF TABLES XXII

ABBREVIATIONS XXIV

NOTATIONS XXVI

1 CHAPTER ONE- INTRODUCTION 1

1.1 Research background 1

1.2 Research significance 2

1.3 Research aims and objectives 3

1.4 Research methodology 4

1.5 Thesis outlines 6

2 CHAPTER TWO- SELF COMPACTING CONCRETE 9

2.1 Introduction 9

2.2 History of SCC developed 9

2.3 Advantages of SCC 10

2.4 Disadvantages of SCC 11

2.5 Materials used in SCC 12

2.5.1 Chemical Admixtures 12

2.5.2 Cement replacement materials 17

2.6 Fresh properties of SCC 20

2.6.1 Filling ability 21

2.6.2 Passing ability 21

2.6.3 Segregation resistance 22

2.6.4 Robustness 22

2.6.5 Consistence retention 23

2.6.6 European Guidelines for SCC 23

2.6.7 Empirical workability test methods 24

2.7 Mix Design Principles for SCC 30

2.7.1 Ozawa's approach 31

2.7.2 CBI's approach 31

2.7.3 LCPC's approach 31

2.7.4 Hwang's approach 32

2.7.5 Ghazi's approach 32

2.7.6 A simple mix design method 33

2.8 Hardened properties of SCC 36

2.8.1 Compressive strength 36

2.8.2 Elastic modulus 37
2.8.3 Permeability 37
2.8.4 Creep 38
2.8.5 Shrinkage 38

2.9 Confined drying shrinkage of concrete 45

2.10 Experimental investigations on drying shrinkage strain of SCC ... 45

2.11 Prediction of concrete shrinkage 47

2.12 Concluding Remarks 47

3 CHAPTER THREE- MATERIALS AND EXPERIMENTAL PROCEDURE 50

3.1 Introduction 50

3.2 Materials 50

3.3 Mix design proportions 53

3.3.1 Pilot study 54
3.3.2 Main mix design proportions 54

3.4 Mixing and specimens preparation 69

3.4.1 Testing procedure 70
3.4.2 Mechanical properties tests 73
3.4.3 Water absorption and density tests 74
3.4.4 Free and confined drying shrinkage strains tests 75

3.5 Concluding remarks 77

4 CHAPTER FOUR- EXPERIMENTAL WORK - RESULTS AND DISCUSSION 78

4.1 Introduction 78

4.2 Test results of fresh properties 78

4.2.2 Passing ability 79

4.2.3 Segregation resistance 79

4.2.4 Slump test 80

4.3 Compressive strength 82

4.4 Flexural strength 84

4.5 Bulk density 85

4.6 Water absorption 87

4.7 Free and confined drying shrinkage strain 88

4.7.1 Free drying shrinkage strain under air and sealed curing 88

4.7.2 Confined and unconfined drying shrinkage strain. 94

4.8 Concluding remarks 100

5 CHAPTER FIVE - PREDICTION OF SELF-COMPACTING CONCRETE DRYING SHRINKAGE STRAINS USING EXISTING MODELS 103

5.1 Introduction 103

5.2 Comparisons of free drying shrinkage strain prediction models. 103

5.2.1 ACI 209R-92 model 104

5.2.2 BS EN 1992 model 104

5.2.3 ACI 209 (Huo) model 105

5.2.4 B3 model 105

5.2.5 GL 2000 model 106

5.3 Assessment of drying shrinkage strains prediction models 108

5.3.1 Effect of compressive strength on drying shrinkage using various models.……...109

5.3.2 Effect of cement and water content on drying shrinkage strain using various models..... 110

5.3.3 Effect of relative humidity on drying shrinkage using different models ……...111

5.4 Experimental database for drying shrinkage strain 112

5.5 Results and analysis 120

5.5.1 Comparison between experimental database and predicted drying shrinkage strain. 120

5.5.2 Evaluation of existing models for predicting drying shrinkage strain.……124

5.6 Concluding remarks 128

6 CHAPTER SIX - PREDICTION OF DRYING SHRINKAGE OF SCC USING ARTIFICIAL NEURAL NETWORK 130

6.1 Introduction 130

6.2 Applications of Artificial neural network 130

6.3 Artificial neural network background 132

6.3.1 Topology of neural networks..... 133

6.4 Training process of neural networks 134

6.5 Experimental database 136

6.5.1 Data normalisation 141

6.6 Construction of ANN model 142

6.6.1 Performance of developed ANNMs models 145

6.7 Parametric study 149

6.7.1 Effect of compressive strength on drying shrinkage strain 150

6.7.2 Effect of water to binder ratio on drying shrinkage strain. 151

6.7.3 Effect of binder content on drying shrinkage strain. 152

6.7.4 Effect of fly ash percentage on drying shrinkage strain. 152

6.7.5 Effect of relative humidity on drying shrinkage strain 153

6.8 Comparison between the prediction given by ANNM1 model and different existing models 154

6.9 Concluding remarks 157

7 CHAPTER SEVEN – CONCLUSIONS AND RECOMMENDATIONS FOR FUTURE WORK 160

7.1 Summary 160

7.2 Conclusions 161

7.2.1 Experimental investigations 161

7.2.2 Analytical investigations 164

7.3 Recommendations for future work 165

REFERENCES 167

APPENDIXE A. PILOT STUDY 179

APPENDIX B. DATABASE OF DRYING SHRINKAGE STRAIN 181

APPENDIX C. STATISTICAL ANALYSIS OF ANN MODELS 191

LIST OF FIGURES

Figure 1-1 Research methodology diagram 6

Figure 2-1 Drying shrinkage against age for concretes with and without SRA (Berke et al., 2003) 16

Figure 2-2 Slump slow apparatus (Alyhya, 2016) 26

Figure 2-3 J-ring apparatus ((Alyhya, 2016) 27

Figure 2-4 L-Box apparatus (Alyhya, 2016) 28

Figure 2-5 V-funnel apparatus (Alyhya, 2016) 30

Figure 2-6 Plastic shrinkage of SCC versus normal concrete (NC) mixes (Turcry et al., 2002)..... 40

Figure 3-1 Grading of coarse and fine aggregates..... 53

Figure 3-2 Trail mix design program flowchart 56

Figure 3-3 Mixing, preparing, casting and curing procedure. 70

Figure 3-4 Viscosity and filling ability of SCC mixes using (a) slump flow test (b) V-funnel test. 71

Figure 3-5 Passing ability of SCC mixes using J- ring test. 72

Figure 3-6 Sieve stability test (a) Slump test for NC mixes (b). 73

Figure 3-7 Photo of test set up of (a) compressive strength (b) flexural strength. 74

Figure 3-8 Free and confined drying shrinkage strain measurements 76

Figure 3-9 Free and confined drying shrinkage strain curing specimens. 77

Figure 4-1 Slump flow and J-ring results..... 81

Figure 4-2 Workability boxes of SCC mixes. 81

Figure 4-3 Effect of fly ash % on compressive strength for mixes with w/b ratio of 0.44 83

Figure 4-4 Effect of fly ash % on compressive strength for mixes with w/b ratio of 0.33. 83
Figure 4-5 91-day flexural strength for NC and SCC mixes with w/c ratios of 0.44 and 0.33 85
Figure 4-6 Effect of fly ash percentage on SCC density. 86
Figure 4-7 Effect of FA content on water absorption of NC and SCC mixes. 87
Figure 4-8 Effect of FA content on free drying shrinkage strain for NCs and SCCs mixes with w/b ratio 0.44 at different ages under air curing. 89
Figure 4-9 Effect of FA content on free drying shrinkage strain for NCs and SCCs mixes with w/b ratio 0.33 at different ages under air curing. 90
Figure 4-10 Effect of FA content on free drying shrinkage strain for NCs and SCCs mixes with w/b ratio 0.44 at different ages under sealed curing. 90
Figure 4-11 Effect of FA content on free drying shrinkage strain for NCs and SCCs mixes with w/b ratio 0.33 at different ages under sealed curing. 91
Figure 4-12 Relation between FA content and free drying shrinkage at 1000 days for different w/b ratios under air curing 92
Figure 4-13 Relation between FA content and free drying shrinkage at 1000 days for different w/b ratios under sealed curing..... 92
Figure 4-14 Relation between 91 days compressive strength and free drying shrinkage at 91 days for different w/b ratios under air curing. 93
Figure 4-15Relation between 91 days compressive strength and free drying shrinkage at 91 days for different w/b ratios under sealed curing. 94
Figure 4-16 Effect of FA content on confined drying shrinkage strain for NCs and SCCs mixes for w/b ratio 0.44..... 95

Figure 4-17 Effect of FA content on confined drying shrinkage strain for NCs and SCCs mixes for w/b ratio 0.33..... 96
Figure 4-18 Effect of FA content on unconfined drying shrinkage strain for NCs and SCCs mixes for w/b ratio 0.44..... 96
Figure 4-19 Effect of FA content on unconfined drying shrinkage strain for NCs and SCCs mixes for w/b ratio 0.33..... 97
Figure 4-20 Relation between FA content and confined drying shrinkage at 1000 days for different w/b ratios. 98
Figure 4-21 Relation between FA content and unconfined drying shrinkage at 1000 days for different w/b ratios. 98
Figure 4-22 Relation between 91 days compressive strength and confined drying shrinkage at 91 days for different w/b ratios. 99
Figure 4-23 Relation between 91 days compressive strength and unconfined drying shrinkage at 91 days for different w/b ratios. 99
Figure 5-1 Effect of compressive strength on drying shrinkage strain using different models. 109
Figure 5-2 Effect of cement content on drying shrinkage strain for different models 110
Figure 5-3 Effect of water content on drying shrinkage strain for B3 model 111
Figure 5-4 Effect of RH % on drying shrinkage strain using different models 112
Figure 5-5 Distribution of cement content of SCCs included in database .. 113
Figure 5-6 Figure 5.6 Distribution of coarse aggregates content of SCCs included in database 114

Figure 5-7 Distribution of fine aggregates content of SCCs included in database 114
Figure 5-8 Distribution of fly ash content of SCCs included in database.... 115
Figure 5-9 Distribution of W/B ratio of SCCs included in database 115
Figure 5-10 Distribution of binder content of SCCs included in database.. 116
Figure 5-11 Distribution of final age of SCCs included in database 116
Figure 5-12 Distribution of relative humidity of SCCs included in database 117
Figure 5-13 Distribution of water content of SCCs included in database ... 117
Figure 5-14 Distribution of 28 days cylinder compressive strength of SCCs included in database 118
Figure 5-15 Comparison between experimental and predicted drying shrinkage strains of SCCs using ACI 209R-92 model 120
Figure 5-16 Comparison between experimental and predicted drying shrinkage strains of SCCs using BSEN-92 model 121
Figure 5-17 Comparison between experimental and predicted drying shrinkage strains of SCCs using ACI 209R-92 (Huo) model 122
Figure 5-18 Comparison between experimental and predicted drying shrinkage strains of SCCs using GL2000 model 122
Figure 5-19 Comparison between experimental and predicted drying shrinkage strains of SCCs using B3 model 123
Figure 5-20 Experimental- to- Predicted values of SCC mixes against ages for ACI 209R-92 model 125
Figure 5-21 Experimental- to- Predicted values of SCC mixes against ages for BSEN-92 model 126

Figure 5-22 Experimental- to- Predicted values of SCC mixes against ages for ACI 209R-92(Huo) model 126
Figure 5-23 Experimental- to- Predicted values of SCC mixes against ages for GL2000 model 127
Figure 5-24 Experimental- to- Predicted values of SCC mixes against ages for GL2000 model 127
Figure 6-1 Artificial neuron model 133
Figure 6-2 Frequency distribution of cement content across the range of 230 tests 138
Figure 6-3 Frequency distribution of fly ash % across the range of 230 tests 138
Figure 6-4 Frequency distribution of W/B ratio across the range of 230 tests 139
Figure 6-5 Frequency distribution of F/Ta ratio across the range of 230 tests 139
Figure 6-6 Frequency distribution of 28-day compressive strength across the range of 230 tests 140
Figure 6-7 Frequency distribution of RH across the range of 230 tests 140
Figure 6-8 Frequency distribution of binder content across the range of 230 tests 141
Figure 6-9 ANNM1 model architecture..... 144
Figure 6-10 ANNM2 model architecture..... 144
Figure 6-11 Performance of ANNM1 model..... 148
Figure 6-12 . Performance of ANNM2 model..... 149

Figure 6-13 Effect of compressive strength on drying shrinkage strain using ANNMs 150
Figure 6-14 Effect of water- binder ratio on drying shrinkage strain using ANNMs 151
Figure 6-15 Effect of binder content on drying shrinkage strain using ANNM1 152
Figure 6-16 Effect of fly ash content on drying shrinkage strain using ANNM2 153
Figure 6-17 Effect of relative humidity on drying shrinkage strain using ANNMs 154
Figure 6-18 Comparison between experimental and predicted drying shrinkage strains of SCCs using ANNM1model and the existing models..... 156
Figure C-1 Screenshot of Performance Plot of ANNM1..... 191
Figure C-2 Screenshot of Performance Plot of ANNM2..... 191
Figure C-3 Screenshot of Training state of ANNM1..... 192
Figure C-4 Screenshot of Training state of ANNM2..... 192
Figure C-5 Screenshot of Training Error Histogram of ANNM1 193
Figure C-6 Screenshot of Training Error Histogram of ANNM2 193
Figure C-7 Screenshot of Training Regression of ANNM1 194
Figure C-8 Screenshot of Training Regression of ANNM2 195

LIST OF TABLES

Table 2-1 Typical mixture proportioning values suggested by EFNARC (2005) 24

Table 3-1 Physical properties and chemical compositions of cement and fly51

Table 3-2 Physical and chemical properties of SP and SRA 52

Table 3-3 Physical properties of coarse and fine aggregates 53

Table 3-4 Proportions of concrete mixtures per m3 57

Table 4-1 Filling ability and viscosity tests, flow slump and V-funnel. 79

Table 4-2 Passing ability and stability tests, J-ring and segregation resistance. 80

Table 4-3 Compressive and flexural strength of NCs and SCCs 82

Table 4-4 Bulk density of NCs and SCCs 86

Table 5-1 Parameters considered by different models for drying shrinkage prediction. 107

Table 5-2 Variables range for each model 108

Table 5-3 Summary of experimental database 119

Table 5-4 Summary of statistical results for drying shrinkage predicted by existing models 124

Table 6-1 Range of components of data sets for drying shrinkage prediction (230 mixtures) 137

Table 6-2 Comparison of different training algorithms 145

Table 6-3 Performance of ANNMs models for different hidden layers neurones created 146

Table 6-4 Effect of relative humidity on drying shrinkage strain using ANNMs 155

Table A-1 Mix proportions of SCC trial mixes 179

Table A-2 Fresh properties and compressive strength of SCC trail mixes. 180

Table B-1 Details of database..... 181

ABBREVIATIONS

The following abbreviations are used in this research:

A%	Air content %
AEAs	Air entraining admixtures
ANNs	Artificial neural networks
ANNMs	Artificial neural network models
B	Binder
C	Cement content
C_{agg}	Coarse aggregate
CFET	Concrete filled elliptical steel tubes
CFT	Concrete-filled steel tubular members
COV	Coefficient of variation
CRMs	Cement replacement materials
DS	Drying shrinkage
DSNC	Drying shrinkage of normal concrete
DSSCC	Drying shrinkage strains of SCC
E	Elastic modulus
FA	Fly ash
F_{agg}	Fine aggregate
GGBS	Ground granulated blast-furnace slag
HRWRA	High-range water reducing admixtures
LS	limestone
MAS	Maximum coarse aggregate size
MAE%	Mean absolute error

MBP	Multi-layered neural network back-propagation
MK	Metakaoline content
NC	Normal concrete
OPC	Ordinary Portland cement
PF	Packing factor of aggregate
SCC	Self-compacting concrete
SF	Silica fume content
SPs	Superplasticisers
SRAs	Shrinkage reducing admixtures
VMAs	Viscosity-modifying admixtures
W/B	Water to binder ratio
W/C	Water to cement ratio

NOTATIONS

The following symbols are used in this thesis:

$\mathrm{A_c}$	Concrete cross-sectional area
γ_{sh,f'_c}	Compressive strength coefficient
ε_{sh}	Drying shrinkage strain
W_{WB}	Content mixing water contents required by GGBS paste
W_f	Content mixing water contents required by FA paste
W_g	Content of coarse aggregates in SCC
W_{gL}	Unit volume mass of loosely coarse aggregates in air
W_{pm}	Total amount of Pozzolanic materials (GGBS and FA)
W_s	Content of fine aggregates in SCC
W_{sL}	Unit volume mass of loosely fine aggregates in air
W_{wc}	Content of mixing water content required by cement
f_{cm}	Mean compressive strength
k_{h_0}	Notional size coefficient
k_h	Relative humidity coefficient
$\beta_{(h)}$	Humidity coefficient
$\beta_{(t)}$	Time of drying coefficient
$\gamma_{sh,RH}$	Humidity coefficient
$\gamma_{sh,c}$	Cement content coefficient
$\gamma_{sh,s}$	Slump coefficient
$\gamma_{sh,tc}$	Initial moist curing coefficient
$\gamma_{sh,vs}$	Member size coefficient

$\gamma_{sh,\Psi}$	Fine aggregate coefficient
$\gamma_{sh,\alpha}$	Air content coefficient
γ_{sh}	Cumulative of correction factors
$\varepsilon_{sh\,\mathrm{u}}$	Ultimate shrinkage
CRD	Difference between the comparator reading of the Specimen and the reference bar at any age
D	Cross section thickness of concrete
d1 and d2	Slump flow
k	Cement type coefficient
T_{500} and $T_{v\text{-funnel}}$	Flow time
t_c	Time of curing
V_{paste}	Paste volume
V_{PB}	Volume of GGBS paste
V_{PF}	Volume of FA paste
V_v	The least void of packing system
W/B	Water binder ratio
W/C	Water cement ratio
α_1	Cement type coefficient
α_2	Curing type coefficient
α_{ds}	Cement type coefficient
ε_{exp}	Experimental value of drying shrinkage
ε_{pred}	Predicted value of drying shrinkage

CHAPTER ONE- INTRODUCTION

1.1 Research background

Basically, SCC consists of the same components as normal concrete (NC) (cement, water, aggregates, admixtures, and mineral additions), but the final composition of the mixture and its fresh characteristics are different. Compared to NC, SCC mixtures are usually designed with high volumes of paste, large quantities of mineral fillers such as limestone (LS), ground granulated blast furnace slag (GGBS), silica fume (SF) and fly ash (FA) and high range water reducing admixtures (HRWRA) with a smaller maximum size of the coarse aggregate. All of those special characteristics of SCC affect the behaviour of concrete in its hardened state such as drying shrinkage (DS) that is considered to be a major concern for concrete deterioration (Gesoğlu et al., 2009). As highlighted by Hwang and Khayat (2008a), SCC can exhibit higher shrinkage compared with normal concrete (NC) due to its great volume of cement paste and low coarse aggregate content. DS is a more significant phenomenon than the other types of shrinkage, it produces tensile stress within the concrete leading to cracking, which enables harmful materials to penetrate into the concrete and effects the economic factors of construction such as durability, serviceability and long-term reliability. Many investigations have been carried out covering free drying shrinkage behaviour of SCC compared to NC. However, there is some discrepancy regarding the magnitude of drying shrinkage strains of SCC (DSSCC) compared to drying shrinkage of normal concrete (DSNC). Moreover, no previous research has been conducted on

confined drying shrinkage strain of SCC and NC. The current study will investigate the main parameters affecting the free and confined drying shrinkage of SCC compared to NC to explain that discrepancy.

1.2 Research significance

As mentioned above, many studies have investigated the behaviour of SCC with various compositions including drying shrinkage. The free drying shrinkage behaviour of SCC has been investigated by several studies. However, there are significant concerns among researchers that SCC may have a different drying shrinkage magnitude compared to NC, and this needs further research. The discrepancy between the experimental results of DSSCC and DSNC could be related to the differences between the concrete mixtures studied, testing conditions, and testing methods (Fernandez-Gomez and Landsberger, 2007). Moreover, most of the previous studies took into account only DS that was determined after a specific time of curing or immediately after demoulding, while other researchers considered DS that started from the setting time, including autogenous shrinkage. In this investigation, in order to compare the DSSCC and DSNC magnitudes, the environmental conditions (relative humidity, temperature and curing type) and concrete condition (casting and testing) were kept same for SCCs and NCs and the measurements of drying shrinkage strain were taken immediately after demoulding.

Furthermore, to date, there has been no research on the confined drying shrinkage strain characteristics of SCCs and NCs. As it is known two types of materials are used to fabricate concrete-filled steel tubular members (CFT), it

is expected that concrete drying shrinkage may cause a circumferential gap between the steel tube and concrete core. None of the previous researchers have examined confined drying shrinkage of NC or SCC. Thus, as part of this investigation, the behaviour and magnitude of confined drying shrinkage of SCC compared to NC will be highlighted. The presented study is part of an ongoing research program to increase the knowledge of the free and confined drying shrinkage strain of SCC and NC.

The proper evaluation of SCC drying shrinkage can provide engineers with the information required of the design process and produce a high quality SCC mix. Thus, it is important to find an appropriate prediction model for SCC drying shrinkage. Computational models using artificial neural network (ANNs) to predict drying shrinkage of SCC and evaluate the influence of SCC ingredients behaviours on the drying shrinkage have not been developed to date. In this research two drying shrinkage prediction models proposed by international codes, three existing models that have been proposed by some researchers, and an artificial neural network model (ANN), have been used to estimate SCC drying shrinkage strain.

1.3 Research aims and objectives

The main aim of this research is to study free and confined drying shrinkage of SCC compared to NC. Experimental work objectives were set together with the modelling objectives to fulfil the final research aim. The principal objectives of the present research are categorised as follows:

- To experimentally investigate the influence of different constituents on fresh and mechanical properties of SCC compared with NC.

- To monitor and examine long term (more than two years) free and confined drying shrinkage magnitude and behaviour of SCC and compare with NC.
- To assess the accuracy of drying shrinkage prediction models proposed by international codes and others, including American Concrete Institute Committee (ACI 209R-92) model, Eurocode 2 (BS EN-92) model, the model modified by Huo (ACI 209R-92 (Huo), the model developed by Bazant and Baweja (B3) and Gardner and Lockman model (GL2000).
- To confirm the predictability of the existing models based on experimental results collected from this work.
- To analytically develop an artificial neural network model (ANNM) for prediction of drying shrinkage strains of SCC, using collected comprehensive database from different sources in the literature together with experimental results obtained from this investigation, and to analyse the effect of key parameters considered in this study on the long term drying shrinkage of SCC.
- To compare between the results given by the ANNM model and the results obtained by the five existing predicted models mentioned above.

1.4 Research methodology

To achieve the above aims and objectives, the current project was undertaken through the following approaches as shown in **Figure 1.1**.

For the experimental campaign the following steps have been performed;

- Eight self-compacting concrete (SCC) mixes have been designed with two different water-cement ratios (0.44 and 0.33) with cement replacement by various percentages (20%. 40% and 60%) of fly ash.
- The procedure and batching of the SCC mix has been developed followed previous mix design methods with some proportions modification.
- Fresh properties of SCC have been tested and checked using; slump flow, J-Ring, V-Funnel and segregation test.
- Two normal concrete (NC) mixes have been tested in order to compare with SCC mixes.
- (100 × 100 × 300 mm) prismatic specimens and (Φ 240×113×100 mm) elliptical specimens have been used to monitor and evaluate free and confined drying shrinkage respectively for SCC and NC under two type of curing conditions (Air and sealed).

Furthermore, the following analytical investigations have been developed:

- Artificial neural networks (ANNs) has been develop using software MATLAB (R2016b) to predict drying shrinkage strain of SCC.
- Existing models, including ACI 209R-92, BS EN-92, ACI 209R-92 (Huo), B3 and GL2000 have been used to predict of drying shrinkage strain of SCC.

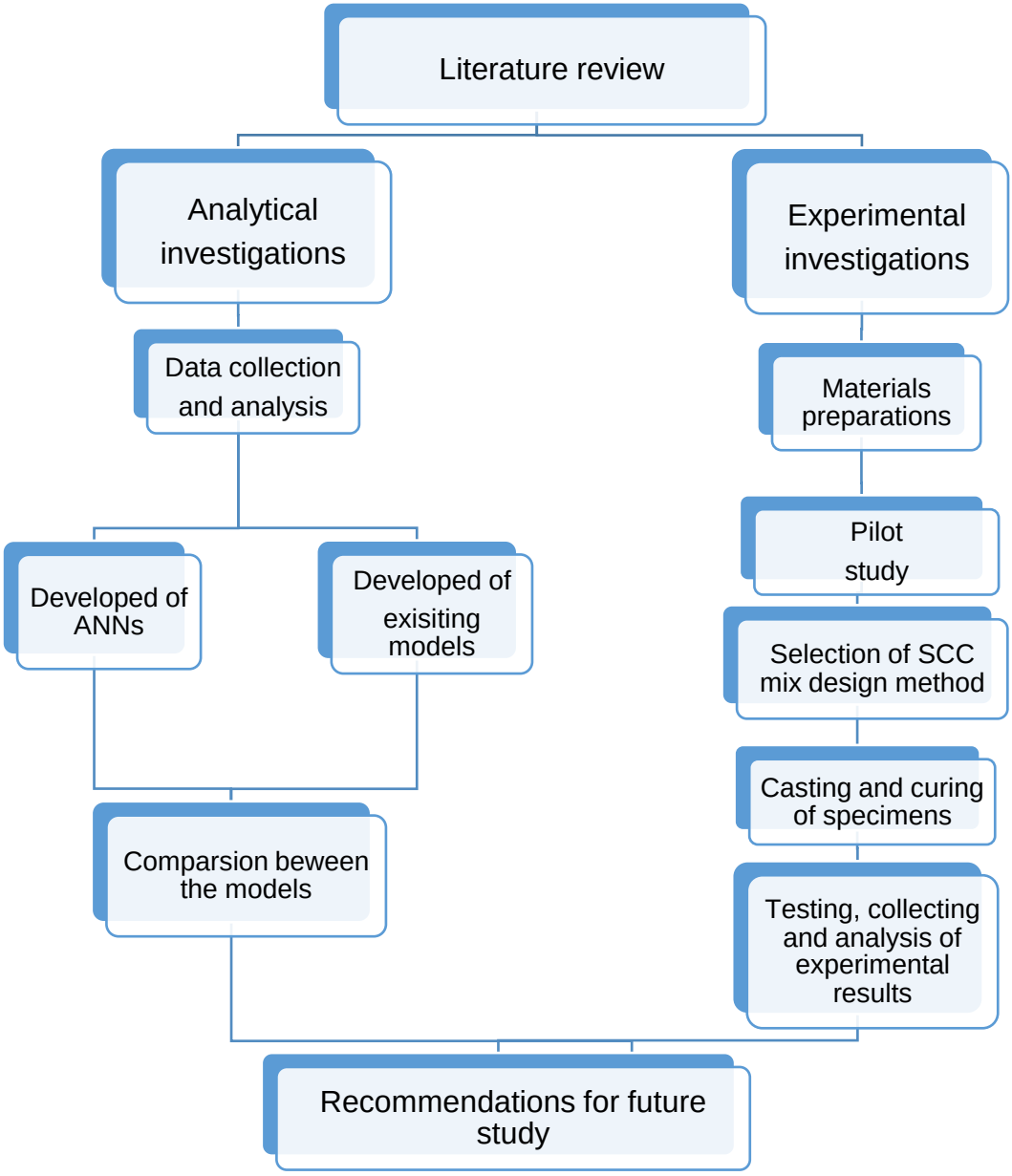

Figure 1-1 Research methodology diagram

1.5 Thesis outlines

In addition to the current chapter including general background about SCC, drying shrinkage of SCC, objectives and scope of this study, this thesis contains other six chapters, which are divided into sections and subsections, following by bibliographical references and appendixes.

Chapter 2 presents a review of the literature relating to SCC including raw materials, fresh properties of SCC, principles of SCC mix design approaches and hardened properties of SCC as well as previous research on free drying shrinkage of SCC, confined drying shrinkage of concrete, followed by computational methods to predict shrinkage of concrete overview.

Chapter 3 introduces the experimental investigation and research methodology in detail covering preparation and mechanical properties of materials used, mix design proportions (Trial and main design), curing and casting of concrete. Also, the testing procedure for measuring the fresh and hardened properties of SCC have been illustrated in this chapter.

Chapter 4 provides experimental test results, which include fresh properties of SCCs such as filling ability, viscosity, segregations and slump test of NCs, in addition to hardened properties of SCCs and NCs including compressive strength, flexural strength, bulk density, water absorption and long term free and confined drying shrinkage strains under two types of curing. This is followed by analysis and discussion of the influence of different constituents on fresh and hardened properties of SCC compared with NC.

Chapter 5 aims to predict SCC drying shrinkage using various computational existing models (ACI 209R-92), BSEN-92, B3, GL2000 and ACI 209R-92 (Huo) covering data selection for SCC drying shrinkage strains, experimental results, and comparison between the different models predicted and calculated of SCC drying shrinkage strains. Finally, based on the experimental results collected from this work, predictability of the existing models has been confirmed.

Chapter 6 in this chapter, prediction of drying shrinkage of SCC using ANNs model, providing background knowledge about ANNs, applications of ANNs, data collected from previous research including parametric studies to investigate the effect of different parameters on the SCC drying shrinkage behaviour, as well as comparison between existing models presented in previous chapters with current computational models have been covered.

Chapter 7 deals with general conclusions involved in Chapters 3 to 6 and provides recommendations and suggestions for future research.

CHAPTER TWO- SELF COMPACTING CONCRETE

2.1 Introduction

The first part of this chapter presents a brief background on history of self-compacting concrete (SCC), advantages and disadvantages of SCC, the principal materials and fresh properties of SCC. As well as this, a description of mix design methods available and hardened properties of SCC is provided. An overview of the shrinkage of SCC and drying shrinkage strain measurements followed by key research on the shrinkage behaviour of SCC and its effects are introduced in the second part of this chapter. An overview of concrete shrinkage prediction is also presented. Concluding remarks are provided at the end of the chapter.

2.2 History of SCC developed

Self-compacting concrete (SCC) was first invented at the University of Tokyo, Japan in the late 1980s, to eliminate noise caused by vibration, improve concrete construction quality, shorten the construction time and minimise skilled labour requirements. The development of SCC was completed in 1988 using the same materials proportions as those used in normal concrete (NC) (Okamura and Ouchi, 2003). At the end of the 1990s SCC technology spread to Europe and North America (Billberg, 1999). The first projects using SCC were a building constructed in Japan in 1990 and the tower of a prestressed concrete bridge in Japan in 1991(Okamura and Ouchi, 2003). SCC started to be of interest in more construction projects in the beginning of the 21st century.

Moreover, in 2004, about fifty percent of all precast prestressed concrete manufacturers shifted to SCC technology (Schindler et al., 2007)

Many definitions of SCC available in the literature; The American Concrete Institute (ACI) (ACI Committee 209, 1992) defines SCC as a “highly flowable, non-segregating concrete that can spread into place, fill the formwork, and encapsulate the reinforcement without any mechanical consolidation.” The BS-EN/206 (2010) defines SCC as “concrete that is able to flow and compact under its own weight, fill the formwork with its reinforcement, ducts, boxouts, etc., whilst maintaining homogeneity”. Many academic institutions and professional societies have been developed some recommendations on the design and applications of SCC in building construction.

2.3 Advantages of SCC

The invention of SCC has significantly benefited the construction industry with a wide range of advantages due to its unique features in quality and economy. Elimination of the need for vibration reduces the number of workers and machinery requirements which reduce construction costs. Okamura and Ouchi (2003) reported that the number of workers can be reduced by 30% from those required if normal concrete (NC) is used in large applications. SCC has good deformability and passing ability with high resistance to segregation which can be placed in heavily reinforced applications and compacted under its self-weight. With no vibration, it accelerates the process of casting concrete and reduces the mixer truck movement and pump operations, which decreases the construction time. Okamura and Ouchi (2003) reported that the construction period may reduced by 20% in huge scale projects where SCC is applied.

2.4 Disadvantages of SCC

SCC has been applied in wider applications. However, besides its benefits there are some disadvantages to using SCC that should be considered. It requires designers with high levels of experience to produce and control the SCC mix to achieve the fresh properties required. SCC is designed with high amounts of chemical admixtures and cementitious materials which may delayed the setting time (Okamura and Ouchi, 2003). In addition, the low content and small size of coarse aggregates in SCC compared to NC lead to increased shrinkage and reduce the modulus of elasticity (Parra et al., 2011, Turcry et al., 2002). Moreover, the drying shrinkage of SCC is higher than that of NC due to high volumes of paste, large quantities of mineral fillers, low coarse aggregates content and high range of water reducing admixture (Hwang and Khayat, 2008b, Kim et al., 1998, Heirman and Vandewalle, 2003). Finally, there are no standard methods or specifications for proportioning SCC materials. However, SCC has been successfully used in many applications, and these disadvantages can be reduced or eliminated. For example, the drying shrinkage risk of SCC can be reduced using chemical admixtures such as shrinkage reduction admixtures (SRA or cementitious material replacements such as fly ash (FA) and ground granulated blast-furnace slag (GGBS). The high material cost can be offset by the reduced labour cost and the importance of high flowability, deformability and passing ability of SCC which are required in a wide range of applications. Therefore, the advantages of using SCC are more significant than the drawbacks.

2.5 Materials used in SCC

SCC can be made with a large range of the same materials as those in normal concrete (NC), but it is generally much more sensitive to changes in material properties. The characteristics of chemical admixtures and supplementary cementitious materials which are principal parameters to improving workability will be described briefly as a part of this chapter.

2.5.1 Chemical Admixtures

The key admixtures used to produce SCC are high-range water reducing admixtures (HRWRA) and viscosity-modifying admixtures (VMA). Other admixtures including air-entraining admixtures (AEA) can also be used successfully in SCC.

2.5.1.1 High – range water reducing admixtures

For achievement of SCC with a high level of workability with great stability, use of high- range water reducing admixtures (HRWRA) is indispensable (Okamura and Ozawa, 1996). The advent of superplasticisers (SPs) and the developments in the admixture technology have made the production of SCC easier, it can increase paste flowability with a slight decrease of viscosity (Khayat, 1999). The superplasticiser complies with ASTM/C494/494M (2017) as Class A and F admixture. Mainly it contains a sulfonic group in the molecule which imparts a negative charge on the cement particles, thus causing dispersion (Nawa et al., 1998, Kim et al., 2000). New researchers have developed polycarboxylic acid-based superplasticiser which able to provide high consistence, proper viscosity and long consistence retention even in a small amount and at low water cement ratio (W/C). It is therefore suitable for

SCC and is the most commonly used superplasticiser. Yamada et al. (2000) have studied the effect of different superplasticisers with different W/C ratio on the consistency of a cement paste. They concluded that where the W/C ratio was below 0.25, the effect of the W/C ratio on consistency was significant. On the other hand, the spread of the paste was more sensitive to a superplasticiser dosage with a W/C ratio higher than 0.35, therefore small fluctuations in the water or superplasticiser content can have a great influence on the consistency of SCC.

Adsorption of superplasticisers has an important effect on SCC, the ability of absorption depends on the electrostatic repulsion, mainly determined by the degree of cement fineness and tricalcium aluminate (C_3A) content (Bonen and Sarkar, 1995). The lower the specific surface and C_3A content in the cement, the lower superplasticiser adsorption (Yamada et al., 2000). The rate of adsorption of SPs is also effected by temperature, with high temperature accelerating the rate of SP adsorption (Liu, 2009). In addition, the effect of superplasticisers also depends on the powders and mixing methods.

Adding superplasticisers causes some delay in the setting time (Uchikawa et al., 1997) due to the adsorbed of polymer chains onto the cement grains and interference with the precipitation of various minerals into solutions which slow the hydration rate (Khayat and Guizani, 1997). Yamada et al. (2000) and Jolicoeur and Simard (1998) found that both initial and final setting were delayed by increasing the sulfonic and carboxylic groups in the aqueous phase of polycarboxylic acidbased superplasticiser. Khayat and Yahia (1997) confirmed that the initial setting time of the paste increased from 5.3 to 11.5

hours with the increase in the superplasticiser dosage from 0 to 0.8% by the mass of cement.

2.5.1.2 Viscosity modifying agents

Viscosity-modifying admixtures (VMA), also known as anti-washout admixtures, generally used for SCC applications to improve segregation resistance, reduce bleeding, increase cohesion (Bury and Christensen, 2002) as well as they may be used as an alternative to increasing the powder content or reducing the water content of a concrete mixture. VMA divides into two categories depended on the mechanism of adsorptive and non-adsorptive (Yammamuro et al., 1997, Nawa et al., 1998). Adsorptive VMAs act on cement. After addition, it is adsorbed onto the surface of the cement particles and forms a structure, which imparts the viscosity of SCC, superplasticisers and VMAs will contest for the adsorption site (Nawa et al., 1998).

Moreover, non-adsorbing VMAs act on water; they increase the plastic viscosity of SCC due to their water soluble polymer chains imbibing some free water (Khayat, 1999). By increasing non-adsorbing VMAs the amount of superplasticisers adsorbed does not change. Therefore, the plastic viscosity of concrete increases, while the spread value may not change (Nawa et al., 1998). For producing SCC with high filling ability and adequate viscosity non-adsorbing VMAs were added. One of the non-adsorbing VMA was in a liquid form (from Sika) and the other one was in a powder form (Welan and Dituan) which were used in Japan, and South America respectively. Both of them are anionic, long-chain biopolymers with sugar backbones substituted with sugar side chains, produced by a controlled aerobic fermentation process (Khayat, 1998).

Petersson and Billberg (1999) reported that by increasing the amount of welan gum the slump decreased, mixes with VMAs lost consistency more quickly than those without VMA. In addition, a small dosage of welan gum led to a higher superplasticiser requirement, which may subsequently affect the performance of SCCs (Khayat, 1995). However, VMA does not affect the saturation of a superplasticiser, although an increase of VMA will decrease the spread and flow time (Schwartzentruber et al., 2006).

Overall, two aspects of VMA must be considered when using SCC, characteristics and interaction of VMAs with superplasticisers. The consistency of SCC should be controlled during the addition of VMAs. Subsequently by testing the consistency retention the compatibility between VMA and superplasticiser can be assessed.

2.5.1.3 Shrinkage Reducing Admixtures

Shrinkage-reducing admixtures (SRAs) are a new type of admixture that has appeared in recent years in concrete engineering. SRA is a chemical admixture (1–2% by mass of cement) based on neopentil glycol, $(CH_2)_2$–C–$(CH_2OH)_2$, or other similar products which reduce the drying and/or autogeneous shrinkage (Berke et al., 2003). According to some researchers SRA can reduce plastic shrinkage (Engstrand, 1997), autogenous shrinkage (Bentz et al., 2001), and especially drying shrinkage (Sato et al., 1983). SRA lowers the surface tension of the pore water solution in the cement paste, thus decreasing the shrinkage stresses and reducing the cracking due to shrinkage (Sato et al., 1983). Berke et al. (2003) tested concretes with and without SRA and they reported that the presence of SRA showed significant reduction with respect to the reference concrete in the drying shrinkage at 1 month from

0.04% to 0.02% as observed in **Figure 2.1**. At 2% SRA dosage, free drying shrinkage can be decreased by 30 – 40% for concrete specimens at 60 days. It also reduces autogenous shrinkage for mortar by 20–30% at 90 days with the same dosage (Rongbing and Jian, 2005).

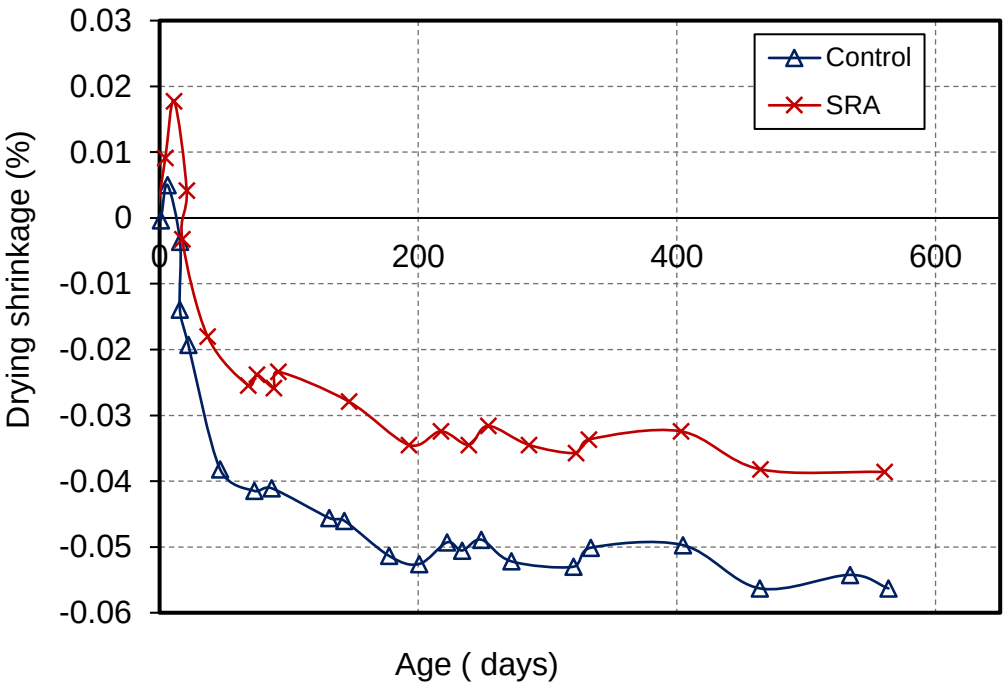

Figure 2-1 Drying shrinkage against age for concretes with and without SRA (Berke et al., 2003)

2.5.1.4 Air Entraining Admixtures

To achieve adequate air content, air bubble size, air bubble spacing, and freeze-thaw cycles resistance, air entraining admixtures (AEAs) are used in SCC (Khayat, 2000, Khayat and Assaad, 2002, Ozyildirim, 2005). It is also used to improve the workability of concrete and to reduce bleeding. AEAs were first discovered in the 1930s when engineers observed that certain roads in the north-east states of USA were more durable that other roads in the same area. (Mailvaganam and Rixom, 2002). Air-entraining agents are made of salts of wood resins, proteinaceous materials, petroleum acids, sulfonated lignin,

organic salts of sulfonated hydrocarbons and certain synthetic detergent (Mehta, 1986). Entrained air bubbles can reduce viscosity, which may reduce the stability of concrete, meaning that other mixtures such as VMAs should be used, and/or by lowering free water content. (Khayat, 2000).

Khayat and Assaad (2002) concluded that yield stress and plastic viscosity should not be too low, which may cause segregation and a loss of air, and not too high, which may increase the internal pressure in air bubbles resulting in loss of air content.

2.5.2 Cement replacement materials

SCC usually requires a high powder content. If only cement is used, SCC has a high cost. Cement replacement materials (CRMs) or mineral admixtures are added to SCC. The CRMs may be used in addition to, or as a partial replacement for, Portland cement in concrete depending on the properties of the materials and the effect required on concrete (Kula et al., 2002), it is a better way to impart high workability to the mix, as well as to reduce the total cost of SCC. CRMs are finely divided materials used in SCC in order to improve workability, durability and reduce heat of hydration, segregation resistance. The principal chemical ingredients in CRMs, silca (SiO_2) and aluminum oxide (Al_2O_3), can react slowly with lime Ca $(OH)_2$ a cement hydration product, resulting in the formation of calcium silicate and aluminate hydrates the pozzolanic reaction. These replacements fill the voids in concrete, improving long term strength and durability by lowering the permeability, reducing shrinkage, creep, chloride ingress and sulphate attack. Also Pozzolanic reaction reduces the thickness and porosity of the interfacial zone which acts between cement paste and aggregate thus improving the bond

strength between the paste and aggregate (Kuroda et al., 2000, Wong et al., 1999).

Due to the reduction in early strength development in mixtures with fly ash or slag, the strength of such mixtures may need to be evaluated at ages beyond 28 days. In some cases, CRMs are used to reduce strength at certain ages because the amount of powder materials needed for workability would result in excessive strength if composed of only Portland cement (Domone, 2006)

The most commonly used CRMs are the ground granulated blast furnace slag (GGBS) and pulverised fuel ash or fly ash (FA), which can be used as binary, ternary (two CRMs in a single mix) and quaternary mixtures.

2.5.2.1 Ground granulated blast furnace slag

Ground granulated blast furnace slag (GGBS) is one of the CRMs widely used in the production of SCC. It is a by-product from the blast furnaces used to make iron. According to its level of reactivity, GGBS is classified by EN 15167-1 and EN 15167-2 (or BS 6699). For equal mass of the total binder (i.e. cement plus GGBS) content in the concrete, the GGBS will produce a larger volume of the binder paste which will increase the segregation resistance and make the concrete easier to work, pump, place and compact. Finer particles in the GGBS (compared with the Portland cement) can also reduce bleeding (Craeye et al., 2010). Güneyisi et al. (2010) studied the effect of GGBS on compressive strength and drying shrinkage of SCC, they concluded that SCC mixtures having GGBS had comparable strength values with 6.2% reduction in drying shrinkage. Saliba et al. (2011) reported that there was no clear destruction in concretes containing GGBS after 140 cycles of freezing and thawing and also

a high resistance to elevated temperatures. However, a high proportion of GGBS may affect the stability of SCCs resulting in reduced robustness with problems of consistency control, while slower setting can also increase the risk of segregation (Heirman et al., 2007, BIBM and ERMCO, 2005).

2.5.2.2 Fly ash (FA)

Fly ash (FA) is collected from the combustion of pulverized coal in electric power generation plants. The particle sizes of fly ash vary from less than 1μm to more than 100μm with the typical particle size measuring less than 20μm. The spherical nature of FA particles reduces the friction between aggregates and increases the workability of concrete. More recently volcanic ash has also been used to produce SCC (Hossain and Lachemi, 2005). FA are classified according to their chemical composition into two major classes : class F and class C. Class F is fly ash normally produced from burning anthracite or bituminous coal, and class C is normally produced from the burning of subbituminous coal and lignite (Halstead, 1986). The difference between class C and class F fly ash as per the ASTM standard is the amount of calcium, silica, alumina, and iron content in the ash ASTM C618/12a (2012). Concretes with fly ash can lead to many improvements in overall concrete properties. FA concrete has been proved to be more durable and resource-efficient than the OPC concrete (Malhotra, 2002). Khatib (2008) reported that using up to 60% as Portland cement replacement can produce SCC with a strength as a high as 40 N/mm^2.

2.5.2.3 Silica Fume (SF)

Silica fume is generally used to increase cohesiveness and reduce segregation and bleeding (BIBM and ERMCO, 2005), as well as increasing compressive strength, modulus of elasticity, and flexural strength and enhancing durability at all ages. Compared to other CRMs, SF increases the strength of concrete at early ages (Pala et al., 2007).

As Park et al. (2005) reported that the use of silica fume at cement replacement rates of 5, 10, and 15% increased yield stress and plastic viscosity significantly. They suggested that silica fume be used to increase plastic viscosity to prevent segregation and that the sharp increase in yield stress be offset by the use of a ternary cementitious system with either fly ash or slag (Alrifai et al., 2013). In spite of SF concretes showing higher compressive strength than conventional ones however, the use of SF with Portland cement gradually increased the drying shrinkage of SCC (Güneyisi et al., 2010).

2.6 Fresh properties of SCC

As mention earlier in this research, SCC has the characteristics of filling ability, passing ability, segregation resistance, robustness and consistence retention and it is important to keep these characteristics during transport and placing. Fresh properties influence not just constructability but also hardened properties like strength and durability. The importance of these properties and their measurement will be described in the following sections.

2.6.1 Filling ability

Filling ability is the ability of the fresh concrete to fill the formwork including areas of complex reinforcement under its own weight. As Bailey (2005b) reported that there are two methods to ensure that the concrete will exhibit proper filling ability; by balancing the w/c with the superplasticizer dosage which will increases the deformability of the paste and by minimizing the inter-particle friction within the mix by reducing the amount of coarse aggregate and increasing the volume of paste.

The slump flow spread and T_{500} time are the most popular tests used to assess the horizontal free flow of SCC for the assessment of concrete flowability (or fluidity). The result is an indication of the filling ability of SCC. More details about slump flow test are presented in section **2.6.7.1**.

2.6.2 Passing ability

Another fresh concrete property that describes SCC flowability is passing ability. Khayat et al. (2004) suggested three parameters that should be considered when evaluating the passing ability of SCC; the geometry and density of reinforcement, the stability of fresh concrete, and the maximum aggregate size and content. These should be optimized to avoid blockage and segregation at the areas of congested reinforcement (BIBM and ERMCO, 2005, Bailey, 2005a, Hwang et al., 2006). To improve resistance to blocking or passing ability, segregation should be reduced using viscosity modifier admixtures (VMAs) or low w/c (Khayat et al., 2004). In order to assess the passing ability of the mix; several tests have been developed including the L-

box and J-ring tests. More details for test procedures are presented in section **2.6.7.2** and **2.6.7.3**.

2.6.3 Segregation resistance

Segregation is the separation of aggregates from paste. Segregation can form around the reinforcement during the casting of a structure and also after the concrete has been poured, settlement of the aggregates can occur and cause weak surfaces and cracking in some elements (BIBM and ERMCO, 2005). There are two types of segregation, the first one is referred to as dynamic, and occurs during placing and the second type is known as static or bleeding, which happens after placing (Kim et al., 2000). To improve segregation resistance, (Bailey, 2005b) suggests minimizing bleeding due to free water and reducing the segregation of solid particles by using VMAs and/or lowering the w/c of the mix. Felekoğlu et al. (2007) suggested that the optimum water/cement ratio for production of SCC is 0.84 to 1.07 by volume, and ratios above or below these limits cause blocking or segregation. The common methods to measure the segregation resistance of the fresh concrete are the sieve segregation resistance, the static segregation column test and the penetration test. The procedure of the sieve segregation test is presented in section **2.6.7.4**.

2.6.4 Robustness

Robustness is the ability of concrete to protect its properties under different situations. The robustness is the capacity of concrete to retain its performance requirements (fresh and hardened properties, including durability) when small variations in the properties or quantities of the constituent materials occur

(Nunes et al., 2006). Variations in water content and SP dosage due to changes in the production process have been observed to cause large variations in fresh properties of SCC. However, using powder and VMA to increase the viscosity, the robustness will improve (Domone, 2007).

2.6.5 Consistence retention

The fresh properties of SCC after mixing should be maintained close to their initial level, usually for 60~90 minutes during transporting and placing (Sonebi and Bartos, 2002, Kasemchaisiri and Tangtermsirikul, 2008). The different effects of powder on the adsorption of water and admixture consistency loss mainly result from the powder-superplasticiser interaction (Khayat, 1999), The water binder ratio (w/p) and the chemical structure of the superplasticiser also affect the consistency retention (Felekoğlu et al., 2007, Yamada et al., 2000).

2.6.6 European Guidelines for SCC

European Guidelines for Self-Consolidating Concrete (BIBM and ERMCO, 2005) have published guidelines for proportioning SCC mixtures with some limitations and specifications based on the mix design methods that have been proposed and the results obtained by other researchers. The European guidelines for SCC mix proportioning are presented in **Table 2.1.**

Table 2-1 Typical mixture proportioning values suggested by EFNARC (2005)

Constituent	Typical range by mass (kg/m^3)	Typical range by volume (litres/m^3)
Powder	380 – 600	
Paste		300 – 380
Water	150 – 210	150 – 210
Coarse aggregate	750 – 1000	270 – 360
Fine aggregate	48 – 55% of total aggregate weight	
Water/powder ratio		0.85 – 1.10

Overall, all these methods have their own requirements depending upon a specific set of materials and relationships which sometimes are not easy to apply to other materials. Mix design of SCC using computing software has become more popular in order to predict SCC properties.

2.6.7 Empirical workability test methods

Due to the lack of standardisation of SCC test methods, the dimensions and details of the empirical test methods can vary within the literature. A number of empirical workability tests (slump flow test, V-Funnel, L-Box test, U-Box test, J-Ring and sieve segregation resistance test) have been proposed and established in practice to measure the workability of SCC. Some of main workability test methods are described in the following subsections.

2.6.7.1 Slump flow test (with T500 and visual stability)

The slump flow test is a modification of the traditional slump test, in which the spread of the material is measured instead of the height reduction, it is the simplest and most commonly used test to evaluate the flow-ability of SCC

(Pashias et al., 1996). The slump flow test evaluates the deformation capacity of SCC under its own weight without external forces against the friction of the base plate. The slump flow tests is usually the test that determines whethers the mix is accepted or rejected at the working site (Utsi et al., 2003). T500 is the time from lifting of the cone to the concrete spreading to a 500 mm diameter, which used to indicate the deformation rate. The higher the T500 value, the lower the deformation rate of concrete. T500 is between 2 and 7 seconds in the case of fresh SCC (Neophytou et al., 2010). However, for very flow-able concrete it is difficult to measure the short time period using the T500 method (Carlswärd et al., 2003). As Bouzoubaâ and Lachemi (2001) have reported the superplasticiser dosage is the main parameter that affects the slump flow, while the water to powder ratio and the fly ash replacement content have only a secondary effect. However, Sonebi (2004) showed that the water to binder (cement+ fly ash) ratio had the greatest effect on the slump flow for SCC incorporating fly ash. Apparatus used to evaluate slump flow is shown in **Figure 2.2**.

2.6.7.2 J-ring test

The J-ring test is used to measure the passing ability of SCC through congested reinforcement. The apparatus as shown in **Figure 2.3** is composed of a ring (300mm diameter and 100mm high) with several reinforcing bars, a slump cone and a rigid plate. The slump cone is placed centrally in the J-Ring and filled with concrete, when it is lifted vertically, the concrete has to pass through the reinforcing bars as it flows across the plate. The passing ability is expressed as the average height difference between the concrete at four different locations.

Tam et al. (2005) developed different geometries of the J-ring and different bar arrangements, in order to study the combined effects of the size and space between the reinforcing bars in practice, the range of the J-ring diameter was increased from 300 mm to 500 mm with even spaces between the bars, they reported that by this modification it is possible to replicate the actual reinforcement in a structure by varying the number, the size or the configurations of the bars.

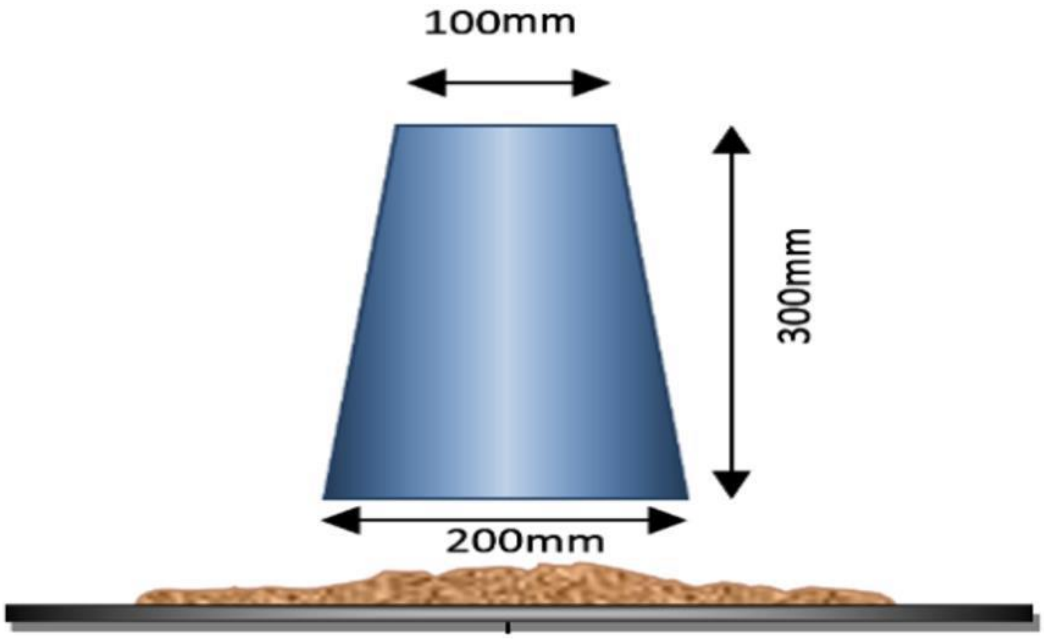

Figure 2-2 Slump slow apparatus (Alyhya, 2016)

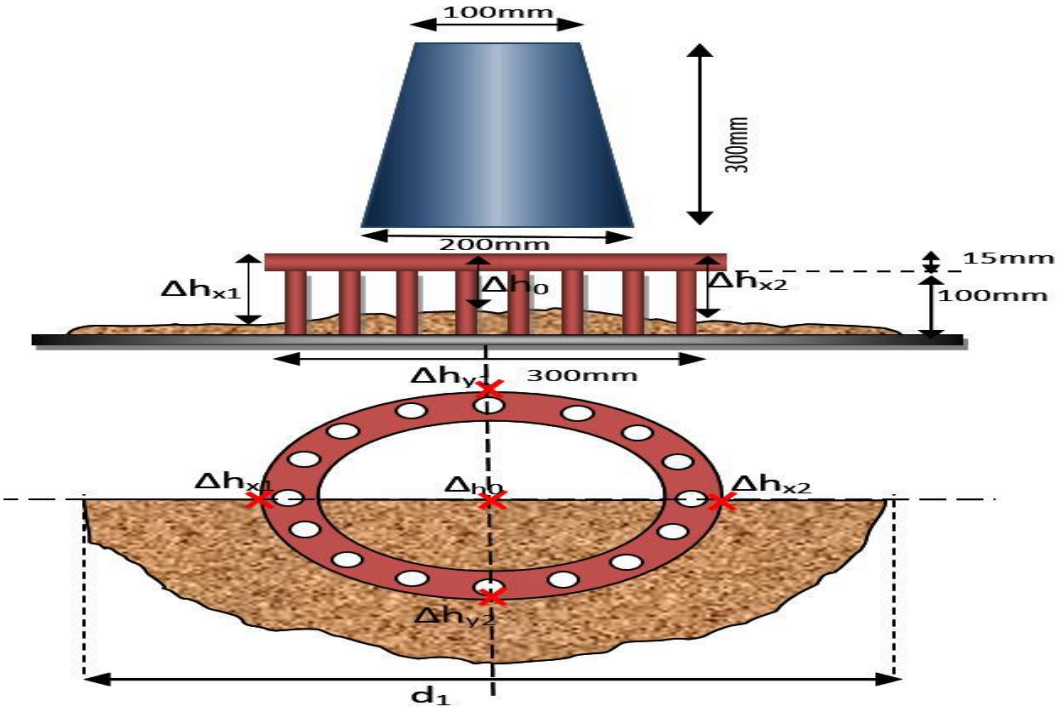

Figure 2-3 J-ring apparatus ((Alyhya, 2016)

2.6.7.3 L- Box and test

The L-box test evaluates the passing ability of SCC in a confined space. The L-box is composed of a long rectangular trough with a vertical column/hopper at one end. The dimensions of apparatus are shown in **Figure 2.4**. A gate is fitted to the base of the column allowing concrete discharges into the horizontal trough. The heights of the concrete at the two ends of the box (H1 and H2) can be measured to evaluate the passing ability. The ratio of H1 to H2 is called the blocking ratio. If the SCC has perfect fresh properties, the blocking ratio is equal to 1. Conversely, the blocking ratio is equal to 0 if the concrete is too stiff or segregated. The blocking ratio is useful for SCC applications involving complex shapes, and congested reinforcement. Also the flow speed can be measured by the time taken to reach a distance of 200 mm (T200) or 400 mm (T400) from the gate. L-boxes of different sizes with different reinforcing bars and gaps were used (Bui et al., 2002, Petersson, 2003). Investigations have

shown that the L-box was sensitive to blocking and that it was more difficult for concrete to pass three rather than two bars (Sedran and De Larrard, 1999).

The test depends on the operator, for example, in regard to the lifting speed of the gate (Nguyen et al., 2006), if the gate was lifted slowly and there was no segregation, the final shape of the concrete was determined by yield stress and there were correlations between the blocking ratio and the ratio of yield stress to specific gravity, the difference between two results with and without steel bars were small which can be used to detect dynamic segregation.

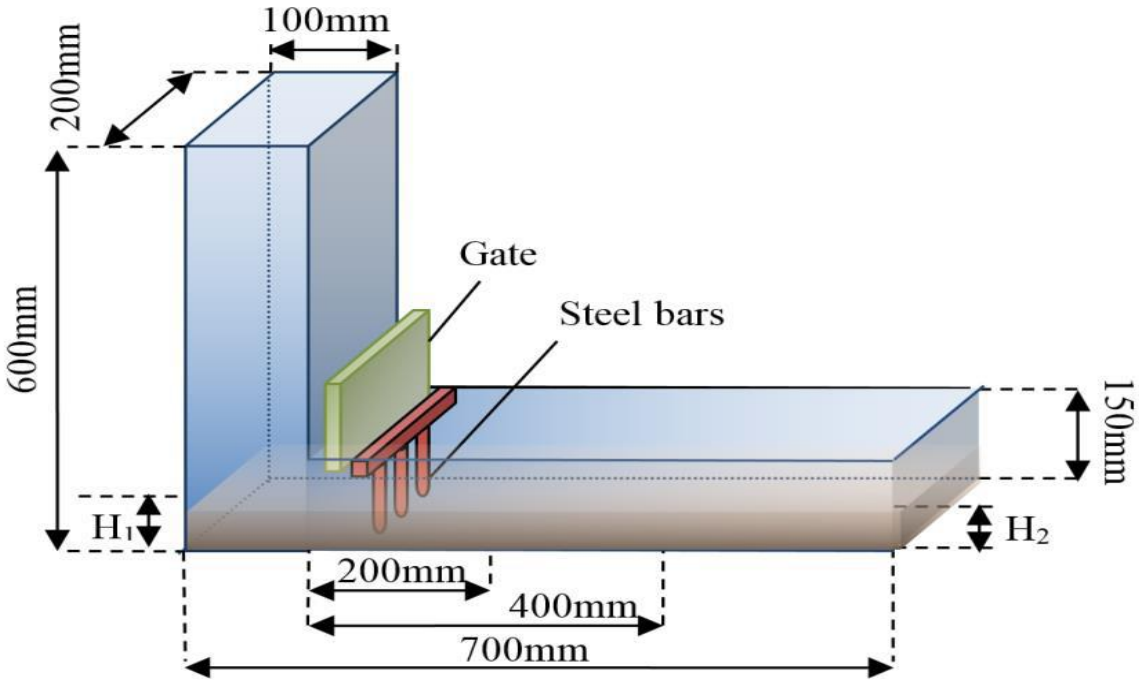

Figure 2-4 L-Box apparatus (Alyhya, 2016)

2.6.7.4 Sieve segregation resistance test

The sieve segregation resistance test is used to assess the resistance of SCC to segregation, which measures the amount of grains passing through a 5 mm sieve after a standard period. It is used to measure the degree of separation of the coarse aggregates and mortar fractions. In this test, 10 litres of fresh SCC are placed into a test container and allowed to settle over a 15 minute

period. The coarse aggregate settles at the bottom and the upper part of the concrete in the container is then wet sieved and the volume of mortar calculated. The more mortar passing through the sieve, the higher segregation index, which indicates the higher risks of segregation in concrete after placing.

2.6.7.5 V- Funnel test

The V-funnel test is performed by measuring the time for the concrete to flow out of the funnel under its own weight. This test is used to evaluate deformation velocity, which is affected by the passing ability and segregation resistance of concrete. The dimensions of the V –funnel apparatus are shown in **Figure 2.5**. A long V-funnel time can relate to either a low deformation capacity due to high inter-particle friction, or blockage of the flow. For example, a concrete with a high slump flow value and a long V-funnel time may indicate that the concrete is segregated and blockage may happen in the outlet gate of the V-funnel. As a result, the V-funnel time is related to plastic viscosity provided there is no segregation and blockage. However, Reinhardt and Wüstholz (2006) demonstrated that the T500 measurement was a better indicator of plastic viscosity than V-funnel time because the V-funnel test was influenced by blockage.

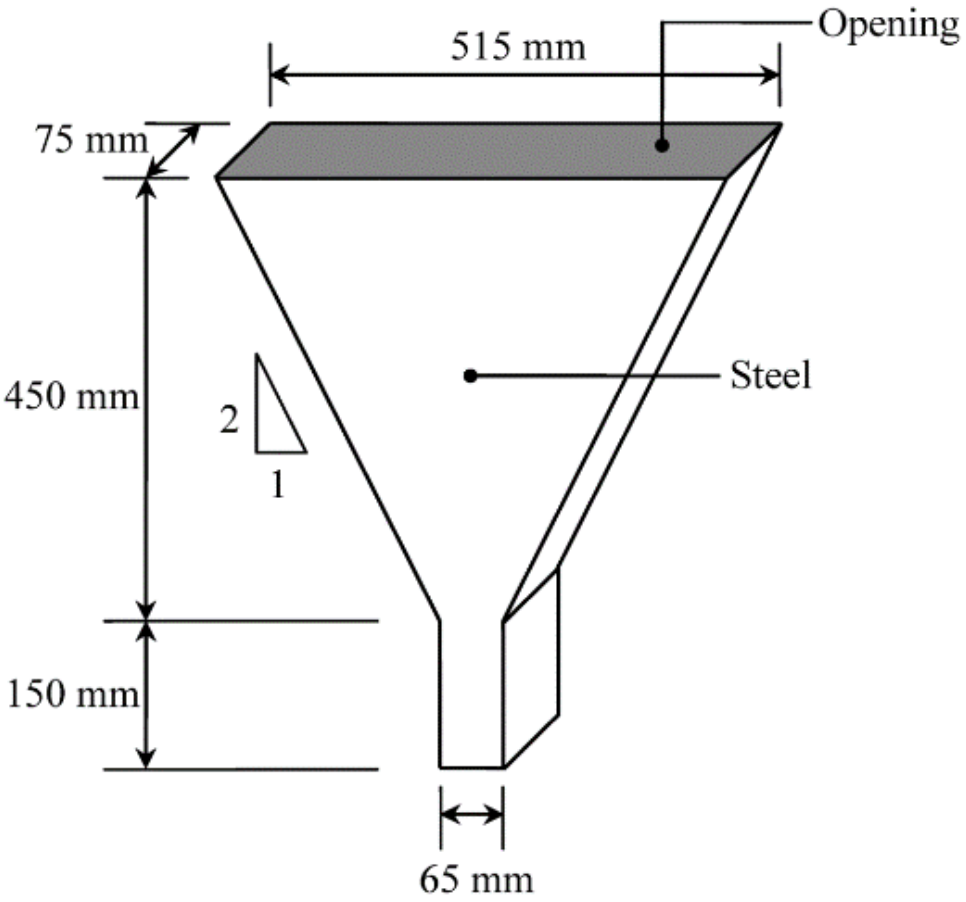

Figure 2-5 V-funnel apparatus (Alyhya, 2016)

2.7 Mix Design Principles for SCC

There are no methods or standard specifications for SCC mix design as known for NC such as ACI or BS methods. Many methods have been developed by different academic institutions and researchers for their purpose with specific limitations and specifications. Selection of SCC proportions requires careful consideration to maintain a proper balance between the requirements of achieved fresh and hardened properties of concrete. Some of the SCC mix design approaches will be briefly described in the following subsections.

2.7.1 Ozawa's approach

This method was proposed by Ozawa (1990) then it was modified by Okamura and Ozawa (1995). The general-purpose of this method is the percentage of coarse aggregate and fine aggregate, which can be determined by 50% and 40% by volume for coarse and fine aggregates, respectively and water to binder ratio (w/b) less than 0.3 with 10% air content and SPs dosage is obtained depending on workability tests of SCC (Skarendahl and Petersson, 2000). However, this approach is suitable only for low w/p ratio and it results in high mortar content which increases the cost of SCC (Su et al., 2001, Su and Miao, 2003).

2.7.2 CBI's approach

The Swedish Cement and Concrete Research Institute together with group of researchers in Thailand (CBI) have developed a SCC mix design approach which is based on the relation between the coarse aggregate content and the paste volume to calculate blocking volume ratio depending on the space between reinforcement. This method mainly considered coarse aggregate and paste volume only, neglecting the fine aggregate, which is one of the main factors effecting the segregation resistance property of SCC (Su et al., 2001, Petersson et al., 2014).

2.7.3 LCPC's approach

The French method of SCC proportions has proposed by Sedran and De Larrard (1999) in Laboratories Central des Pons et Chaussees (LCPC). It is based on the content of binders and the rheological tests of fresh concrete to find the relationship between the packing density with and without vibration,

then software program was run to obtain the SCC proportions. Number of trail mixes should be carried out to select the water content. However, it is not easy to carry out the LCPC approach without purchasing software (de Larrard and Sedran, 2002). Additionally, there are limitations of workability tests that should be considered when following this method such as slump flow and plastic viscosity (Su et al., 2001, Chai, 1998).

2.7.4 Hwang's approach

Another mix design method is Hwang's method which has been widely used in Taiwan. It depends on a densified mixture design algorithm which designs the mix into two parts including aggregate, fly ash and GGBS in the first part and water, cement and superplasticizer in the other part (Su et al., 2001, Chai, 1998, Hwang and Hung, 2005). However, this method was proposed by using a maximum size of coarse aggregate of 20 mm, although the maximum aggregate size suggested for use in SCC is 10mm. In addition, FA and GGBS were added in this approach as a ratio of aggregate instead of cement which is different from NC (Chai, 1998).

2.7.5 Ghazi's approach

All previous methods gave only general guidelines for the proportioning of SCC, with an emphasis on the fresh properties of SCC rather than concrete strength, and this method developed a mixture proportioning approach for designing SCC mixtures with particular reference to compressive strength and taking into consideration the effect of the grading of fine and coarse aggregate. The compressive strength range was expanded to cover 15 to 75 MPa and the maximum cement content was limited to 557 kg/m^3. The maximum weight of

water and air content in the mixture were obtained according to the maximum coarse aggregate size (MAS). The coarse aggregate content depended on the MAS and fine aggregate fineness modulus (Ghazi and Al Jadiri, 2010). It is easy to follow and apply this approach which can be used to design concrete that achieves a particular compressive strength and simultaneously meets the fresh concrete requirements of SCC.

2.7.6 A simple mix design method

Another mix design approach for self-compacting concrete (SCC) was proposed by Su et al. (2001) based on lowering the amount of cement. First, the amount of aggregate required was determined depending on the unit volume mass and packing factor of aggregate (PF). A PF value between 1.12 and 1.16 was recommended by Su et al. (2001) to meet the rank requirements of fresh properties specified. Then the cement content was selected according to the compressive strength required. After that, the w/c ratio was obtained according to previous studies and the amount of water can be determined based on the results. Finally, powder materials such as FA, GGBS and SPs can be set according to the weight and volume of concrete. This approach was applied with some modifications for all SCC mix design in this investigation. The procedures of this mix design are summarised in the following steps:

1- Calculation of coarse and fine aggregate

Coarse and fine aggregate content can be calculated from the following equations:

$$W_g = \text{PF} \times W_{gl} \left(1 - \frac{s}{a}\right) \quad 2.1$$

W_s = PF × W_{sl} ($\frac{S}{a}$) 2.2

where W_g is the amount of coarse aggregates (kg/m^3), W_s is the amount of fine aggregates (kg/m^3), W_{gl} is the unit volume mass of loosely piled coarse aggregates in air (kg/m^3), W_{sl} is the volume mass of loosely piled fine aggregates in air (kg/m^3), PF : packing factor, the ratio of mass of aggregates in a tightly packed state to that in a loosely packed state in air, $\frac{S}{a}$ is the volume ratio of fine to total aggregate.

2- Calculation of cement content

Cement content is calculated from the following equation:

C = $\frac{f'_c}{20}$ 2.3

where C is the amount of cement (kg/m^3) and f'_c is the compressive strength (psi).

3- Mixing water required by cement calculations

This is obtained from the following equation:

w_{wc} = ($\frac{W}{C}$) C 2.4

where w_{wc} is the amount of mixing water (kg/m^3) and $\frac{W}{C}$ is the water/cement ratio by weight.

4- Fly ash content (FA) and (GGBS) contents calculations

It is more complicated to calculate the amount of alternative materials, the volume of FA paste (V_{Pf}) and GGBS paste (V_{PB}) :

$$V_{\mathrm{Pf}} + V_{\mathrm{PB}} = 1 - \frac{W_g}{1000\times G_g} - \frac{W_s}{1000\times G_s} - \frac{C}{1000\times G_c} - \frac{W_{wc}}{1000\times G_w} - V_a \quad (2.5)$$

where $G_g$is coarse aggregates specific gravity, $G_s$is fine aggregates specific gravity, G_c is cement specific gravity, G_w is water specific gravity, V_a is the air content in SCC (%). If the total content of Pozzolanic materials (GGBS and FA) in SCC is W_{pm} (kg/m^3), where the FA percentage is A% and the GGBS percentage is B% by weight.

$$V_{\mathrm{Pf}} + V_{\mathrm{PB}} = \left(1 + \frac{W}{F}\right) \times A\% \times \frac{W_{pm}}{1000\times G_f} + \left(1 + \frac{W}{S}\right) \times B\% \times \frac{W_{pm}}{1000\times G_B} \quad (2.6)$$

where G_f,G_B, G_c, W/F and W/S are obtained from tests, A% and B% are given, and $V_{\mathrm{Pf}} + V_{\mathrm{PB}}$ can be obtained from Eq (2.5). Hence, W_{pm} can be calculated using Eq. (2.6). Also, W_f(FA content in SCC, Kg/m^3) and W_B (GGBS content in SCC, Kg/m^3) can be calculated from Equations below:

$$W_f = A\% \times W_{pm} \quad (2.7)$$

$$W_B = B\% \times W_{pm} \quad (2.8)$$

Mixing water contents required by FA paste and GGBS paste are calculated by equations below:

$$W_{wf} = \left(\frac{W}{F}\right) \times W_f \quad (2.9)$$

$$W_{wB} = \left(\frac{W}{S}\right) \times W_B \quad (2.10)$$

5- Calculation of mixing water content needed in SCC

The amount of mixing water is the total amount of water content needed for cement, FA and GGBS in mixing. Therefore, it can be obtained from the following equation:

$W_W = W_{wc} + W_{wf} + W_{wB}$ 2.11

6- SP dosage calculation

The dosage of SP can be obtained using Eqs (2.12 and 2.13) if the dosage of SP is equal to n% of the amount of binders and its solid content of SP is m%

SP dosage: W_{sp} = n% (C + W_f +W_B) 2.12

Amount of water in SP: W_{wsp} = (1- m %) W_{sp} 2.13

2.8 Hardened properties of SCC

The hardening properties of SCC are similar to normal concrete with regard to strength (Petersson and Billberg, 1999). The main difference between SCC and NC is that SCC has a lower coarse aggregate content with a small maximum coarse aggregate size and a higher powder content. SCC and NC could have similar hardened properties if they are made with similar raw materials and designed to achieve similar strengths (ACI237R, 2007). Moreover, the European guidelines for SCC stated that SCC and NC designed for similar strength should achieve comparable mechanical properties (BIBM and ERMCO, 2005). Some of these hardened properties are explained briefly in the following sections including compressive strength, elastic modulus, permeability, creep and shrinkage.

2.8.1 Compressive strength

The compressive strength is the most important characteristic of concrete. There is no difference in strength between SCC and normal concrete when the water powder ratio is similar. Domone (2007) and Sonebi and Bartos (2002) reported that compressive strength is affected more by the powder content

than by the w/p ratio. However, the European guidelines for SCC reported that compared with traditional vibrated concrete, SCC with a similar water cement or cement binder ratio usually has a slightly higher strength, due to an improved interface transition zone between the aggregate and hardened paste (BIBM and ERMCO, 2005).

2.8.2 Elastic modulus

The elastic modulus (E) is defined as the ratio between stress and strain. It is effected by the type and amount of aggregate, a high E value of aggregate will increase the elastic modulus of concrete. The elastic modulus of SCC is lower than the elastic modulus of NC, due to the high paste volume of SCC (BIBM and ERMCO, 2005). Parra et al. (2011) and Turcry et al. (2002) confirmed that the modulus of elasticity of SCC is normally 2% lower than that of traditional vibrated concrete. However, Skarendahl and Petersson (2000) reported that for similar compressive strength, there is no clear difference in the modulus of elasticity between SCC and traditional vibrated concrete. Moreover, also Schindler et al. (2007) reported that E values obtained for the SCC mixtures are in reasonable agreement with the elastic stiffness assumed during the design of conventional concrete structures. E values of SCC and NC made with the same low powder content (less than 400 kg/m^3) are similar (Mörtsell and Rodum, 2001).

2.8.3 Permeability

Permeability is defined as the ease with which fluids, both liquids and gases can enter into or move through the concrete. The ease with which air or other gases penetrate the concrete is related to the water permeability and therefore

the durability of concrete. Permeability is mainly affected by moisture in the concrete, cementitious materials, extent of curing and moisture of the concrete (Neville, 1998, Hoseini et al., 2009). Schonlin and Hilsorf (1988) concluded that concrete made with a higher w/c ratio shows a higher permeability for the same duration of curing and the same curing temperature. The porosity of SCC is lower than that of NC of the same compressive strength, due to the higher content of powder and lower water content (Zhu et al., 2004, Tragardh, 1999).

2.8.4 Creep

Creep is defined as the continued deformation of concrete with time for a constant applied stress. Creep takes place in the cement paste and it is influenced by its porosity, water/binder ratio, cement type and aggregate volume. When the porosity of the cement paste reduces, creep reduces while strength increases. As the aggregates restrain the creep of the cement paste, the higher the volume of aggregate the lower the creep will be. (BIBM and ERMCO, 2005). SCC shows a greater initial elastic deformation, but the permanent strain induced by creep in SCC is lower compared to normal concrete, Raghavan et al. (2002) reported that the rate of creep was reduced by 33% for normal concrete and 50% for SCC between 7 and 28 days.

2.8.5 Shrinkage

Shrinkage of concrete is the contraction due to the loss of the gel water caused by evaporation or by hydration of cement, and also by carbonation (Neville and Brooks, 1987). Usually there are four stages that occur in the shrinkage of concrete, and they are: plastic, autogenous, drying and carbonation shrinkage. Shrinkage results in cracks and these cracks cause a weakness in

the concrete. Neville (1998) concluded that concretes with a higher paste volume and a lower aggregate volume exhibit greater shrinkage deformations.

2.8.5.1 Plastic shrinkage

This type of shrinkage takes place while the cement paste is plastic (before it has set); it undergoes a volumetric contraction whose magnitude is of the order of 1% of the absolute volume of dry cement. The shrinkage induces tensile stresses in the surface layers because they are restrained by the non-shrinkage inner concrete, and, since the concrete is very weak in its plastic state, plastic cracking at the surfaces occurs, which can extend quite deeply into concrete (Neville and Brooks, 1987, Dhir and Jackson, 1996).

The main factors that influence the plastic shrinkage are: w/c ratio, and size of coarse aggregate and consistency of the mix. Plastic shrinkage cracks may form in a random manner or be roughly parallel to each other. The cracks are often almost straight, ranging in length from 25 mm to 2 m but are usually 300 to 600 mm long. They can be up to 3 mm wide at the surface but usually taper quickly over their depth but may penetrate right through a concrete element. These cracks form a weakness in the concrete and will be widened and/or extended by subsequent drying shrinkage and thermal movement (Almusallam et al., 1998).

Turcry and Loukili (2003) measured free plastic shrinkage of SCC and NC by a device using laser sensors for the same evaporation rate, they reported that the plastic shrinkage amount of SCC was found to be at least two times higher compared to that of NC as shown in **Figure 2.6**. The plastic shrinkage of SCC reduced at early age using SRA by 25% for a w/c ratio of 0.43 (Saliba et al.,

2011). Initial plastic shrinkage can be reduced by moist-curing products. Providing a continuous water source to the concrete as it cures will help to fill the capillary pores and the hydration reaction continues to take place (Gambhir, 2013).

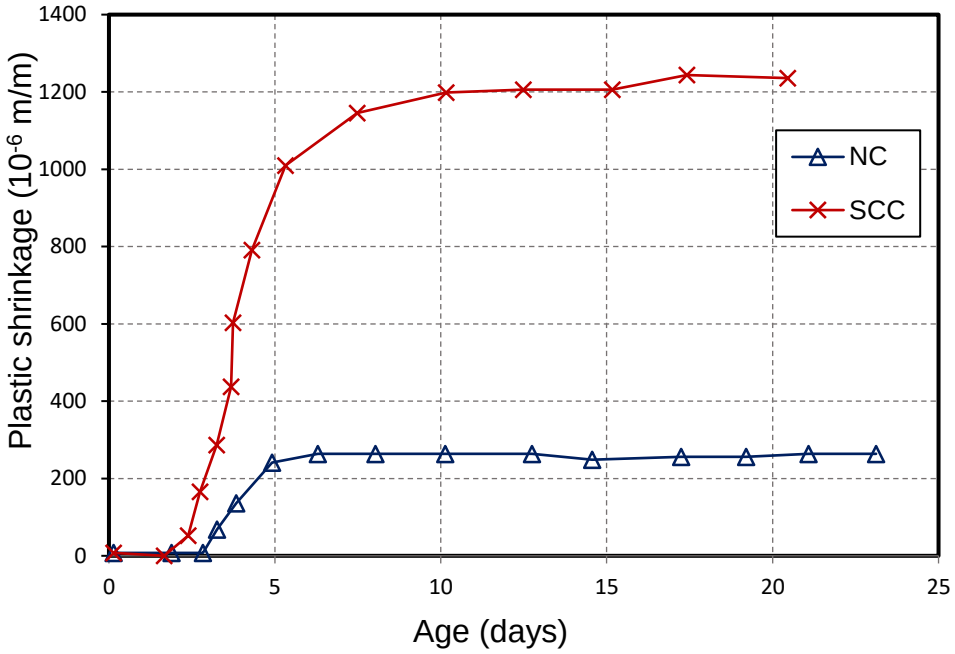

Figure 2-6 Plastic shrinkage of SCC versus normal concrete (NC) mixes (Turcry et al., 2002)

2.8.5.2 Autogenous Shrinkage

This is caused by loss of water used up in hydration, in normal strength concrete, autogenous shrinkage is very small, typically 50 to 100 $\times 10^{-6}$ (μstrain), but it can be large in high performance concrete. The factors that influence the rate and magnitude of autogenous shrinkage are: chemical composition of cement, the initial water content, temperature, and time (Neville and Brooks, 1987, Dhir and Jackson, 1996). Autogenous shrinkage tends to increase at higher temperatures, with higher cement content, and possibly with finer cements, and with cements which have a high C3A and C4AF content. At a constant content of blended cement, a higher content of fly ash leads to

lower, autogenous shrinkage. At very low water/cement ratios (below 0.40), autogenous shrinkage is very high (Neville, 1998). Autogenous shrinkage occurs in cement-based materials with a w/c-ratio lower. Alrifai et al. (2013) studied the evolution of the autogenous shrinkage of SCC for W/C ratios varying between 0.47 and 0.67 and they concluded that the autogenous shrinkage is clearly observed at low W/C ratios. The addition of fine powders can have an important role in the autogenous shrinkage process.

2.8.5.3 Carbonation Shrinkage

The carbon dioxide (CO_2) present in atmosphere reacts in the presence of moisture with the hydrated cement minerals, carbonating $Ca(OH)_2$ to $CaCO_3$. The carbonation slowly penetrates beyond the exposed surface of concrete. The shrinkage due to carbonation occurs mainly at intermediate humidity (Gambhir, 2004). The actual rate of carbonation depends on the permeability of the concrete, its moisture content, and on the CO_2 content and relative humidity of the ambient medium. Carbonation neutralizes the alkaline nature of the hydrated cement paste and thus the protection of steel from corrosion is vitiated. Consequently, if the full depth of cover to reinforcement is carbonated and moisture and oxygen can ingress, corrosion of steel and possibly cracking will result (Neville, 1998). Poor-quality concrete suffers carbonation earlier and deeper than good-quality dense concrete (Dhir and Jackson, 1996). The extent of carbonation can be determined by treating a freshly broken surface with phenolphthalein - the free Ca $(OH)_2$ is coloured pink while the carbonated portion is uncoloured (Neville and Brooks, 1987).

2.8.5.4 Drying Shrinkage Strains

Drying shrinkage occurs over time as pore water that is not consumed in the hydration reaction evaporates, resulting in internal strain causing the concrete to shrink. About 14 to 34% and 40 to 80% of 20-year shrinkage occurs within the first 2 weeks and the first 3 months, respectively (Neville and Brooks, 1987). At the end of one year, the rate of shrinkage drops down to nearly one-half the initial value, concrete that is stored in 100% relative humidity does not shrink; instead, it swells (Somayaji, 2001). Drying shrinkage cracks in large sections are induced by tensile stresses because of the internal restraint caused by differential shrinkage between the surface and the interior of the concrete (Neville, 1998). It causes different kinds of construction building cracks which affect the long term serviceability and durability of concrete.

2.8.5.4.1 Factors affecting drying shrinkage behaviour of SCC

The rate and amount of drying shrinkage strain is influenced by various factors. The most important factors are mixture composition, curing conditions, ambient exposure conditions, and element geometry. Some of concrete composition such as; aggregate, cement type and content, water cement ratio as well as cement replacement will be explained briefly in the following sections.

2.8.5.4.1.1 Effect of water-binder ratio on drying shrinkage

The general idea when assessing drying shrinkage is that concrete with a high w/b ratio will have a higher drying shrinkage because there is more unbound water (Holt and Leivo, 2004). These findings are supported by Burlion et al. (2005), who used various w/c ratios (0.25-0.60) and indicated that as the w/c ratio decreases from 0.60 down to 0.25, the magnitude of drying shrinkage

decreases. Moreover, Bissonnette et al. (1999) reported that the reduction of the W/C ratio from 0.50 to 0.35 resulted in a slightly lower shrinkage.

2.8.5.4.1.2 Effect of aggregate on drying shrinkage

The aggregates which have low elastic modulus and exhibit moisture movement themselves (many natural crushed rock and gravel aggregates undergo changes of volume to a greater or lesser extent, as they take up or lose water) can cause large shrinkage. Concrete using sandstone may shrink as much as one using limestone. Drying shrinkage increases as maximum size of aggregate decreases (Mindess et al., 2003). However, maximum aggregate size and grading of the aggregate do not influence the magnitude of concrete with a given volume of aggregate and a given water-cement ratio, the maximum size affect the voids volume and aggregate content of similar strength concrete mixtures, therefore, larger aggregate allows more aggregate content and leads to lower shrinkage (Gambhir, 2004). The use of aggregates with high stiffness and low shrinkage decreases drying shrinkage (BIBM and ERMCO, 2005). SCC can exhibit higher shrinkage compared with NC due to its great volume of cement paste and low coarse aggregate content as well as small maximum aggregate size.

2.8.5.4.1.3 Effect of cement content and type on drying shrinkage

Normally high fines and cement content and a higher paste volume are used in making SCC than in making NC. The higher the paste content the greater the drying shrinkage and the total shrinkage of SCC is increased due to its higher volume of paste (Rozière et al., 2007). However, shrinkage may not affected much by the cement content if the water content per unit volume is constant. The types of cement also have different influences on the shrinkage,

the rapid-hardening cement shrinks somewhat more than the others. Effect of mineral admixture on drying shrinkage.

The use of a higher content of paste, powder and superplasticiser in SCC all may contribute to higher shrinkage and creep than in NC. However, the replacement of cement with fly ash, limestone filler, or slag may reduce drying shrinkage (Loser and Leemann, 2009, Poppe and De Schutter, 2005, Khatib, 2008, Gesoğlu et al., 2009), while some researchers consider that the limestone fines content has no significant effect and the addition of silica fume is reported to increase shrinkage (Gesoğlu et al., 2009). On the other hand, Bouzoubaâ and Lachemi (2001) studied the effect of high volumes of fly ash on the drying shrinkage of self-compacting concretes and they stated that no difference was noticed between drying shrinkage of SCC without fly ash and SCC with fly ash.

2.8.5.4.2 Measurement of Drying Shrinkage strain

Several test methods have been developed to assess the free drying shrinkage strain of concrete mixtures. Length change of hardened hydraulic cement mortar and concrete according to ASTM/C157 (2008) is a popular method used to evaluate free shrinkage of concrete. This test method covers the determination of the length changes that are produced by causes other than externally applied forces and temperature changes in hardened concrete. This approach have been applied by many researchers (Güneyisi et al., 2010, Hwang and Khayat, 2010, Khatib, 2008, Gao et al., 2012, Bouzoubaâ and Lachemi, 2001, Turcry et al., 2006). Test set up is explained in detail in chapter 3. Drying shrinkage strain could be also determined by the mass loss due to water evaporation (Gao et al., 2012).

2.9 Confined drying shrinkage of concrete

Instead of traditional reinforced concrete columns, concrete filled steel tubes (CFT) have been used as columns for construction buildings. Many composite column sections shapes such as circular, rectangular and square have been used in building design. However, elliptical hollow sections have been recently introduced to the construction market and are becoming more popular contemporary building design due to their pleasing appearance.

In the case of CFT filled with self-compacting concrete confined drying shrinkage strain may occur and it might cause a gap to form between the concrete and steel tube which could affect their composite action. As Roeder et al. (1999) reported, the bond transfer between the steel tube and the concrete infill depends on radial displacements due to the confined drying shrinkage. None of the previous researchers have examined confined drying shrinkage of NC or SCC. Thus, as part of this investigation, the behaviour and magnitude of confined drying shrinkage of SCC compared to NC will be highlighted.

2.10 Experimental investigations on drying shrinkage strain of SCC

SCC mixtures are usually designed with high volumes of paste, large quantities of mineral fillers such as finely crushed limestone or fly ash and high range water reducing admixtures and the maximum size of the coarse aggregate is smaller. All of those special characteristics of SCC may have a significant influence on its shrinkage behaviour. Drying shrinkage strain (DS) is considered as a major concern for concrete deterioration, it produces tensile stress within concrete leading to cracking, which enables harmful materials to

penetrate the concrete, affecting long term concrete durability. Some discrepancy remains regarding the drying shrinkage strains of SCC (DSSCC) compared to drying shrinkage of normal concrete (DSNC). For example, Kim et al. (1998), Rols et al. (1999), Chan et al. (2003), Klug and Holschemacher (2003), Chopin et al. (2003), Turcry and Loukili (2003), Heirman and Vandewalle (2003), Turcry et al. (2006), Loser and Leemann (2009), Valcuende et al. (2012) and Bhirud and Sangle (2017) pointed out that SCC can exhibit higher shrinkage compared with NC. However, other investigators such as Persson (2001), Bouzoubaa and Lachemi (2001), Pons et al. (2003), Vieira and Bettencourt (2003), Poppe and De Schutter (2005), Seng and Shima (2005), Collepardi et al. (2005), Pierard et al. (2005) and Assié et al. (2007) concluded that the shrinkage strains of SCC are equivalent to those of NC with similar compressive resistance, and in some cases it was even found that the shrinkage of SCC was lower than NC (Proust and Pons, 2001, Heirman et al., 2007, Huynh et al., 2018). The discrepancy between the experimental results of DSCC and DSNC could be related to the differences in concrete mixtures studied, testing conditions, and testing methods (Fernandez-Gomez and Landsberger, 2007). Moreover, most of the previous studies took into account only DS that was determined after a specific time of curing or immediately after demoulding, while other researchers considered DS that started from the setting time, including autogenous shrinkage. In this investigation, in order to compare between DSSCC and DSNC magnitude the environmental conditions (relative humidity, temperature and curing type) and concrete condition (casting and testing) were kept same for SCCs and NCs

and the measurements of drying shrinkage strain were taken immediately after demoulding.

2.11 Prediction of concrete shrinkage

There are many empirical models associated with the accuracy of shrinkage strains prediction of concrete. According to a review of the literature for these types of prediction models the most widely discussed and used models are American Concrete Institute Committee (ACI 209R-92) model (ACI Committee 209, 1992), the Eurocode (BS EN- 92) model (Eurocode2, 2004), the model modified by Huo et al. (2001) (ACI 209R-92 (Huo)) model, the model developed by Bazant and Baweja (2000) (B3 model) and GL2000 model proposed by Gardner (2004). In addition, there are many other models and proposed models that are in use. However, it appears that all of these models are compared to at least one of the two models mentioned above. Moreover, artificial neural networks (ANNs) have been widely utilized in many applications of civil engineering to model and estimate concrete properties. ANN model was used by Bal and Buyle-Bodin (2013) to predict the drying shrinkage of NC and he reported that ANN model describes correctly the evolution with time of drying shrinkage. None of previous studies developed ANN model to predicted drying shrinkage of SCC. More details about the existing models and ANN model to predict drying shrinkage of SCC has been presented in chapters five and six.

2.12 Concluding Remarks

SCC has been successfully used in wide areas such as buildings, bridges, marine structures and tunnels. The use of SCC has many advantages

including reduce the need for skilled labour during construction and shortening concrete placing time. Moreover, it provides a calm construction environment, and it can promote innovations in the construction system. However, it needs a high standard of quality control for its production and formwork for SCC may also need to be strengthened, as well as the high cost of the admixtures used. The standard tests for normal concrete are not adequate for SCC, several mix design methods have been proposed and some are still under development. Each has its distinguishing features and advantages. The choice of method should depend on the mix purpose and experience of the mix design method.

The main fresh properties needed to achieve good mix design are; high deformability, good segregation resistance and a non-blocking property (passing ability). Almost any material that is suitable for normal concrete can be used for SCC. The influence of cement replacement materials (GGBS, FA and SF) on the characteristics of SCC was discussed with an emphasis on the fresh state of SCC. It was concluded that CRMs enhance self-compacting ability, fluidity, cohesiveness and segregation resistance. Moreover, effect of chemical admixtures (HRWRA, VMA, SRA and AEA) on SCC properties also were reviewed.

In general SCC has the same level of hardened properties and better durability compared to normal concrete of the same strength. However, there are unresolved arguments when considering some hardened properties such as drying shrinkage strain magnitudes of SCC compared to NC. Moreover, none of these studies were conducted on confined drying shrinkage of SCC and NC. Therefore, in this investigation experimental work will be designed to cover the

effect of key parameters effecting on free and confined drying shrinkage strain of SCC and NC.

According to a review of the literature for prediction of shrinkage of SCC, several researchers have studied and developed models to predict shrinkage of SCC. None of the previous researchers developed an ANN model to improve the accuracy of the shrinkage strain prediction of concrete. Thus, the aim of the analytical work of this research is to develop an ANN model using collected data from different experimental investigations available in the literature together with experimental results obtained from this investigation to predict drying shrinkage of SCC. In addition, the results obtained by the ANN model will be compared with the results obtained by some existing predicted models reviewed in the chapter.

CHAPTER THREE- MATERIALS AND EXPERIMENTAL PROCEDURE

3.1 Introduction

This chapter presents the experimental program and methodology and the constituent material properties that were used in this study. The mix design approaches for the study have been selected according to pilot work. A series of experiments, including fresh properties such as; slump, slump flow, J-ring, V-funnel and segregation resistance have been conducted. Hardened properties such as; compressive strength, flexural strength, water absorption, concrete density have been examined. Free and confined drying shrinkage strain measurements are also carried out over the long term as a part of this chapter.

3.2 Materials

The materials used in various experiments are given below.

Cement: Ordinary Portland cement (OPC), CEM I 52.5N complying with EN 197-1:2011 was used for all of the experimental work in this study. Physical properties and chemical compositions of the cement as provided by the supplier are given in **Table 3.1.**

Fly ash: Fly ash BS EN 450 -1, fineness category S, loss on ignition category B, grey colour was used as a partial replacement of Portland cement. Physical properties and chemical compositions of the fly ash as provided by the supplier are presented in **Table 3.1**.

Admixtures: A high range water reducing admixture (HRWRA) superplasticizer (SP) complying with BS EN 934-2:2001 was employed to achieve a suitable workability for SCC mixes. A shrinkage reducing admixture (SRA 895) was used to reduce significantly the drying shrinkage strains of SCCs. Physical and chemical properties of SP and SRA provided by the supplier are given in **Table 3.2.**

Table 3-1 Physical properties and chemical compositions of cement and fly

Cement replacement materials	Cement (CEMI 52.5 N)	Fly ash (450-S)
Physical properties		
Specific gravity	3.15	2.15
Blaine specific surface area, m^3/kg	400	461
28 days Compressive strength, (MPa)	60.0	-
Initial setting time (Mins)	150	-
Soundness, expansion (mm)	1	< 0.1
Chemical composition, %		
S_iO_2	20.10	51
AL_2O_3	5.04	29
Fe_2O_3	2.28	7.6
C_aO	36.24	2.5
M_gO	2.50	1.5
SO_3	3.39	0.9
K_2O	0.62	2.36
$N_{a2}O$	0.28	-
CI	0.05	< 0.05
LOI	2.87	1.6

Table 3-2 Physical and chemical properties of SP and SRA

Properties	Superplasticizer (SP)	Shrinkage reducing admixture (SRA)
Name	Glenimum C315	MasterLife SRA 895
Form	Liquid	liquid
Colour	Yellowish	colorless
pH value	5 – 8	-
Specific gravity	1.10 ± 0.03	1.01 ± 0.02
Dosage range	0.10-1.10% of binder content	0.50-2.0 % of binder content

Aggregates: All SCC and NC concrete mixtures were prepared with a crushed coarse limestone aggregate (C_{agg}) with a maximum size of 10 mm and a local natural sand (F_{agg}) with a maximum aggregate size of 4.75 mm. For each aggregate, the relative density on saturated dry basis and dry, water absorption (% of dry mass), and apparent specific gravity were determined in accordance with (ASTM/C127, 2015) and bulk density of aggregates were measured in accordance with (ASTM/C29/C29M, 2009). The determination of the percentage of evaporable moisture in a sample of aggregates were tested according to (ASTM/C566, 2013). All materials were collected and stored in the laboratory to ensure their constant absorption characteristics and keep the same environmental conditions throughout the test program. Results obtained of physical properties of the aggregates are summarized in **Table 3.3**. The particle size distributions of coarse and fine aggregates were within the limits set by (ASTM/C33M, 2013) Grading of the aggregates with the ASTM limits are plotted in **Figure 3.1**.

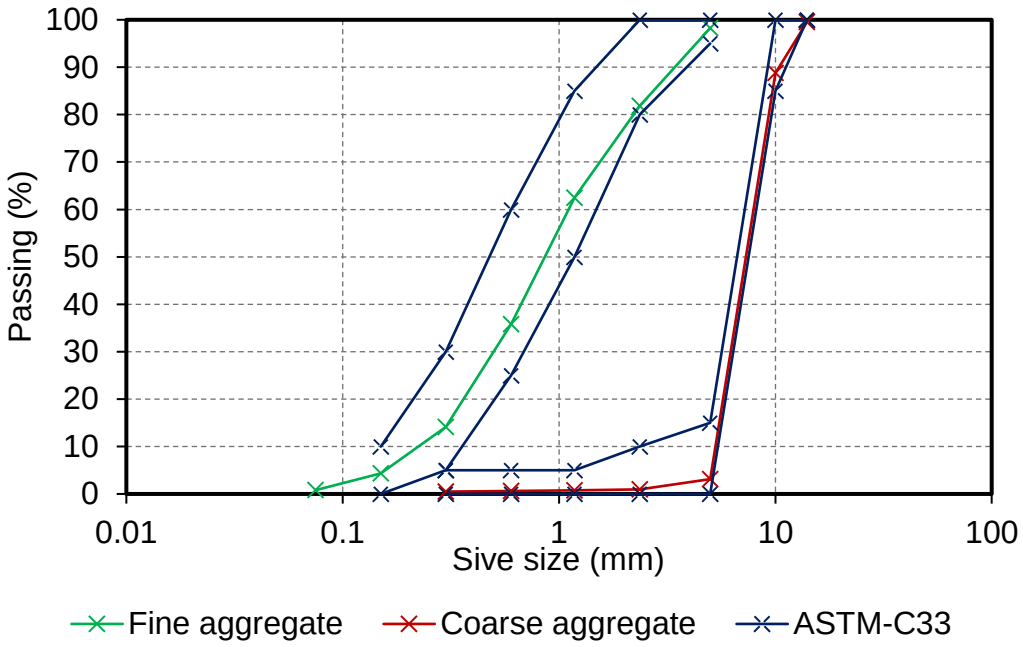

Figure 3-1 Grading of coarse and fine aggregates

Table 3-3 Physical properties of coarse and fine aggregates

Property of aggregate	Coarse aggregate	Fine aggregate
Relative density (SSD)	2.55	2.51
Relative density (Dry)	2.58	2.54
Absorption (% of dry mass)	0.42	0.60
Apparent specific gravity	2.61	2.60
Water content (kg/m^3)	0.61	1.47
Bulk density (kg/m^3)	1500	1400
Fineness modulus	7.20	2.90

3.3 Mix design proportions

The mix design proportions can be broken down into two phases: a pilot study and a main mix design.

3.3.1 Pilot study

As mentioned early in this research, there is no standard method for SCC mix design and many academic institutions, admixture, ready-mixed, precast and contracting companies have developed their own mix proportioning methods. SCC is largely affected by the characteristics of materials and the mix proportions. The purpose of the pilot study was to evolve a procedure for mix design of SCC. Several trials for the mix design of NC and SCC were carried out in this research. For SCC mixes the simple mix design method of SCC proposed by Su et al. (2001) with some modification in the mix proportions was adapted. The weight-batching method according to the Building Research Establishment was also considered for NC mixes (Teychenné et al., 1975). A flow chart of the experimental trial mix program is illustrated in **Figure 3.2**. Mix proportions of the trial mixes are presented in **Appendix A (Table A.1)**. In addition, the results of this pilot work for acceptance characteristics for SCC such as slump flow, J-ring, V-funnel and segregation resistance are summarised in **Appendix A (Table A.2)** Furthermore, the strength characteristics in term of compressive strength at 7 and 28 days are presented as well in **Appendix A (Table A.2).**

3.3.2 Main mix design proportions

According to the results achieved from the pilot work in the previous section, a total of 8 SCCs mixtures were designed following the SCC mix design method proposed by Su et al. (2001) with some modification in the mix proportions. Two NCs mixtures chosen as control mixes, using the weight-batching method according to the Building Research Establishment, were also considered (Teychenné et al., 1975). All concrete mixtures were designed at two water-

binder ratios (w/b) of 0.44 and 0.33. The replacement ratio of fly ash (FA) for SCCs mixes were 20%, 40% and 60% by weight of the binder. For all SCC mixes the packing factor (PF), air content (A %) and volume ratio of fine aggregates to total aggregates were assumed to be equal to 1.16, 1.5 and 53%, respectively. Mixture proportions of the eight SCC (SCC-0.44, SCC-0.33, SCC-0.44-20, SCC-0.44-40, SCC-0.44-60, SCC-0.33-20, SCC-0.33-40 and SCC-0.33-60) and two NCs (NC-0.44 and NC-0.33) mixtures are summarized in **Table 3.4.**

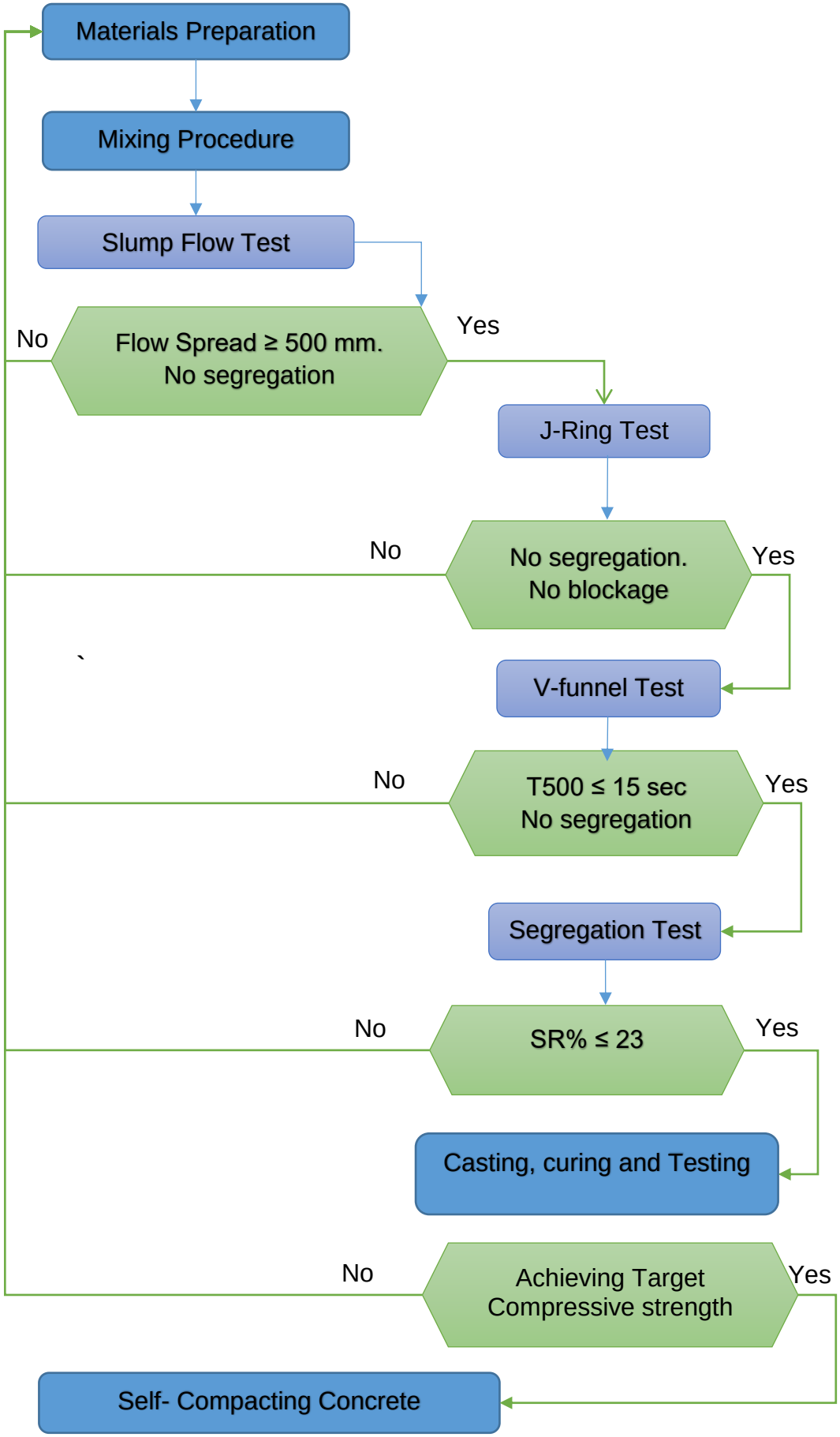

Figure 3-2 Trail mix design program flowchart

Table 3-4 Proportions of concrete mixtures per m3

Mix ID	W/B	B	C	FA	W	C_{agg}	F_{agg}	SP	SRA	A
	ratio				(Kg)				(%)	
NC-0.44	0.44	466	466	0	205	924	755	0	0	0
NC-0.33	0.33	622	622	0	205	883	640	0	0	0
SCC-0.44	0.44	450	450	0	198	780	890	1	0	1.5
SCC-0.33	0.33	550	550	0	180	780	890	1	0	1.5
SCC-0.44-20	0.44	450	360	90	198	780	890	1	1	1.5
SCC-0.33-20	0.33	550	440	110	180	780	890	1	1	1.5
SCC-0.44-40	0.44	450	270	180	198	780	890	1	1	1.5
SCC-0.33-40	0.33	550	330	220	180	780	890	1	1	1.5
SCC-0.44-60	0.44	450	180	270	198	780	890	1	1	1.5
SCC-0.33-60	0.33	550	220	330	180	780	890	1	1	1.5

W/B: Water to binder ratio, B: Binder content, C: Cement content, FA: Fly ash content,

W: Water content, C_{agg}: Course aggregates content, F_{agg}: Fine aggregates content,

SP: Superplasticizer, SRA: Shrinkage reducing admixture, A: Air content.

3.4 Mixing and specimens preparation

All concrete mixtures were prepared in 0.08 m^3 batches using a drum mixer. For SCC mixtures the ingredients were poured into the laboratory counter mixer in the following order; coarse aggregate (C_{agg}), fine aggregate (F_{agg}), cement (C), fly ash (FA), water mixed with admixtures (HRWRA and SRA); the same procedure is followed for the NC mixtures without fly ash and admixtures. This procedure was adopted for all of the mixes in order to minimize the risk of a possible disparity between the homogeneity of each mix. Dry ingredients (aggregates and binder (B)) were mixed for 3 minutes, then water (with HRWRA and SRA for SCC mixtures only) was gradually added in 15 seconds and the mixing continued for 3 minutes followed by a 2 minutes final mix. The top of the mixer was covered to prevent evaporation during the mix period in accordance with (ASTM/C192/C192M, 2015). For each concrete mixture, different sizes (cubes and prisms) of concrete specimens were prepared and cast in steel moulds for testing water absorption, density, compressive strength, flexural strength and drying shrinkage strains. All of the specimens (cubes and prisms) were not subjected to any compaction other than their own self weights except for NC specimens. After casting, the specimens were kept covered in a controlled chamber at 20±2^{0}C for 24 h until demoulding and then cured as presented in the following sections. Mixing, casting and curing of specimens are shown in **Figure 3.3**.

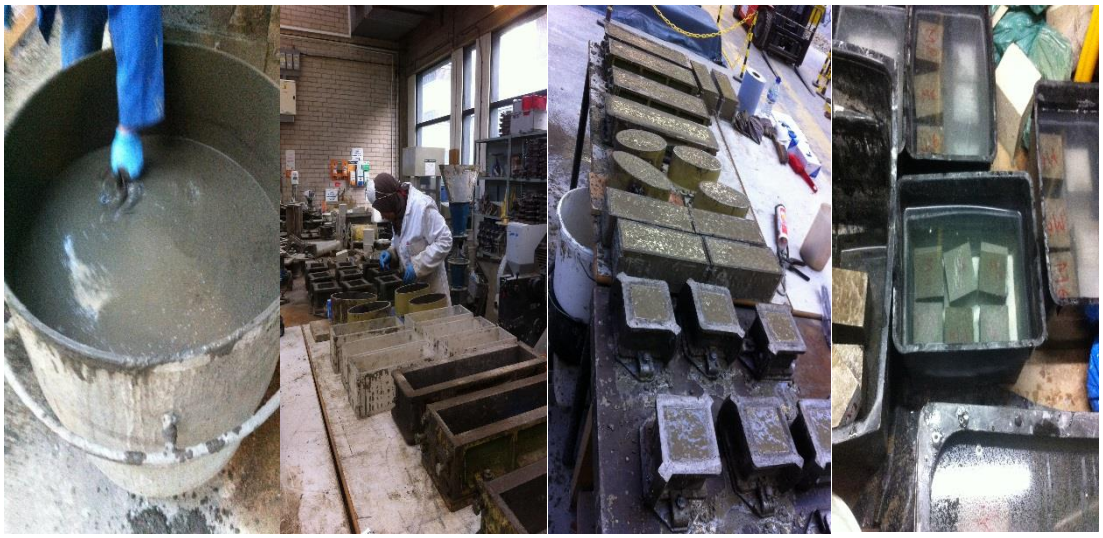

Figure 3-3 Mixing, preparing, casting and curing procedure.

3.4.1 Testing procedure

3.4.1.1 Fresh properties tests

In this section, tests on the fresh state of normal and self-compacting concretes are described. Self-compacting concrete is characterized by viscosity, filling ability, passing ability and resistance to segregation and it is important to keep these characteristics during transport and placing. For all fresh properties tests, concrete was dropped back into the mixer after testing and remixed for 1 minute before another test was taken to simulate the concrete slowly stirred in the drum mixer.

3.4.1.1.1 Filling ability and viscosity

The viscosity of SCC was evaluated using the slump flow test, the flow spread and T_{500} time representing horizontal free flow of the mass of concrete after release of a standard slump cone to a diameter of 500 mm. The assessment of SCC filling ability which represents the ability of fresh concrete to distort and flow under its own weight without vibration or extra assistance into the

formwork was measured using V-funnel test. **Figure 3.4** shows the horizontal spread of SCC mixes using flow slump test and v-funnel test.

Figure 3-4 Viscosity and filling ability of SCC mixes using (a) slump flow test (b) V-funnel test.

3.4.1.1.2 Passing ability

The passing ability of SCC determines how well the concrete can flow through confined and constricted spaces and narrow openings that exist between reinforcing bars in real reinforced concrete structural elements. For this purpose, a 300mm diameter J-ring apparatus with ten steel rods (each of diameter 16 mm and 100mm height) was used. The flowing and passing ability of the SCC mix are shown in **Figure 3.5.**

Figure 3-5 Passing ability of SCC mixes using J- ring test.

3.4.1.1.3 Segregation resistance

The sieve stability test (screen stability test) for segregation resistance was used to measure static segregation of SCCs and to remain the concrete homogeneous in composition while in its fresh state as shown in **Figure 3.6 (a)**. All SCC fresh properties were determined according to the European Guidelines for SCC (BIBM and ERMCO, 2005).

3.4.1.1.4 Slump test

To measure the workability of NC mixes, slump test accordance to (ASTM/C143/C143M, 2015) was used **(Figure 3.6 (b)**).

Figure 3-6 Sieve stability test (a) Slump test for NC mixes (b).

3.4.2 Mechanical properties tests

Compressive strength was measured by testing three cube specimens with 100×100×100 mm size in accordance with (BS-12390-3, 2009). The specimens were cast, left covered with a plastic sheet in a controlled room at 20± 2 ^{o}C for 24h until demoulding. Thereafter, the specimens were placed in water for curing until tested at 7, 28 and 91 days using the compressive strength testing machine as showed in **Figure 3.3 (a)** at a constant rate of 0.2 MPa/s with a maximum load capacity 3000-KN and the results were obtained as the average.

Flexural strength was measured by testing two prism specimens, 100×100×500 mm in size in accordance with (ASTM/C78/C78M, 2015). The test was performed using a testing machine **Figure 3.3 (b)** with a constant rate of 0.05MPa/s until fracture. The curing condition for prism specimens were the same as those for the compressive strength specimens.

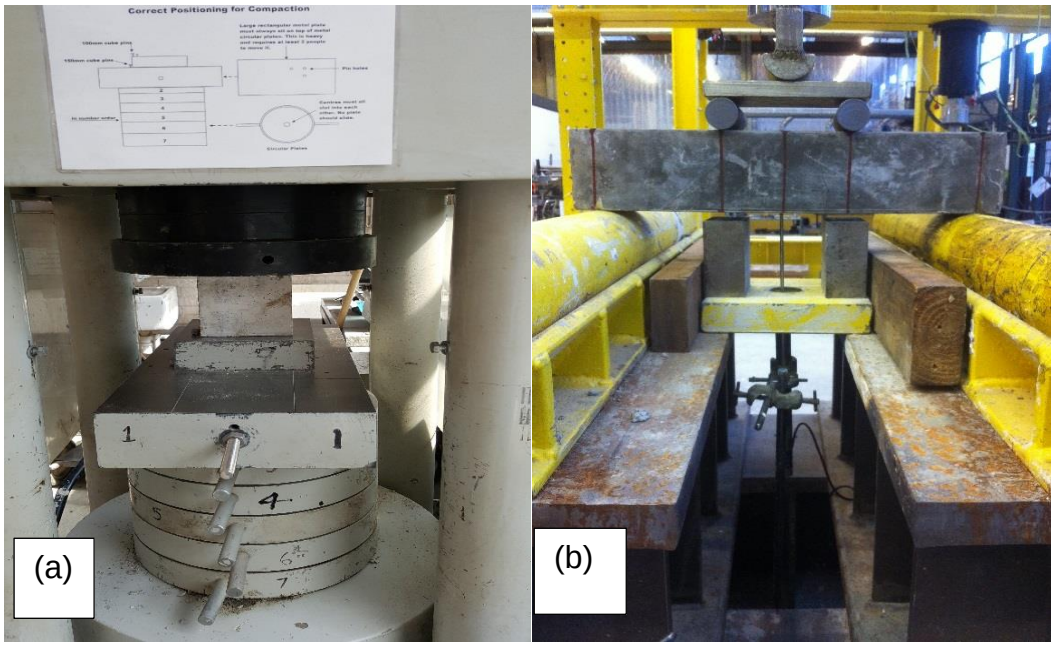

Figure 3-7 Photo of test set up of (a) compressive strength (b) flexural strength.

3.4.3 Water absorption and density tests

A water absorption test according to (BS1881-122, 1983) was used to determine the amount of water absorbed which indicates the degree of porosity of concrete materials. The concrete density was determined according to (BS1881-114, 1983). Specimens were placed in a dry oven at 100±5 °C for 24 h. After removing each specimen from the oven, it was allowed to cool in dry air to a temperature of 20 to 25°C and the average weight of the oven dry specimens (OD) was recorded (A). Immediately after drying and cooling, the specimens were completely immersed in water at 21°C for 24 h. The specimens then were turned to a saturated surface dry state (SSD) by removing water from the surface using a moist cloth. Then the average weight of the specimens was taken (B). The water absorption as a percentage was calculated as the ratio of water mass absorbed to that of the dry mass of the

specimen. The density of concrete was determined as the ratio of dry mass to the volume mass of the specimen and expressed as a percentage.

Water absorption was calculated using the formula below;

$$\text{Water absorption (\%)} = \frac{\mathbf{B-A}}{\mathbf{A}} * \mathbf{100} \quad (1)$$

Density of concrete was determined following the formulas below;

$$\text{Density}_{(OD)}\ (kg/m^3) = \frac{\mathbf{A}}{\mathbf{V}} \quad (2)$$

where **V** is the volume of the specimen.

3.4.4 Free and confined drying shrinkage strains tests

The determination of drying shrinkage strain was conducted on the prisms of 100×100×300 mm in size for free drying shrinkage strain measurements, and to evaluate confined drying shrinkage strain tests, Φ (240×113)×100 mm elliptical specimens were used . All specimens were cast in three layers and covered with a plastic sheet to prevent moisture loss and then demoulded after 24 ± 2 hrs. Demec points were fixed on the top surface of the specimens by using an epoxy adhesive. The variation in length between these points when the specimens were exposed to shrinkage conditions was measured using a dial gauge extensometer that was 220 mm long with an accuracy of 0.001 mm/division. The drying shrinkage strain measurements were monitored for the long term at 4, 7, 14, 21, 28, 50, 91, 112, 224, 365, 500, 730, 900 and 1000 days after an initial reading at 24 hours after demoulding. At each measurement age, the drying shrinkage of the specimen was calculated for the same side and direction as the other ages to reduce the error in the readings (**Figure 3.4**). The average of three specimens were taken for each type of curing (air and sealed curing). During testing the specimens under air

curing were left to air cure in a controlled room at 23 ± 2°C with a relative humidity of 50± 5 % and the others for sealed curing were covered with plastic sheeting and left in same room as shown in **Figure 3.9**. The tests were carried out following the (ASTM/C157, 2008) for determination of length change in hardened cement mortar and concrete. The drying shrinkage strains were calculated using the formula below;

$$\varepsilon_{sh} = \frac{CRD - initial\ CRD}{G} \quad (1)$$

where $\boldsymbol{\varepsilon_{sh}}$ is the drying shrinkage strain of the specimen (mm/mm), CRD is the difference between the comparator reading of the specimen (mm) and the reference bar at any age, initial CRD is the difference between the comparator reading of the specimen and the reference bar at first reading, G is the gauge length (220 mm).

Figure 3-8 Free and confined drying shrinkage strain measurements

Figure 3-9 Free and confined drying shrinkage strain curing specimens.

3.5 Concluding remarks

A series of laboratory tests were performed on SCC mixes and NC mixes in order to achieve the experimental part of the research objectives. The detail features, procedures, specimen preparation, mixing, casting and testing set up were discussed in detail. Both fresh and hardened properties testing of SCCs and NCs were discussed. During handling and testing, concrete was always inspected to ensure the homogeneity. Test results and measurements obtained from the experimental work will be discussed in details and presented in the next chapter of this research. All tests were carried out in accordance with British standards (BS-1881), the American Society for Testing and Materials (ASTM-2015) and the European Guidelines for SCC-2005.

CHAPTER FOUR- EXPERIMENTAL WORK - RESULTS AND DISCUSSION

4.1 Introduction

This chapter presents the results of experimental work and measurements that carried out in chapter three. The main aim of this chapter is to present test results of fresh properties of SCCs such as filling ability, passing ability, viscosity and resistance to segregation and hardened properties such as compressive and flexural strengths, water absorption and density of SCCs and NCs. In addition, free drying shrinkage strain under two types of curing (air and sealed), confined and unconfined drying shrinkage strain are presented and discussed.

4.2 Test results of fresh properties

The fresh properties of SCCs were evaluated by the slump flow test, J-ring test, V-funnel and sieve stability test according to EFNARC (BIBM and ERMCO, 2005). The average time spent on completing each test was up to 15 mins by three people.

4.2.1.1 Filling ability and Viscosity

The viscosity and filling ability of SCCs were evaluated using the slump flow test (slump flow diameter and T_{500mm}) and the V-funnel test (time taken by concrete to completely exit through the funnel). The results slump flow and v-funnel tests are summarised in **Table 4.1**. The flow spread (diameters) for all mixes was in a range of 655 – 808 mm and the time which the concrete took to exit the v-funnel ($T_{v\text{-}funnel}$) was between 6.5 and 11 sec. A slump flow of 600±

50 – 850 mm and a funnel time of 5 – 15 sec were required (BIBM and ERMCO, 2005).

Table 4-1 Filling ability and viscosity tests, flow slump and V-funnel.

Mix ID	Slump flow test			V-funnel test
	d1 (mm)	d2 (mm)	T_{500} (sec)	$T_{v\text{-funnel}}$ (sec)
SCC-0.44	760	780	1.78	9.1
SCC-0.33	660	650	5.00	11
SCC-0.44-20	790	780	2.70	8.7
SCC-0.33-20	810	770	3.44	10
SCC-0.44-40	670	630	2.97	7.3
SCC-0.33-40	770	820	3.20	9.3
SCC-0.44-60	710	740	2.50	6.5
SCC-0.33-60	780	835	4.00	8.1

d1 and d2; slump flow (mm) and T_{500} and $T_{v\text{-funnel}}$; flow time

4.2.2 Passing ability

In order to assess the passing ability of SCCs and to ensure that SCCs be able to pass through congested reinforcement, a J-ring test was used. For a J-ring value below 500 mm, the concrete might have had insufficient flow to pass through highly congested reinforcement (Nagataki and Fujiwara, 1995). The SCC mixes in this work were acceptable with J-ring values between 560- 795 mm (see **Table 4.2**.)

4.2.3 Segregation resistance

To evaluate the homogeneity of the SCCs, a sieve stability test (screen stability test) was used. The measured segregation resistance as a percentage for each of the SCCs is included in **Table 4.2**. The segregation ratio for all mixes ranged between 10– 19 %. When the segregation ratio stayed ≤ 23% of the weight of the sample, the resistance to segregation ability was considered to be acceptable (BIBM and ERMCO, 2005).

Table 4-2 Passing ability and stability tests, J-ring and segregation resistance.

Mix ID	J-ring test			Segregation test		
	d1 (mm)	d2 (mm)	T_{500} (sec)	W_p	W_c	%
SCC-0.44	700	720	3.19	501	4855	10.3
SCC-0.33	560	590	7.00	556	4710	11.8
SCC-0.44-20	770	760	3.00	593	4772	12.3
SCC-0.33-20	770	830	5.10	816	4894	14
SCC-0.44-40	540	580	2.13	945	4800	14.8
SCC-0.33-40	790	770	4.13	1088	4808	16
SCC-0.44-60	580	570	1.6	488	4815	17
SCC-0.33-60	805	785	3.61	943	4824	19

Wp; weight of passed concrete and Wc ; weight of net concrete

4.2.4 Slump test

The workability of NCs was measured by a slump test. There was a significant reduction in workability when the slump decreased from 110mm to 63mm for a decrease in w/b ratio from 0.44 to 0.33.

A comparison between workability of experimental results and specifications of European guidelines are plotted in **Figure 4.1**. As observed throughout this experimental work, the workability of SCC mixes containing FA were achieved at a constant water to binder ratio. Therefore, using FA will reduce water demand for a given workability. SCCs made with a w/b ratio of 0.44 were more workable than those made with a w/b ratio of 0.33. Most of the mixtures showed good homogeneity and cohesion. To analyse the workability results of SCCs, the concept of workability is presented in **Figure 4.2** using boxes, where mixes within the area are acceptable SCC (Esquinas et al., 2018). The mixes inside the box in the section named “Proper SCC area" are regarded as suitable and acceptable SCCs, whereas the other mixes which are located in

the area named “marginal area” are acceptable as SCCs but a slight segregation could occur. None of the mixes in the present investigation were found to be in the unacceptable SCC area.

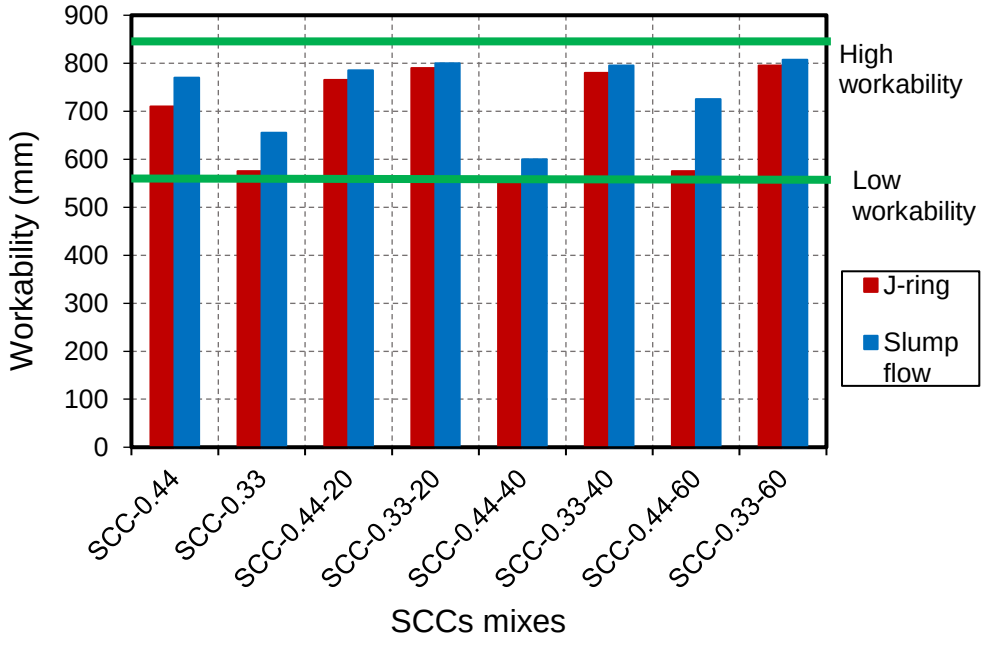

Figure 4-1 Slump flow and J-ring results

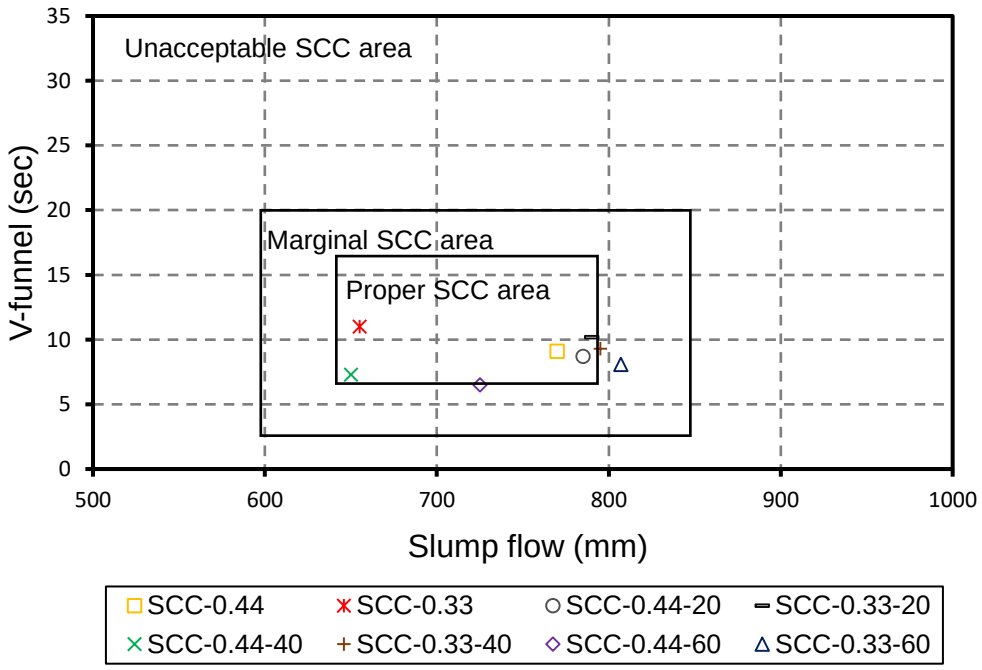

Figure 4-2 Workability boxes of SCC mixes.

4.3 Compressive strength

The compressive strengths of eight SCC mixes and two NC mixes are shown in **Table 4.3.** Normal concretes, NC-0.44 and NC-0.33 achieved compressive strengths of 48.65 MPa and 63.65 MPa at 28 days, respectively compared with self-compacting concretes, SCC-0.44 and SCC-0.33, which reached 55.10MPa and 70.13 MPa at 28 days, respectively. It is clear that for the same water - binder ratio, SCCs have higher compressive strength than NCs. This is mainly attributed to the improved interface transition zone between the aggregate and hardened paste due to the absence of vibration of SCCs.

Table 4-3 Compressive and flexural strength of NCs and SCCs

	Compressive strength (MPa)			Flexural strength (MPa)
Mix ID	7(days)	28(days)	91(days)	91(days)
NC-0.44	43.2	48.65	54.09	4.66
NC-0.33	50.90	63.47	70.25	5.85
SCC-0.44	46	55.1	62.77	5.04
SCC-0.33	59.7	70.13	77.51	6.18
SCC-0.44-20	37.42	45.28	52.12	5.37
SCC-0.33-20	42.13	53.81	66	6.57
SCC-0.44-40	19.9	32.65	36.62	4.56
SCC-0.33-40	39.5	42.25	61.83	5.90
SCC-0.44-60	9.7	21.63	31.65	3.17
SCC-0.33-60	19.9	31.56	43.51	4.07

It is observed that the compressive strength of SCCs decreased with an increase in the percentage of FA as illustrated in **Figure 4.3** and **Figure 4.4.**

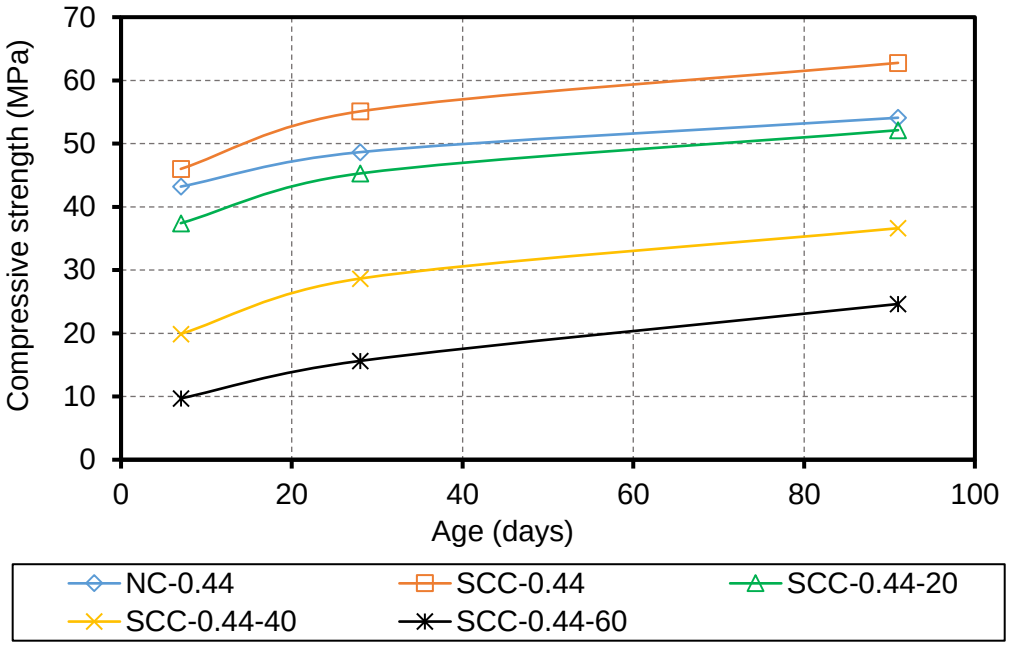

Figure 4-3 Effect of fly ash % on compressive strength for mixes with w/b ratio of 0.44

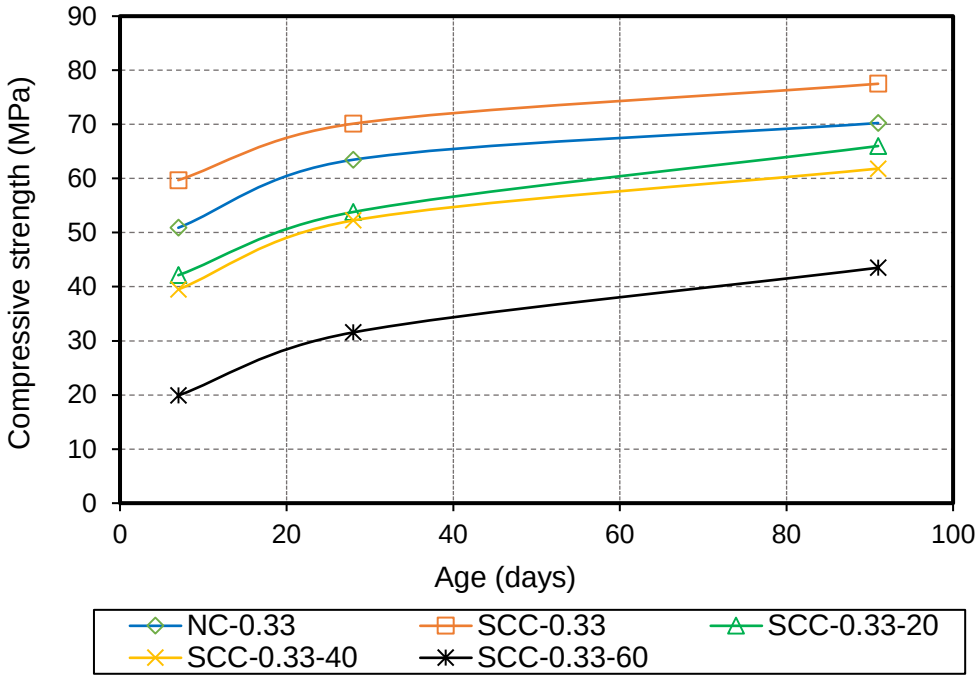

Figure 4-4 Effect of fly ash % on compressive strength for mixes with w/b ratio of 0.33.

This reduction is normally anticipated and is mostly due to the fact that FA needs more time to form the sodium alumino-silicate hydrate (N-A-S-H) gels to build up the mechanical properties (Ismail et al., 2014). The same conclusions have been drawn by Khatib (2008) and Bouzoubaa and Lachemi (2001).

All SCCs mixes achieved acceptable 28-day compressive strengths of about 30 MPa. However, SCCs mixes with 60% FA and a w/b ratio of 0.44 had a 28-day compressive strength of 21.63 MPa. Moreover, a long-term compressive strength at 91 days of above 30 MPa was achieved for SCC mixes containing up to 60% FA as cement replacement (SCC-0.44-60 and SCC-0.33-60). As expected, the compressive strength increased as the w/b ratio decreased at all test ages.

4.4 Flexural strength

All mixes result of flexural strength are shown in **Table 4.3**. A slight increase was observed for the flexural strength of SCCs from 5.07 MPa to 5.37 MPa with a w/b ratio of 0.44 and from 6.18 MPa to 6.57 MPa with a w/b ratio of 0.33 containing 0% FA and 20% FA, respectively. However, by increasing FA from 40% to 60% for SCCs with both w/b ratios (0.44 and 0.33), the flexural strength decreased. A similar reduction in flexural strength of SCCs containing FA has been observed by Iqbal et al. (2017). This reduction of flexural strength of SCCs may be justified on the basis that the SCC compressive strength decreased which has a direct relationship with flexural strength of concrete. The NC flexural strengths were 4.66 MPa and 5.85 MPa for NCs with w/b ratios

of 0.44 and 0.33, respectively. This relationship is graphically represented in **Figure 4.5** from which this behaviour can be clearly observed.

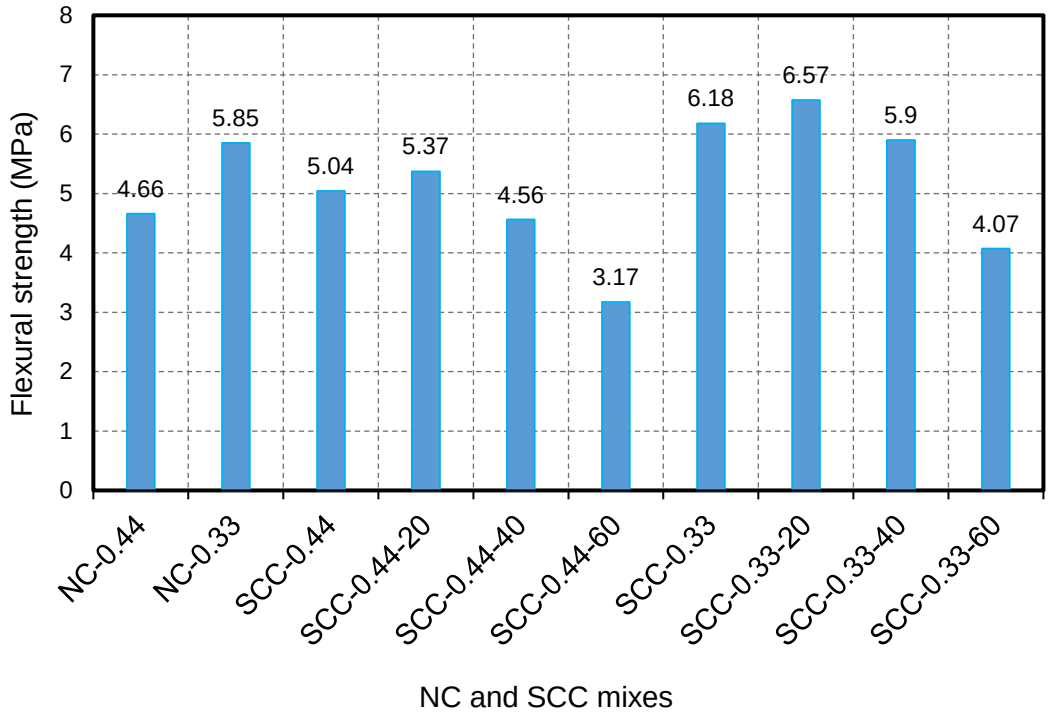

Figure 4-5 91-day flexural strength for NC and SCC mixes with w/c ratios of 0.44 and 0.33

4.5 Bulk density

The bulk densities for NC and SCC mixes for different w/b ratios are presented in **Table 4.4**. Each value of bulk density represents the average of three samples. The density slightly increased as the w/b ratio decreased from 0.44 to 0.33 for both NCs and SCCs which can be attributed to a reduction in the water content from 198 to 180 kg/m^3. Furthermore, at the same w/b ratio, the density of SCC showed a systematic reduction as FA increased due to the lower density of FA compared with ordinary Portland cement (OPC) as shown in **Figure 4.6**. Even though SCC proportions are different to NCs, a slight difference in density of SCCs compared to NCs has been observed in this

study, agreeing with the findings of Khatib (2005), indicating the good self-compaction of SCCs.

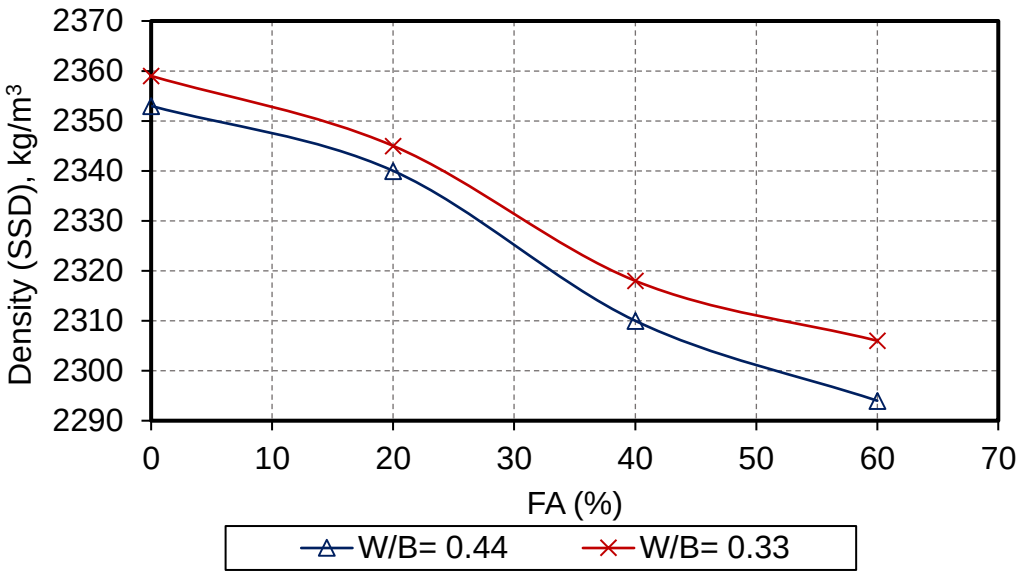

Figure 4-6 Effect of fly ash percentage on SCC density.

Table 4-4 Bulk density of NCs and SCCs

Mix ID	FA (%)	Bulk density (kg/m^3)
NC-0.44	0	2230
NC-0.33	0	2238
SCC-0.44	0	2227
SCC-0.33	0	2241
SCC-0.44-20	20	2217
SCC-0.33-20	20	2236
SCC-0.44-40	40	2129
SCC-0.33-40	40	2178
SCC-0.44-60	60	2108
SCC-0.33-60	60	2141

4.6 Water absorption

Water absorption is generally used as a significant factor for quantifying the durability of cementitious systems. The influence of various degrees of FA content on water absorption for NCs and SCCs is illustrated in **Figure 4.7**. It can be noticed that there is an increase in water absorption for SCCs with increasing FA content. SCC mixes showed lower absorption compared to NC mixes. This is an indicator of good compaction achieved by the concrete self-weight. Due to the increase of workability of SCCs containing fly ash, the compaction is expected to be better. All SCC and NC mixes having w/b ratios of 0.33 showed lower water absorption than those made with w/b ratios of 0.44 and this could be attributed to their capillary and pore networks being somewhat disconnected, which restrains the water penetration depth. It is observed that the water absorption for all mixes varied between 4.6% and 8.8%. All concrete mixes had low absorption characteristics (less than 10%) which was in good agreement with the results reported by Siddique (2013).

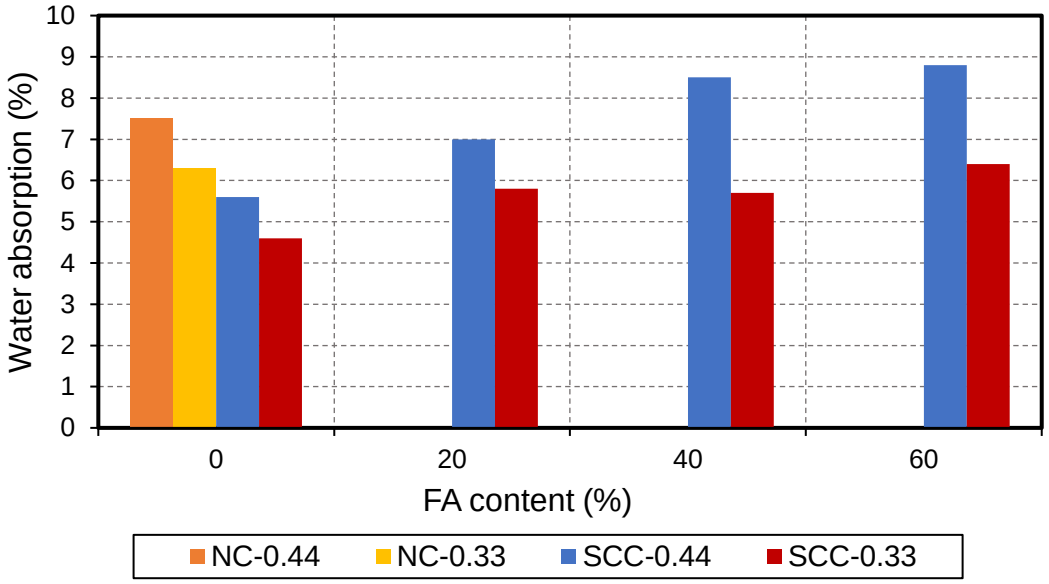

Figure 4-7 Effect of FA content on water absorption of NC and SCC mixes.

4.7 Free and confined drying shrinkage strain

As mentioned early in this research drying shrinkage strain is considered as an important durability property, controlling the deterioration of concrete structures. Experimental results of free drying shrinkage strain under two different curing, confined and unconfined drying shrinkage strain of NCs and SCCs are discussed and presented in the following sections.

4.7.1 Free drying shrinkage strain under air and sealed curing

Free drying shrinkage strain of eight SCC mixes and two NCs under air and sealed curing for two types of water to binder ratios (0.44 and 0.33) were studies and presented in **Figure 4.8** to **Figure 4.11**.

The free dying shrinkage strains of NCs (DSNC) and SCCs (DSSCC) at 1000 days range between 316 and 695 microstrain, respectively. SCCs exhibited 10 to 15 % higher drying shrinkage strains compare d to NCs for the same w/b ratio at different ages of drying. Free drying shrinkage strain results under air curing were slightly higher than the same concrete mixes under sealed curing. The effect of FA content on drying shrinkage strains and the variations with time for NCs and SCCs made with different w/b ratios (0.44 and 0.33) under different curing type (air and sealed) are illustrated in **Figure 4.8** to **Figure 4.11.** It is observed that the DSNC and DSSCC were slightly similar at the very early ages, whereas there was a considerable change in the long-term. It can be seen from **Figure 4.8** to **Figure 4.11** that the effect of replacing the cement by FA was to reduce the drying shrinkage strains remarkably at 40% and 60% FA replacement, but for all of the compositions the drying shrinkage strain

increased with the increase of w/b ratio. At high FA content used in this study (60%), the long term drying shrinkage strain (at 1000 days age) for SCCs was reduced to 49 % compared with the SCCs without FA which was consistent with the finding of Khatib (2005). The drying shrinkage of concrete depends on three controlling factors; w/b ratio, the volume of paste in concrete and the rate of hydration. In this study each of the five mixes had the same w/b ratio and paste volume. However, cement replacement by fly ash reduced the lime content from the mix as FA has a significantly low lime content in this study (2.5%). Due to the reduction of lime content, the rate of hydration of concrete reduced. As a result, fly ash concrete exhibited a lower degree of drying shrinkage compared to conventional concrete (Siddique, 2004, Saha and Sarker, 2017). It is clear that, the majority of concrete drying shrinkage strain occurred in the first three months. Afterwards, the long term drying shrinkage strain up to 1000 days was steady for all mixes.

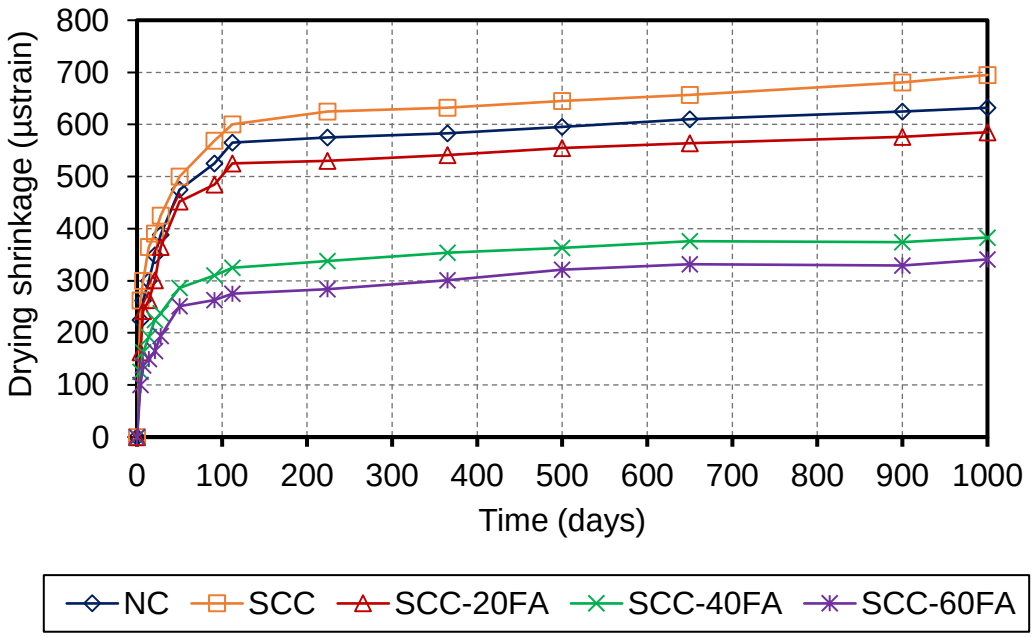

Figure 4-8 Effect of FA content on free drying shrinkage strain for NCs and SCCs mixes with w/b ratio 0.44 at different ages under air curing.

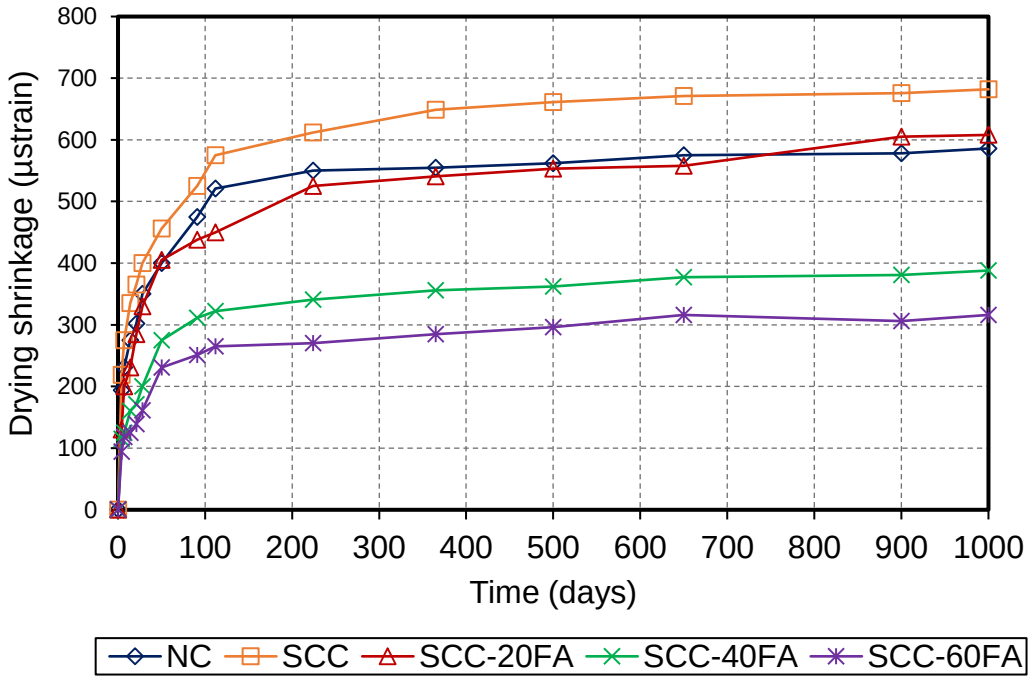

Figure 4-9 Effect of FA content on free drying shrinkage strain for NCs and SCCs mixes with w/b ratio 0.33 at different ages under air curing.

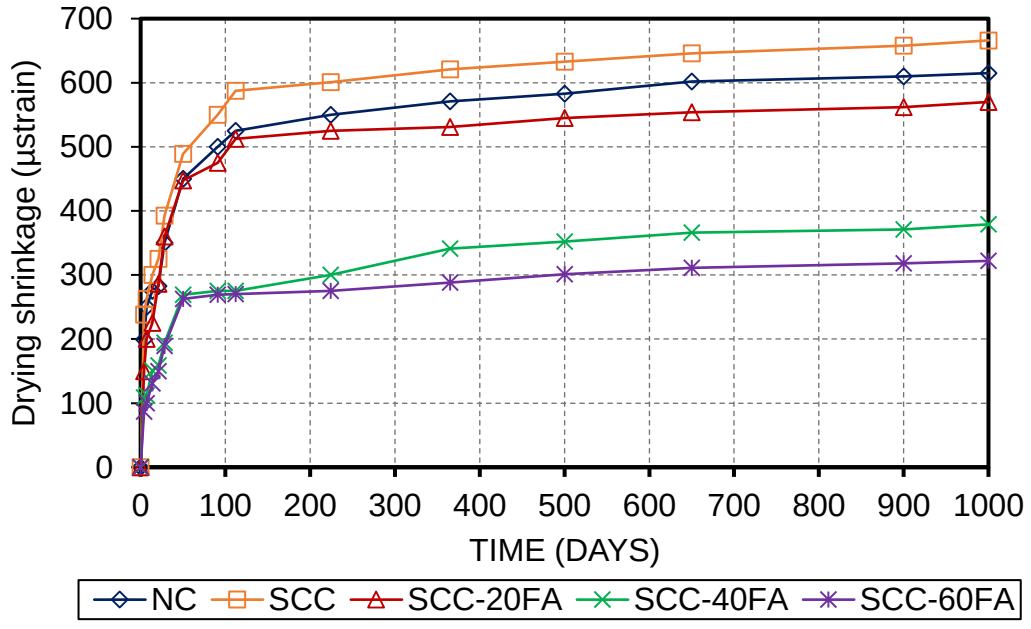

Figure 4-10 Effect of FA content on free drying shrinkage strain for NCs and SCCs mixes with w/b ratio 0.44 at different ages under sealed curing.

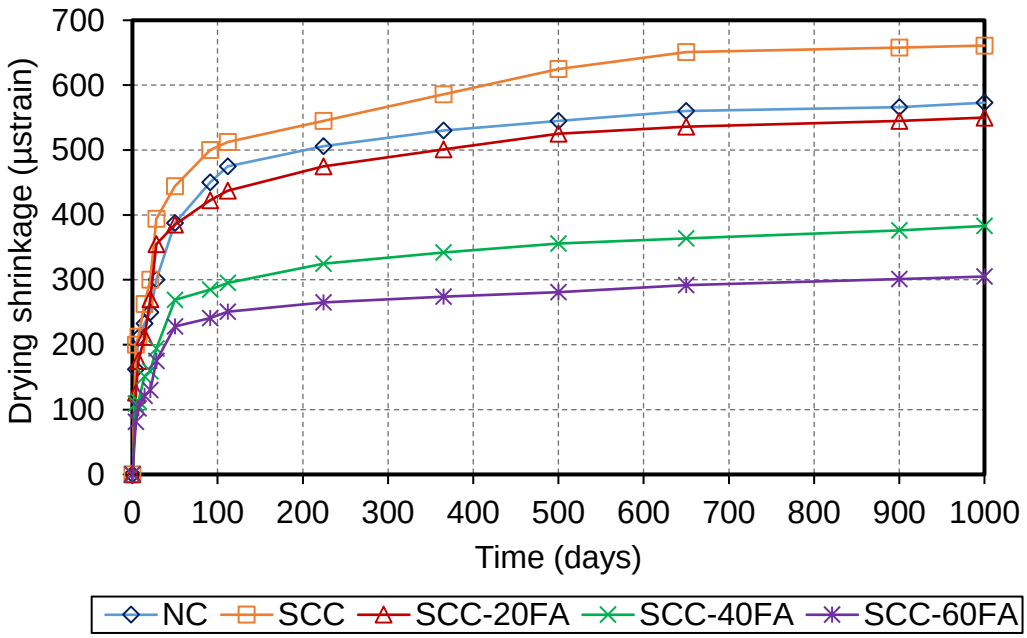

Figure 4-11 Effect of FA content on free drying shrinkage strain for NCs and SCCs mixes with w/b ratio 0.33 at different ages under sealed curing.

4.7.1.1 Effect of fly ash content and compressive strength on free drying shrinkage strain for different types of curing.

Figure 4.12 and **Figure 4.13** illustrate the relationship between FA content and drying shrinkage strain at 1000 days. There is a linear relation between FA content and drying shrinkage strain with R^2 = 0.951 and 0.950 for SCCs under air curing for the two w/b ratios 0.44 and 0.33, respectively and with R^2= 0.962 and 0.983 for SCCs under sealed curing for w/b ratios 0.44 and 0.33, respectively indicating a strong correlation for both w/b ratios. Khatib (2008) reported a linear relationship between drying shrinkage against FA content of R^2 = 0.96 with a reduction in drying shrinkage by increasing FA content.

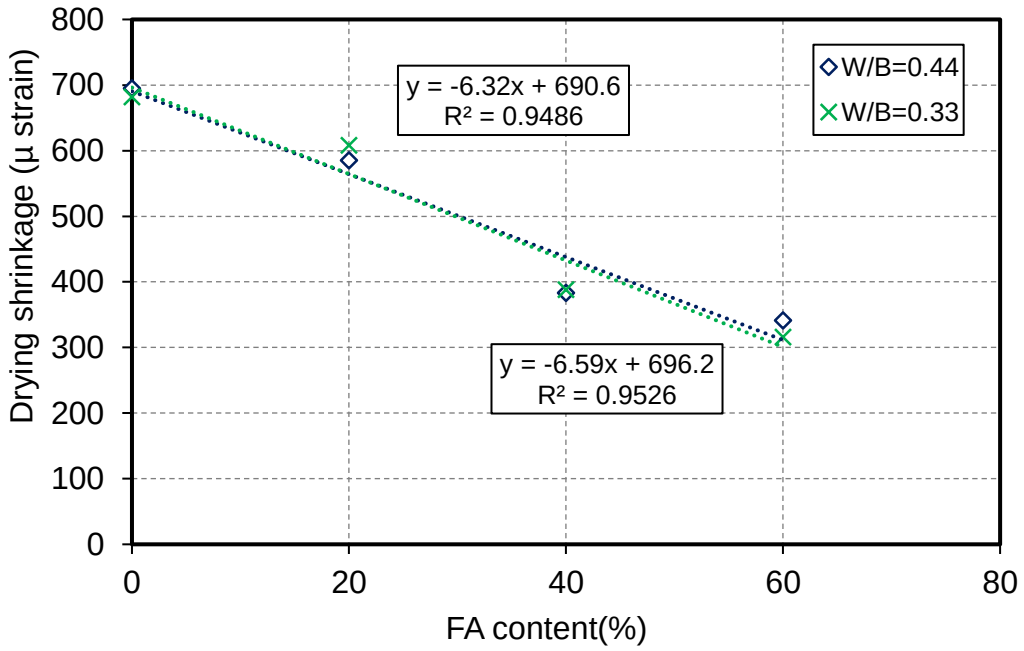

Figure 4-12 Relation between FA content and free drying shrinkage at 1000 days for different w/b ratios under air curing

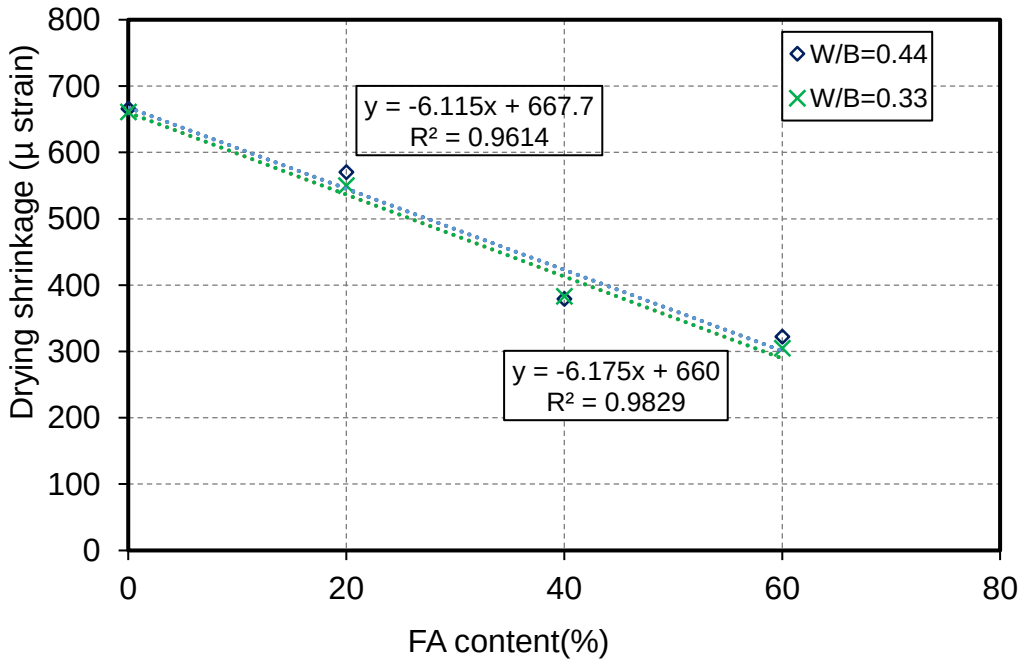

Figure 4-13 Relation between FA content and free drying shrinkage at 1000 days for different w/b ratios under sealed curing

Figure 4.14 and **Figure 4.15** correlate the drying shrinkage at 91 days with the compressive strength at 91 days. It is clear that SCCs with a w/b ratio of

0.44 showed greater drying shrinkage strains than those with a w/b ratio of 0.33. At the same time SCCs with a w/b ratio of 0.33 which had higher compressive strengths exhibited reductions in the drying shrinkage. SCCs with the same w/b ratio displayed an increase in compressive strength when drying shrinkage increased and a linear relationship was obtained with R^2 = 0.975 and 0.866 for NCs and SCCs under air curing with w/b ratios of 0.44 and 0.33 respectively and for NCs and SCCs under sealed curing with R^2 = 0.972 and 0.840 for w/b ratios of 0.44 and 0.33 respectively indicating a good correlation. As it is already known, by increasing the w/b ratio, the compressive strength decreased. Consequently, drying shrinkage increased. The opposite trend was achieved in this study for, similar to previous studies (Persson, 2001, Khatib, 2008) due to the presence of FA content which caused reductions in both compressive strength and drying shrinkage.

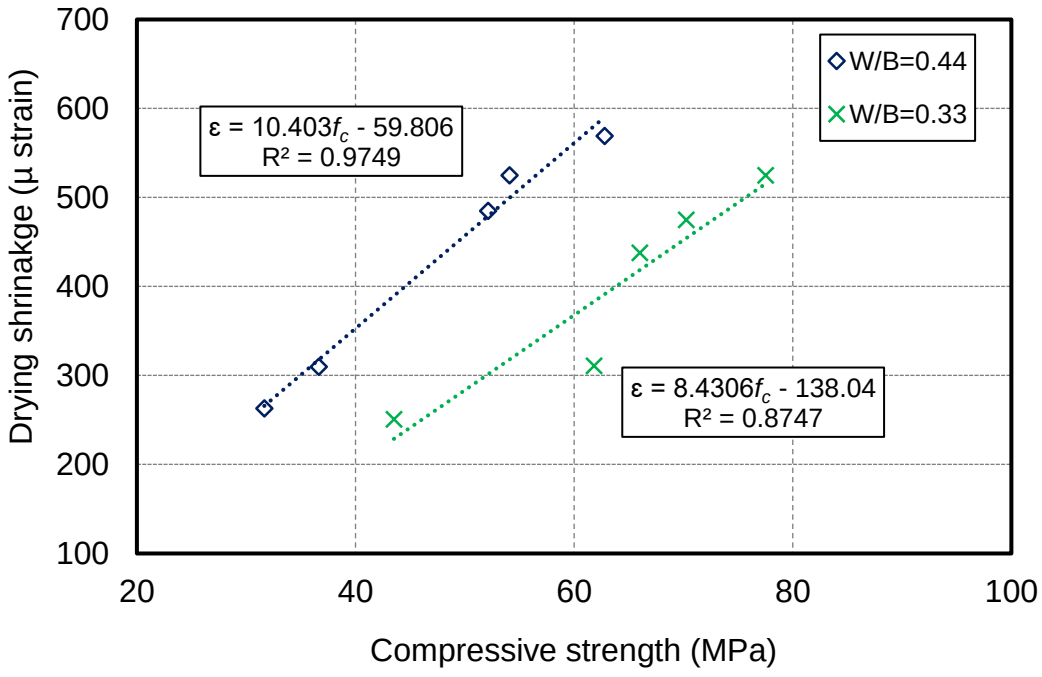

Figure 4-14 Relation between 91 days compressive strength and free drying shrinkage at 91 days for different w/b ratios under air curing.

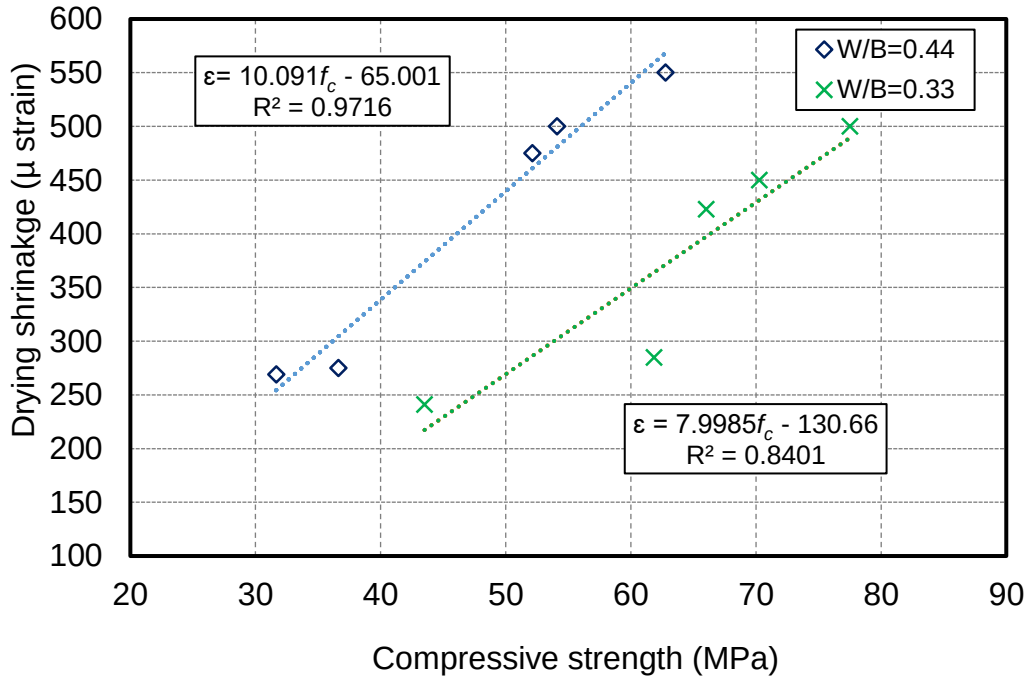

Figure 4-15Relation between 91 days compressive strength and free drying shrinkage at 91 days for different w/b ratios under sealed curing.

4.7.2 Confined and unconfined drying shrinkage strain.

In order to study confined and unconfined drying shrinkage strain, eight SCC mixes and two NCs, cast in elliptical moulds (which are popular for use in building construction), with two types of water binder ratios (0.44 and 0.33) were examined. The results of confined and unconfined of drying shrinkage for SCCs and NCs are illustrated in **Figure 4.16** to **Figure 4.19.** In general, SCCs present 12 to 20% greater drying shrinkage strain than NCs for both confined and unconfined drying shrinkage strain as shown in **Figure 4.16** to **Figure 4.19.** Unconfined drying shrinkage specimens exhibited higher values than the confined ones for the same mixes and this could be attributed to the evaporation of water from the explosed sample sides for the unconfined concrete samples.

For the confined concrete samples only the top surface was exposed. The effects of FA replacement by cement on confined drying shrinkage strain behaviour are similar to those of free drying shrinkage strain, and there was a reduction in confined drying shrinkage strain of SCCs with 60 % of FA by up to 46 % compared with SCCs mixes without FA.

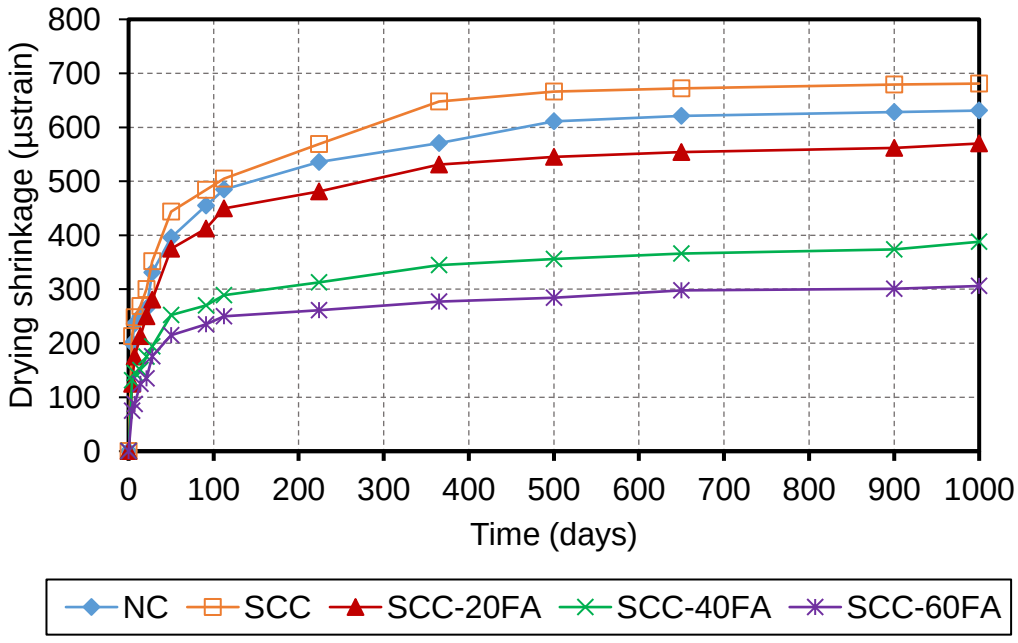

Figure 4-16 Effect of FA content on confined drying shrinkage strain for NCs and SCCs mixes for w/b ratio 0.44.

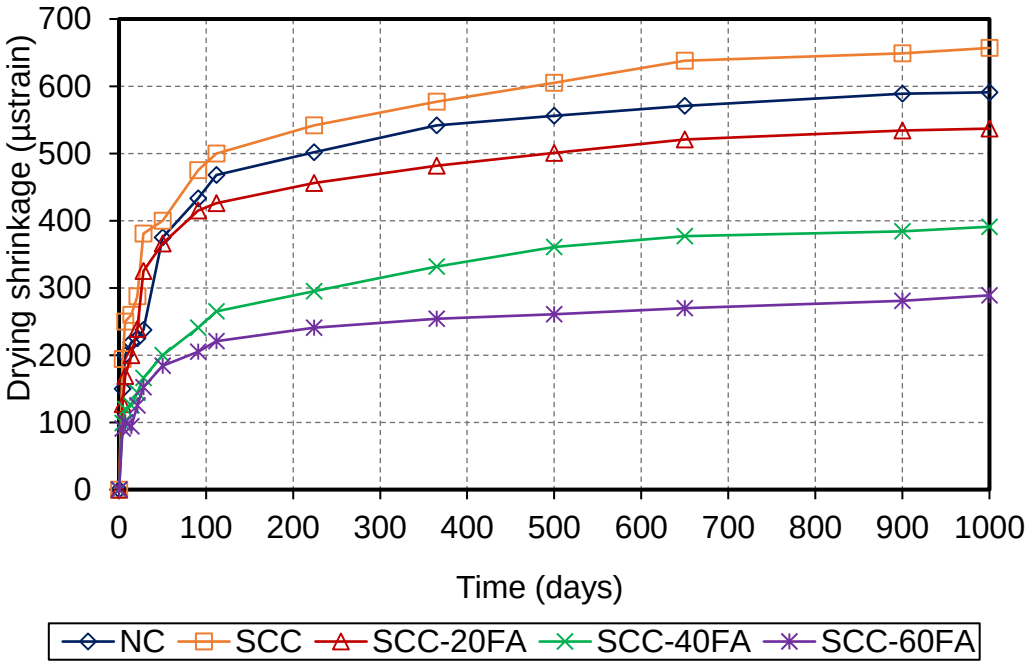

Figure 4-17 Effect of FA content on confined drying shrinkage strain for NCs and SCCs mixes for w/b ratio 0.33.

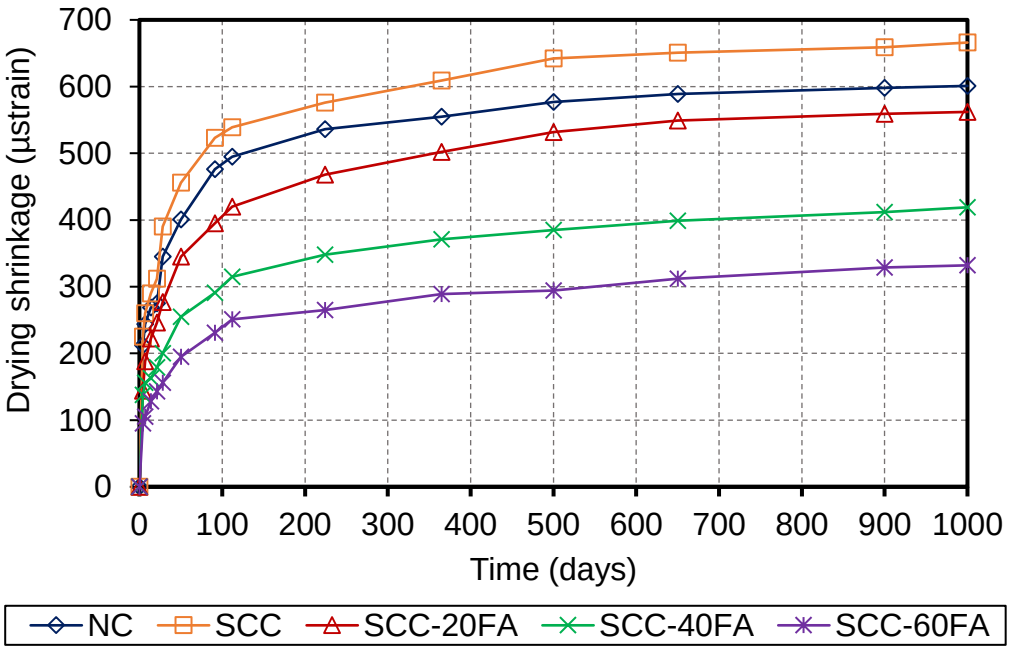

Figure 4-18 Effect of FA content on unconfined drying shrinkage strain for NCs and SCCs mixes for w/b ratio 0.44

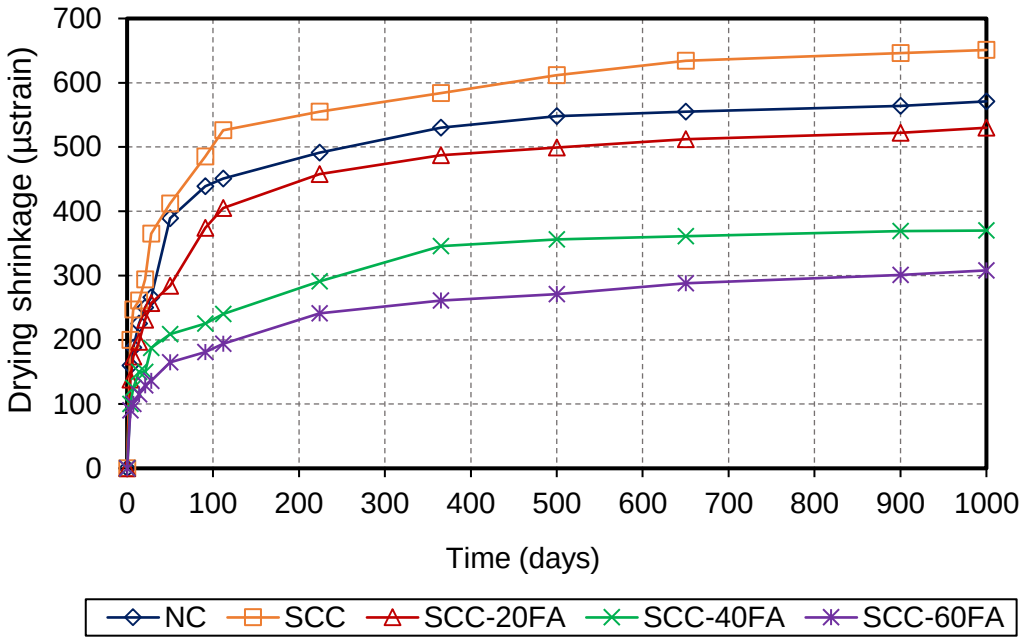

Figure 4-19 Effect of FA content on unconfined drying shrinkage strain for NCs and SCCs mixes for w/b ratio 0.33.

4.7.2.1 Effect of fly ash content and compressive strength on confined and unconfined drying shrinkage strain.

As mentioned earlier in this chapter there is a clear linear relation between the percentage of FA and drying shrinkage strain of SCCs. **Figure 4.20** and **Figure 4.21** show the relationship between FA content and confined and unconfined drying shrinkage strain at 1000 days. From **Figure 4.20** and **Figure 4.21** below it is observed that the confined drying shrinkage strain of SCCs decreased with an increase in the percentage of FA from 20 to 60 % with both w/b ratios (0.44 and 0.33) and R^2 values indicating a good correlation for confined and unconfined SCCs.

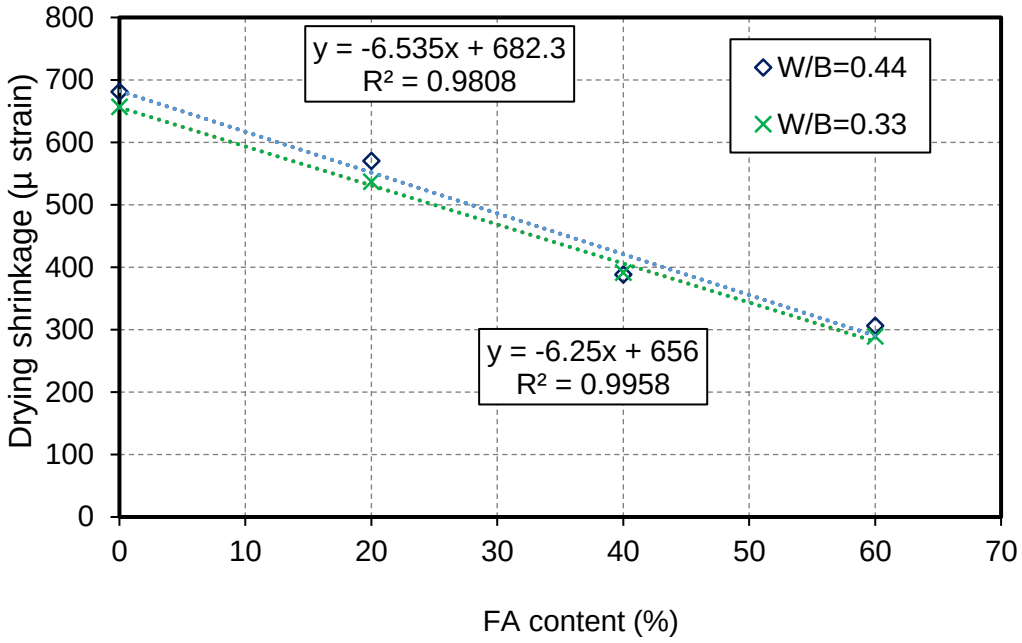

Figure 4-20 Relation between FA content and confined drying shrinkage at 1000 days for different w/b ratios.

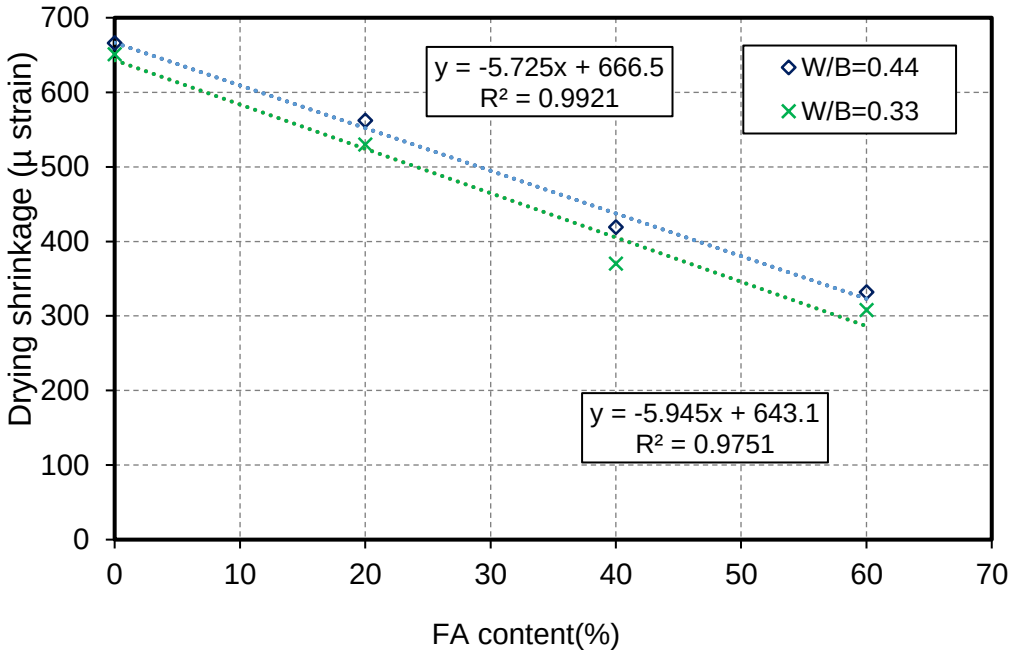

Figure 4-21 Relation between FA content and unconfined drying shrinkage at 1000 days for different w/b ratios.

Figure 4.22 and **Figure 4.23** correlate the confined and unconfined drying shrinkage at 91 days with the compressive strength at 91 days.

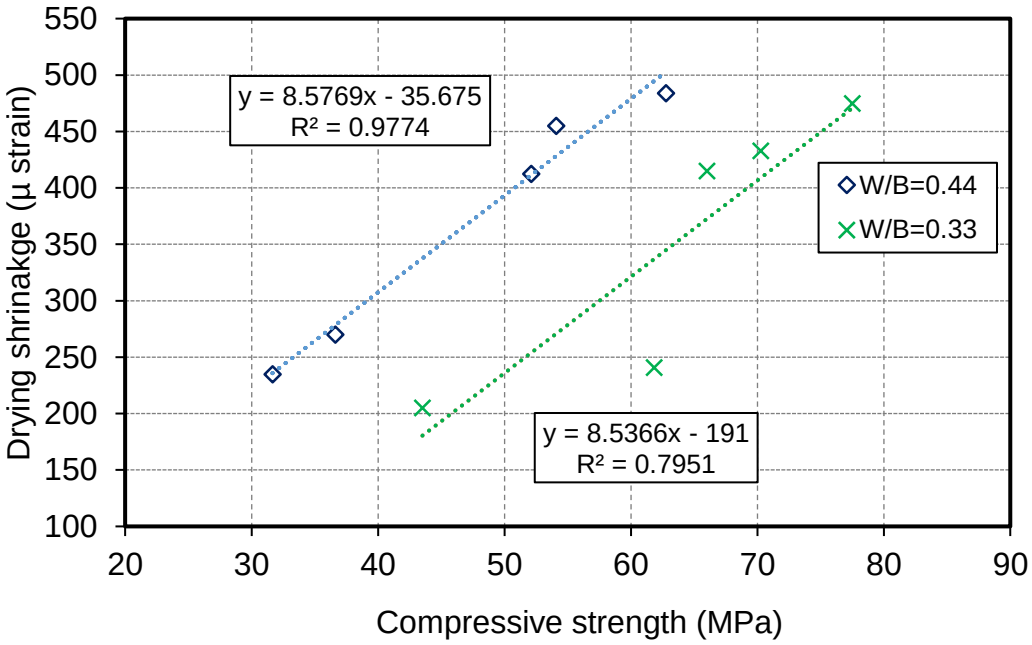

Figure 4-22 Relation between 91 days compressive strength and confined drying shrinkage at 91 days for different w/b ratios.

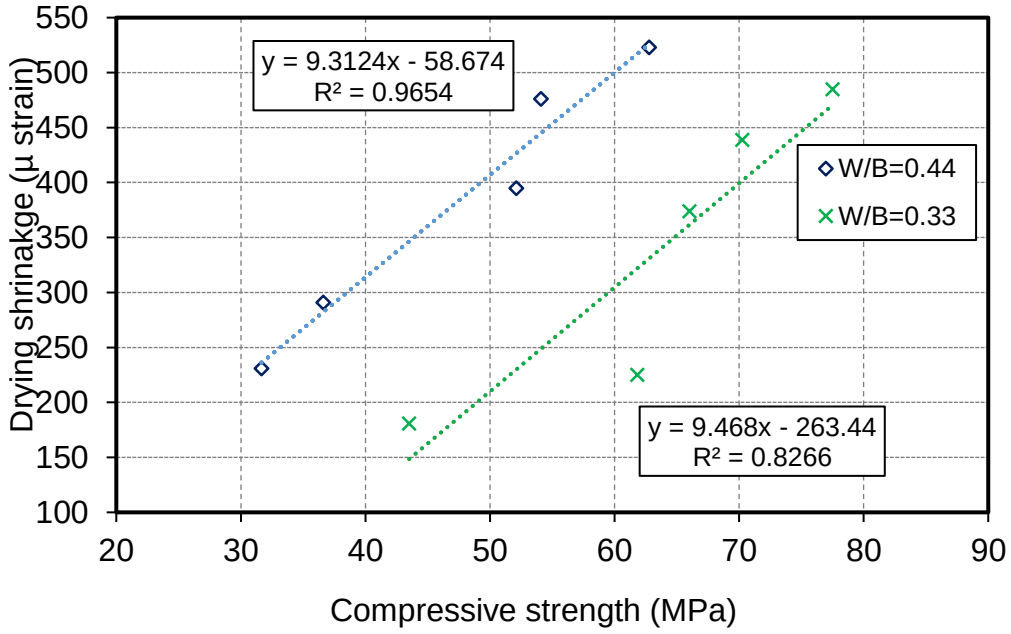

Figure 4-23 Relation between 91 days compressive strength and unconfined drying shrinkage at 91 days for different w/b ratios.

It is clear that confined drying shrinkage strain exhibited the same behaviour as the free drying shrinkage strain. SCCs with a w/b ratio of 0.44 showed higher drying shrinkage strains than those with a w/b ratio of 0.33. For confined and unconfined drying shrinkage strain at same w/b ratio there is a linear relationship between compressive strength and drying shrinkage with R^2 shown in the figure indicating a good correlation. It is clear that by increasing compressive strength for both w/b ratios (0.44 and 0.33), the confined and unconfined drying shrinkage strain increased.

As mentioned earlier in this research concrete filled elliptical tubes (CFET) have been used in construction due to the advantages over reinforced concrete members. In the case of CFET filled with self-compacting concrete confined drying shrinkage strain will occur and it might cause a gap to form between the concrete and steel tube which could affect their composite action. The bond transfer between the steel tube and the concrete infill depends on radial displacements due to the confined drying shrinkage (Roeder et al., 1999). Based on the experimental study of the confined drying shrinkage strain of NCs and SCCs in this research it is possible to reduce confined drying shrinkage of SCCs using FA up to 60 % with a long term compressive strength above 30 MPa.

4.8 Concluding remarks

In this investigation, several SCC mixes proportioned with different fly ash percentages and two types of w/b ratios were prepared in the concrete laboratory and found to meet the necessary self-compacting criteria and the

target compressive strength. Based on the test results of fresh and mechanical properties of SCCs and NCs, the following conclusions can be highlighted:

- The addition of fly ash can significantly improve the fresh properties of SCC. The higher the percentage of fly ash, the higher the workability of SCC. Viscosity, passing ability, filling ability and segregation resistance were accepted within the limits required.
- The compressive strength and flexural strength decreased with the increase of fly ash content due to the lack of lime content. SCCs without fly ash gave the highest values of compressive and flexural strength at 7, 28 and 91 days of age. Using up to 60% of FA as cement replacement can produce SCC with a compressive strength as high as 30 MPa. For the same water - binder ratio SCCs have higher compressive and flexural strengths than NCs.
- The water absorption of SCCs increased considerably when FA was used. However, the bulk density of SCCs showed a systematic reduction with increase of FA content for all SCCs. All SCC and NC mixes having w/b ratios of 0.33 absorbed less water than those made with w/b ratios of 0.44. SCC mixes absorbed less water than NC mixes.
- SCCs exhibited 5 to 10 % higher free drying shrinkage than NCs made with a similar w/b ratio up to an age of 91 days. SCC long-term drying shrinkage from 356 to 1000 days was higher than NCs.
- FA reduced the rate of hydration and thus the drying shrinkage of SCCs containing FA was considerably lower than that of the control concrete.
- Unconfined drying shrinkage mixes exhibited higher values than the confined ones for the same mixes this could be attributed to the

exposure of unconfined concrete samples to the air, allowing evaporation from all sample sides whereas confined concrete samples were exposed on the top surface only.

- Using FA up to 60% as cement replacement reduces confined drying shrinkage strain of SCCs by up to 46 % compared with SCCs mixes without FA.
- This investigation showed that confined drying shrinkage could be very detrimental to the bond between concrete and steel tube which may affect their composite action.
- CFET filled with self-compacting concrete containing FA up to 60% are recommended for use in construction in order to prevent confined drying strain.

CHAPTER FIVE - PREDICTION OF SELF-COMPACTING CONCRETE DRYING SHRINKAGE STRAINS USING EXISTING MODELS

5.1 Introduction

The significance of this chapter is to assess the accuracy of the drying shrinkage prediction models proposed by international codes including the ACI 209R-92 model (ACI Committee 209, 1992) and the BS EN-92model (Eurocode2, 2004) as well as the drying shrinkage prediction models suggested by researchers Huo model (Huo et al., 2001), the B3 model B3 (Bazant and Baweja, 2000), and the GL 2000 model (Gardner, 2004). The drying shrinkage values determined by the five models were compared against a large experimental data base collected from the literature together with the experimental results presented in chapter four.

5.2 Comparisons of free drying shrinkage strain prediction models

There are several empirical models that have been developed over several years to improve the accuracy of shrinkage strain prediction of concrete and parameters necessary for the calculations and these models vary in complexity and precision. The prediction models selected for comparison in this study are the American Concrete Institute Committee (ACI 209R-92) model, the Eurocode 2 (BS EN-92) model, the model modified by Huo (ACI 209R-92 (Huo), the model developed by Bazant and Baweja (B3) and Gradner and Lockman model (GL2000). The characteristics of these models are described in the following sections.

5.2.1 ACI 209R-92 model

This is an empirical model developed by Branson Christiason, it is the current model recommended by American Concrete Institute. The shrinkage strain $\varepsilon_{sh}(t, t_c)$ at age of concrete t (days), measured from the start of drying at t_c(days), is calculated by Eq.

$$\varepsilon_{sh}\ (t - t_c) = \frac{(t-t_c)}{f+(t-t_c)}\ \varepsilon_{sh\,u} \qquad 5.1$$

where; the values of f are 35 and 55 for moist curing and steam curing, respectively, (t, t_c) is the time from the end of the initial curing and $\varepsilon_{sh\,\mathrm{u}}$ is the ultimate shrinkage strain defined as:

$$\varepsilon_{sh\,u} = 780\ \gamma_{sh}\ \times 10^{-6}\ (\mathrm{mm/mm}) \qquad 5.2$$

$$\gamma_{sh} = \gamma_{sh,tc}\,\gamma_{sh,RH}\,\gamma_{sh,vs}\,\gamma_{sh,s}\,\gamma_{sh,\Psi}\,\gamma_{sh,c}\,\gamma_{sh,\alpha} \qquad 5.3$$

where; γ_{sh} represents the cumulative product of the following correction factors: Initial moist curing coefficient ($\gamma_{sh,tc}$), humidity coefficient ($\gamma_{sh,RH}$), member size coefficient ($\gamma_{sh,vs}$), slump coefficient ($\gamma_{sh,s}$), fine aggregate coefficient($\gamma_{sh,\Psi}$), cement content coefficient ($\gamma_{sh,c}$), air content coefficient ($\gamma_{sh,\alpha}$).

5.2.2 BS EN 1992 model

This model is presented by BS EN 1992-1-1:2004, the shrinkage strain $\varepsilon_{\mathrm{cd}}(\mathrm{t})$ at time t for shrinkage beginning at time $\mathrm{t_c}$ is calculated using the following expressions:

$$\varepsilon_{cd}(t) = \beta_{ds}\ (t,t_s)\ k_{h_0}\ \varepsilon_{cd,0} \qquad 5.4$$

$$\beta_{ds} = \frac{t-t_c}{(t-t_c)+0.04\sqrt{h_0{}^3}} \quad 5.5$$

$$\varepsilon_{cd,0} = 0.85\left[(220 + 110.\propto_{ds1}).\exp(-\propto_{ds2}.\frac{f_{cm}}{f_{cm0}}\right].10^{-6}.\beta_{RH} \quad 5.6$$

$$\beta_{RH} = 1.55\ \left[1 - \left(\frac{RH}{RH_0}^3\right)\right] \quad 5.7$$

where; t is the age of the concrete at the moment considered, in days; t_c is the age of the concrete (days) at the start of drying, K_h is a coefficient depending on the notional size h_0 , and h_0 is the notional size (mm) of the cross-section = $2A_c$ /u

where; A_c is the concrete cross-sectional area and u is the perimeter of that part of the cross section which is exposed to drying.

5.2.3 ACI 209 (Huo) model

This model is the same as ACI 209R-92, and additional modification factors for compressive strength at 28 days (f'_c) are considered as presented in formula below:

$$\varepsilon_{sh}\ (t - t_c) = \frac{(t-t_c)}{(45-0.3625\ f'_c+(t-t_c))}\ \ \varepsilon_{sh\,\mu} \quad 5.3$$

$\varepsilon_{sh\,u}$= 780 γ_{sh} × 10^{-6} (mm/mm) 5.4

$$\gamma_{sh} = \gamma_{sh,tc}\gamma_{sh,RH}\gamma_{sh,vs}\gamma_{sh,s}\gamma_{sh,\psi}\gamma_{sh,c}\gamma_{sh,\alpha}\gamma_{sh,f'_c} \quad 5.6$$

5.2.4 B3 model

The B3 model is the latest version in a number of shrinkage prediction methods. It was developed by Bazant and Baweja in 1997. The version presented is the short form of model B3, the mean shrinkage strain $\varepsilon_{sh\,(t)}$, in the cross section at age *t*, measured from start of drying t_c is obtained as follows:

$$\varepsilon_{sh}(t) = \varepsilon_{shu}\, k_h\, S(t) \quad 5.7$$

where; ε_{shu} is the ultimate shrinkage, K_h is the humidity dependence coefficient, and $S_{(t)}$ is the time dependence coefficient.

$$\varepsilon_{shu} = \propto_1 \propto_2 [0.019\ w^{2.1}\ (f'_c)^{-028} + 270] \times 10^{-6} \quad 5.8$$

where; $\propto_1$ is the cement type dependence coefficient, $\propto_1$ is the curing condition dependence coefficient, w is the water content dependence coefficient and f'_c is the 28 days cylinder strength (MPa).

$$S_{(t)} = \tanh \sqrt{\frac{(t-t_c}{\tau_{sh}}} \quad 5.9$$

where; τ_{sh} is the shrinkage half time which is dependent on member size

$$\tau_{sh} = 4.9(D)^2 \quad 5.10$$

where; D; cross section thickness of concrete (mm).

5.2.5 GL 2000 model

This model was published by Gradner and Lockman in 2001. Shrinkage $\varepsilon_{sh\,(t)}$, at any age *t* after exposure to drying at age t_c is determined from the following expression:

$$\varepsilon_{sh}(t) = \varepsilon_{shu}\ \ \beta_{(h)}\ \beta_{(t)} \quad 5.11$$

where; ε_{shu} is the ultimate shrinkage, $\beta_{(h)}$ is the humidity coefficient, and $\beta_{(t)}$ is the coefficient to allow for time of drying.

$$\varepsilon_{shu} = 1000k\ (\frac{30}{f_{cm28}})^{0.50} \times 10^{-6} \quad 5.12$$

where; k is the cement type coefficient, f_{c28} is the cylinder compressive strength (MPa)

$\beta_{(h)}$ = (1-1.18 h^4)

where; h is relative humidity

$$\beta(t) = \left[\frac{t-t_c}{t-t_c+0.12\times(\frac{V}{S})^2}\right]^{0.5} \quad 5.13$$

where; v/s is the volume /surface ratio (mm)

The main parameters considered by each model to predict drying shrinkage strain are summarized in **Table 5.1.**

Table 5-1 Parameters considered by different models for drying shrinkage prediction.

Parameters	ACI 209R-92	BSEN-92	ACI 209R-92 (Huo)	GL2000	B3
Cement content	√	x	√	x	x
Water content	x	x	x	x	√
Fine aggregate content	√	x	√	x	x
Air content	√	x	√	x	x
slump	√	x	√	x	x
Cement type	x	√	x	√	√
Curing time	√	√	√	x	√
Specimen size	√	√	√	√	√
Relative humidity	√	√	√	√	√
Curing conditions	√	x	√	x	√
Compressive strength	x	√	√	√	√

5.3 Assessment of drying shrinkage strains prediction models

To assess the quality of predictive models, the influence of various parameters on the drying shrinkage strain as predicted by various models are studied. A range of parameters for each model was used to assess the models. The limitations of the variables considered for each model are listed in **Table 5.2.** The main parameters considered in this study were compressive strength, cement content, water content and relative humidity.

Table 5-2 Variables range for each model

Parameters	ACI209 R-92	BSEN-92	ACI209R (Huo)	GL2000	B3
Compressive strength (MPa)	-	20-100	60-80	16-82	17-70
Cement content (kg/m^3)	279-446	-	400-445	160-719	160-720
Water content (kg/m^3)	-	-	-	-	60-600
Relative humidity (%)	40-100	40-100	40-100	20-100	40-100

5.3.1 Effect of compressive strength on drying shrinkage using various models.

Figure 5.1 shows the relation between compressive strength and drying shrinkage strain predicted by different models. Compressive strength of concrete is considered as the main parameter for calculating drying shrinkage strain using BSEN-92, ACI 209r-92 (Huo), GL2000 and B3 models. However, it is not considered for calculation of the drying shrinkage of concrete using the ACI 209R-92 model. From **Figure 5.1** it can be observed that there was a clear decrease in drying shrinkage strain predicted with the increase of compressive strength using BSEN-92, ACI 209R-92 (Huo) and GL2000 models. Moreover, only a small reduction in drying shrinkage strain with increasing compressive strength was predicted using the B3 model.

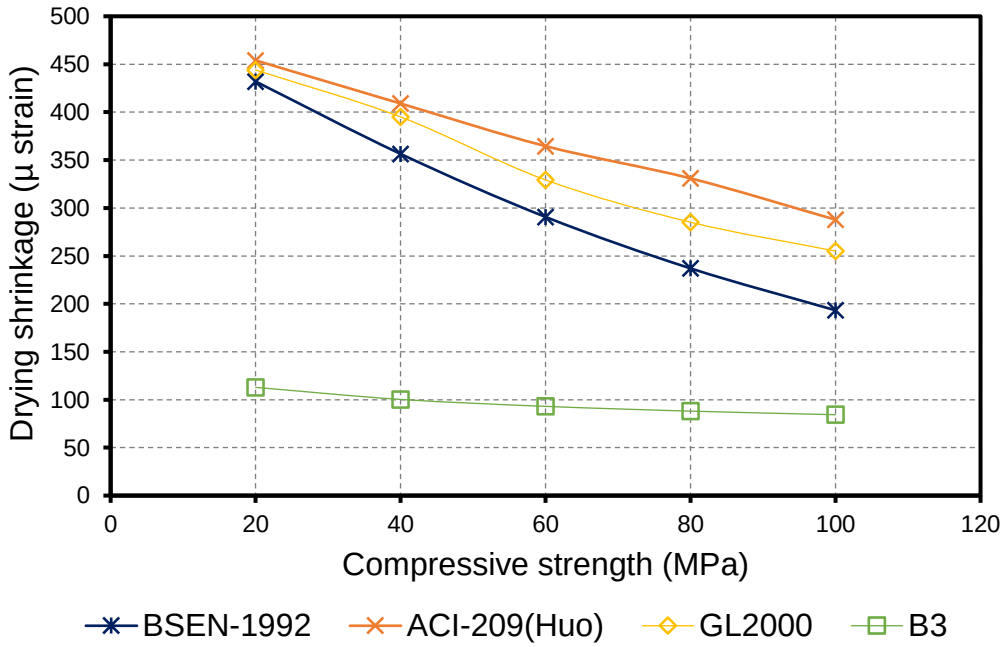

Figure 5-1 Effect of compressive strength on drying shrinkage strain using different models.

5.3.2 Effect of cement and water content on drying shrinkage strain using various models.

The influence of cement and water content on drying shrinkage is illustrated in **Figure 5.2** and **5.3**. Cement content is considered as one of parameters by ACI 209R-92 and ACI 209R-92 (Huo) to calculate drying shrinkage strain and it is not taken into account by other existing models used in this study. Moreover, the only model of the existing models used that considered water content as one of the parameters to calculate drying shrinkage strain is the B3 model. There is an increase in drying shrinkage strain predicted with the increase in cement content using ACI 209R-92 and ACI 209R-92 (Huo) models as shown in **Figure 5.2.** The increase of water content which was considered as one of the main parameters in the B3 model induces an increase of the drying shrinkage strain predicted as illustrated in **Figure 5.3.**

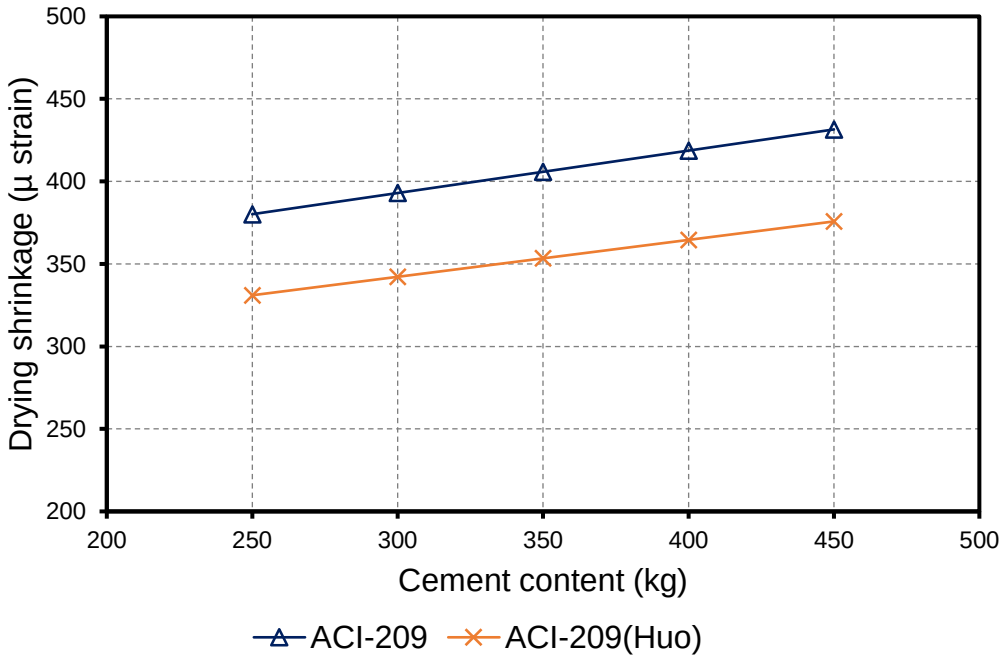

Figure 5-2 Effect of cement content on drying shrinkage strain for different models

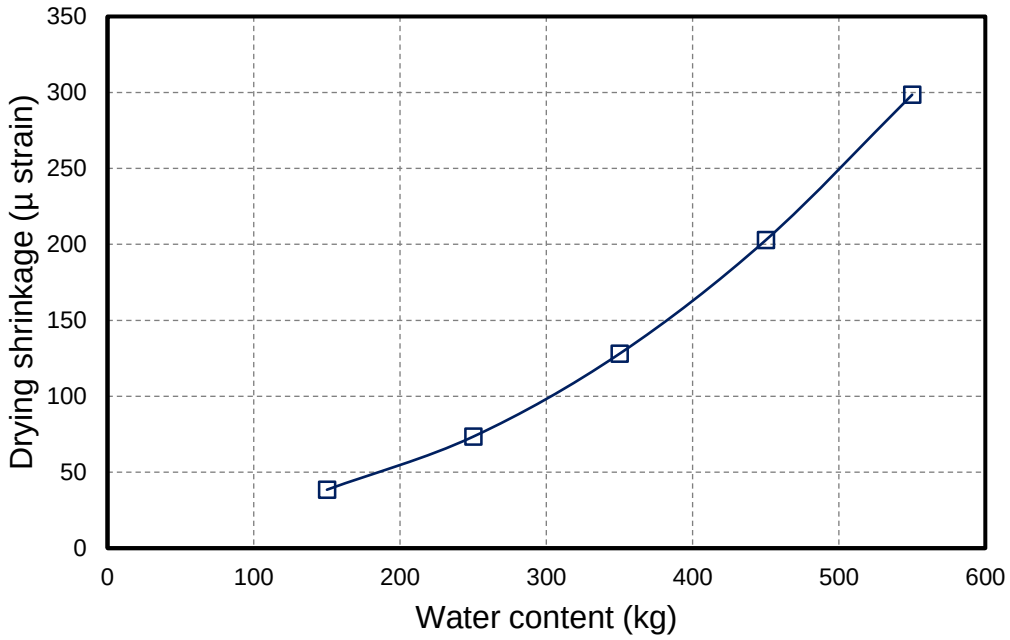

Figure 5-3 Effect of water content on drying shrinkage strain for B3 model

5.3.3 Effect of relative humidity on drying shrinkage using different models

Relative humidity (RH) is one of the more important parameters affecting long term drying shrinkage of concrete and it is considered by all of the models used in this investigation. Figure 5.4 depicts a clear reduction of drying shrinkage predicted by all models when RH increases.

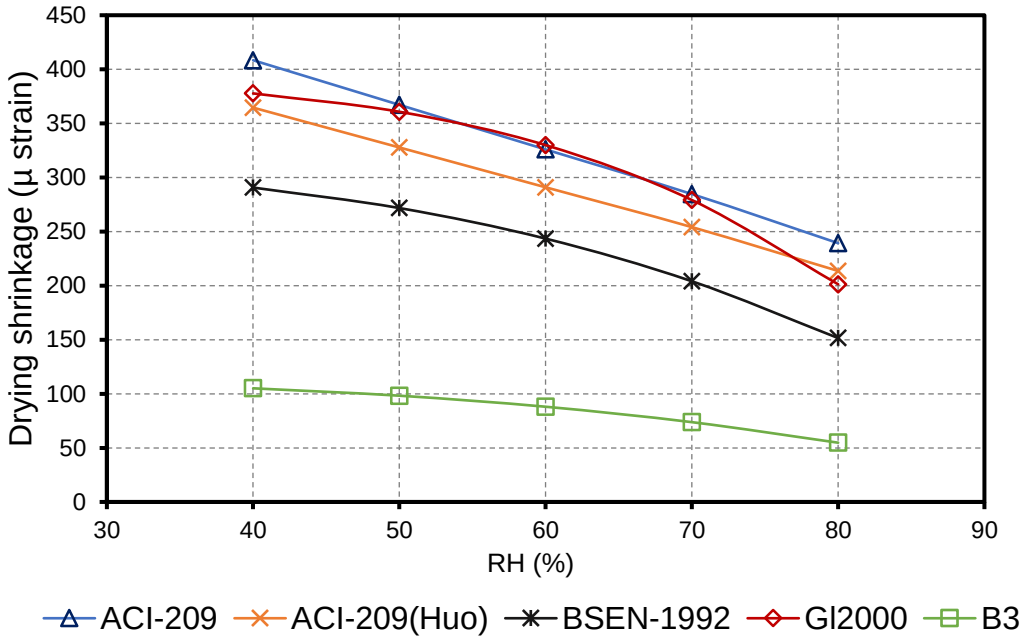

Figure 5-4 Effect of RH % on drying shrinkage strain using different models

5.4 Experimental database for drying shrinkage strain

The experimental results included in the database for studying the applicability of various drying shrinkage strain prediction models were produced by collecting a total of 230 sets of various mixes with different material proportions from different experimental investigations available in the literature (Bouzoubaa and Lachemi, 2001, Proust and Pons, 2001, Collepardi et al., 2002, Chopin et al., 2003, Vieira and Bettencourt, 2003, Assié et al., 2003, Horta, 2005, Poppe and De Schutter, 2005, Turcry et al., 2006, Rozière et al., 2007, Heirman et al., 2008, Khatib, 2008, Loser and Leemann, 2009, Gesoğlu et al., 2009, Hwang and Khayat, 2010, Khayat and Long, 2010, Gao et al., 2012, Valcuende et al., 2012, Aslani and Maia, 2013, Valcuende et al., 2015, Bhirud and Sangle, 2017, Oliveira et al., 2017, Huynh et al., 2018, Esquinas et al., 2018, Atmaca et al., 2018) together with experimental results obtained from this investigation.

Table 5.3 presents a summary of the SCC mixes included in the database. The experimental database included test results from 27 different investigations, with a total of 230 SCC mixes. Additional information regarding the age of concrete curing (t_c), final age of concrete drying (t), relative humidity (RH), type of cement, fine to total aggregate ratio and filler type are also given in **Table 5.3.** The frequency distributions of different parameters are represented graphically as histograms in **Figure 5.5 to 5.14.** More details about experimental results from different sources in the literature can be found in **Appendix B (Table B.1)**.

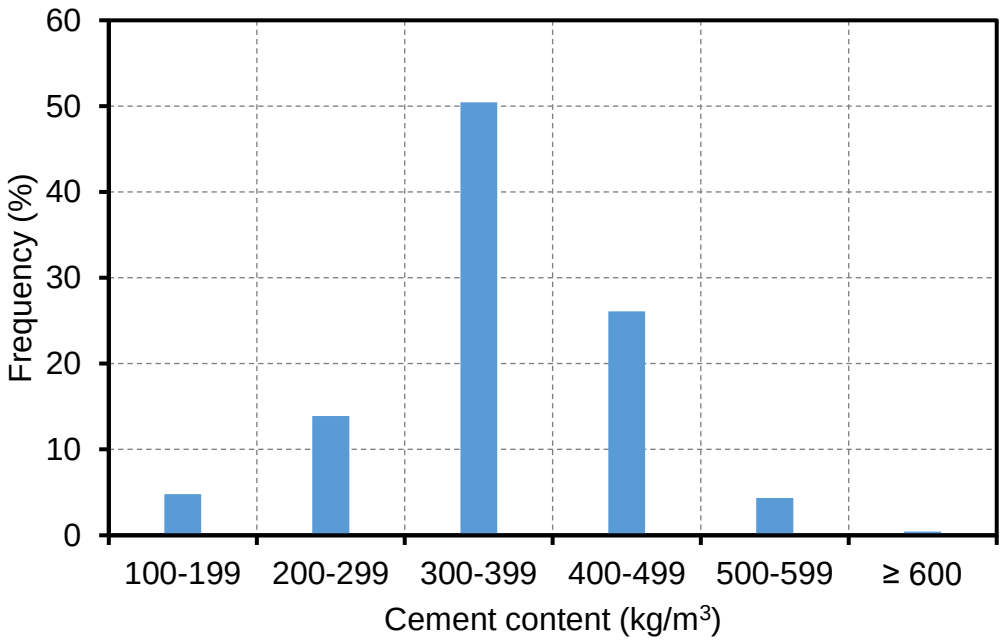

Figure 5-5 Distribution of cement content of SCCs included in database

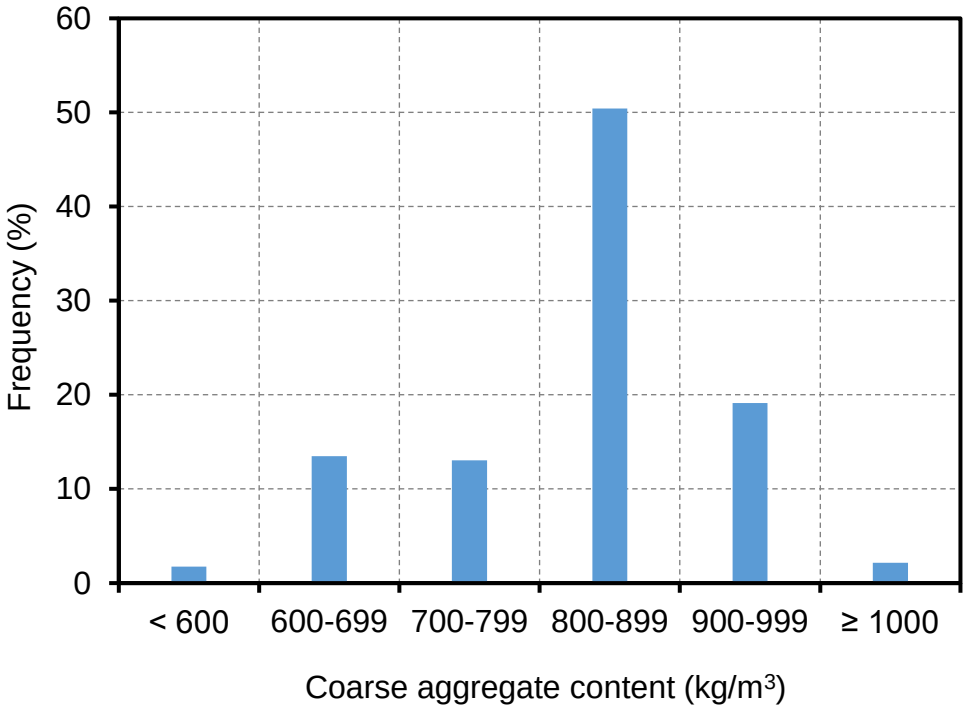

Figure 5-6 Figure 5.6 Distribution of coarse aggregates content of SCCs included in database

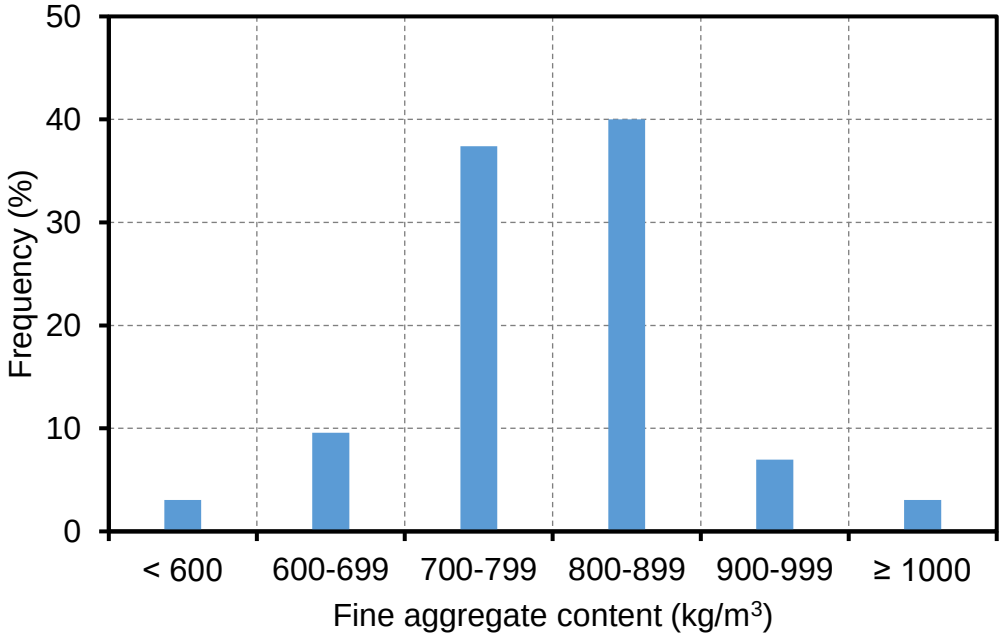

Figure 5-7 Distribution of fine aggregates content of SCCs included in database

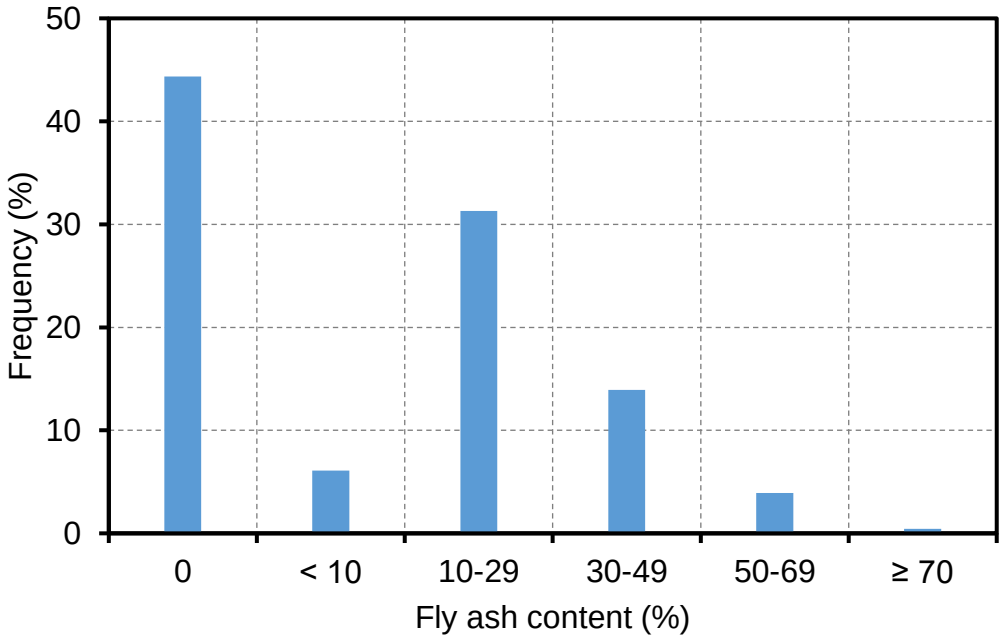

Figure 5-8 Distribution of fly ash content of SCCs included in database.

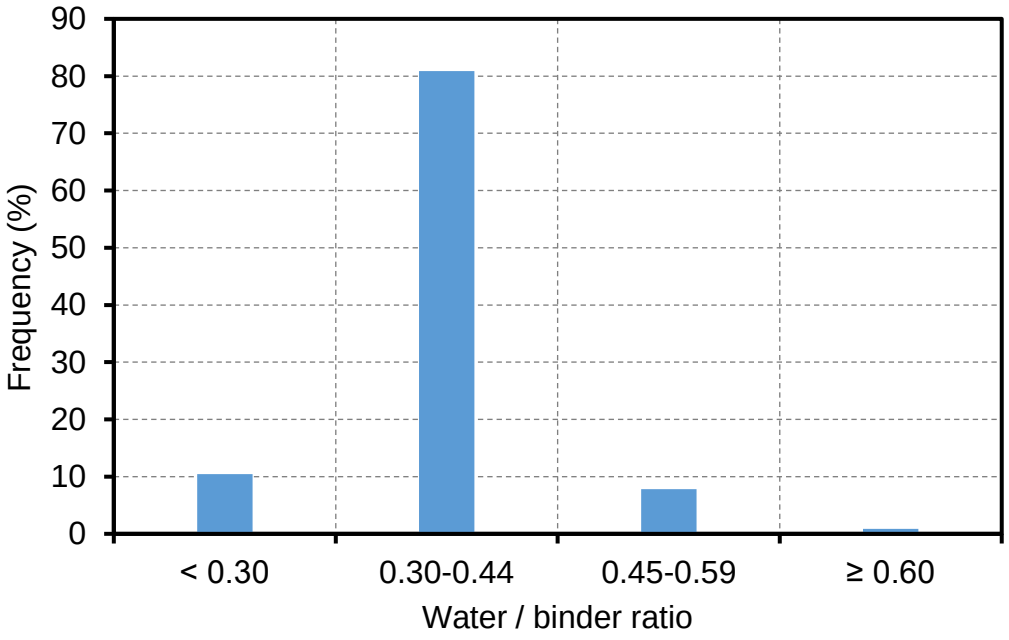

Figure 5-9 Distribution of W/B ratio of SCCs included in database

.

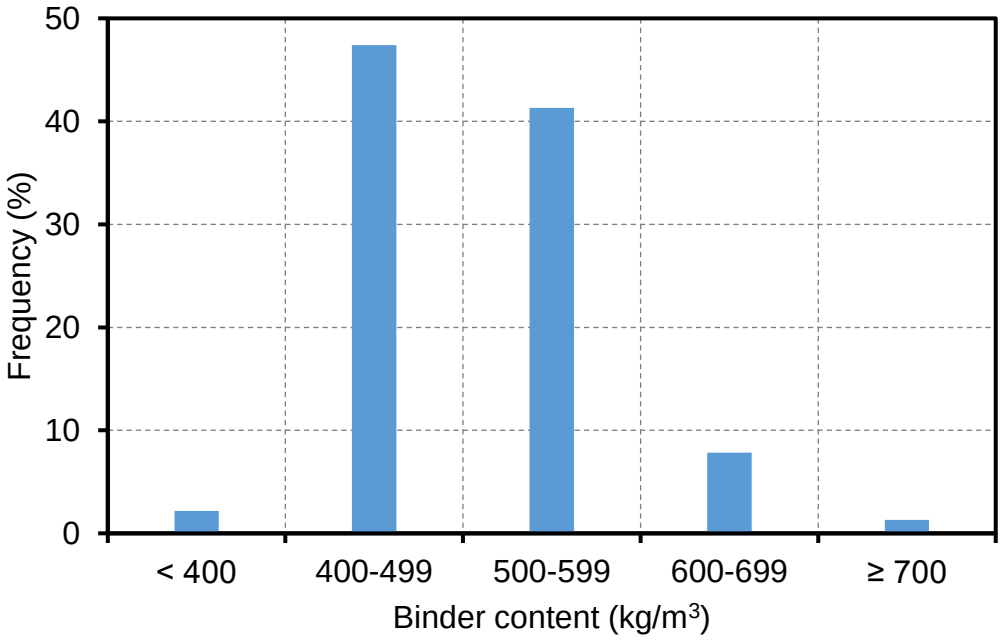

Figure 5-10 Distribution of binder content of SCCs included in database.

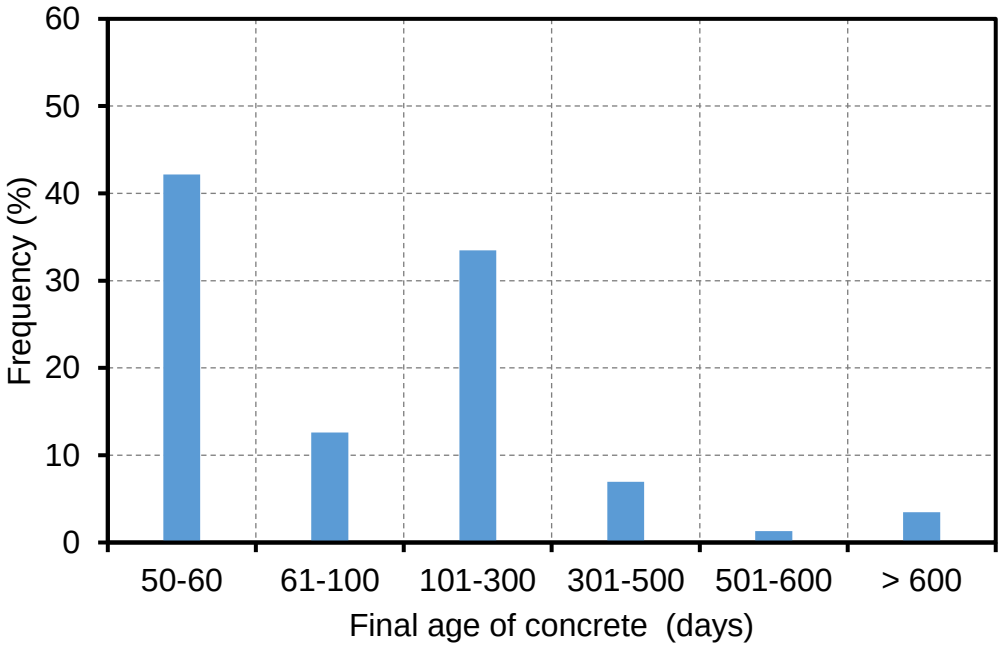

Figure 5-11 Distribution of final age of SCCs included in database

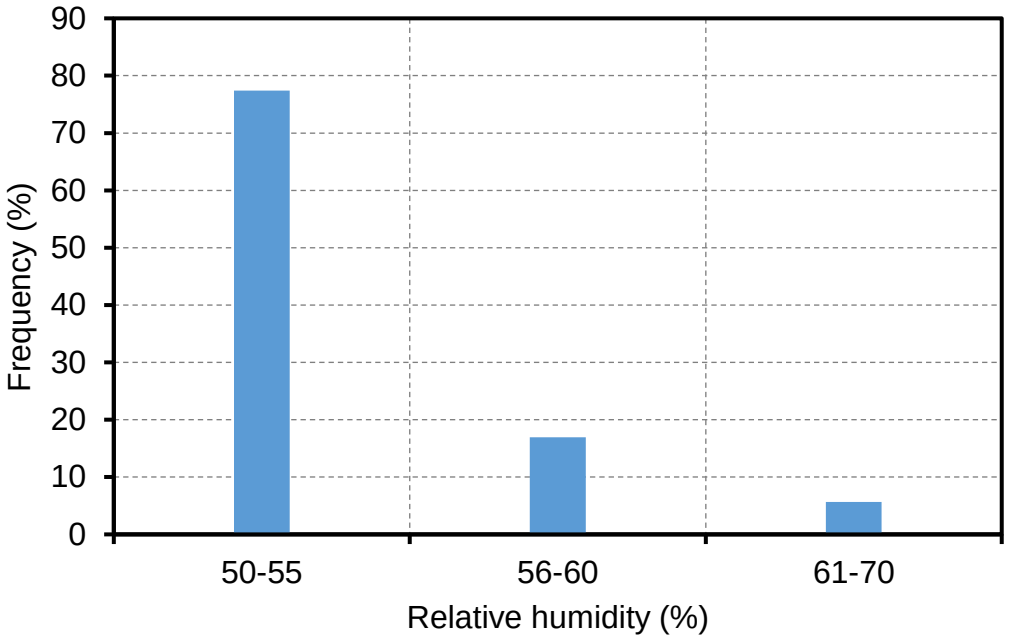

Figure 5-12 Distribution of relative humidity of SCCs included in database

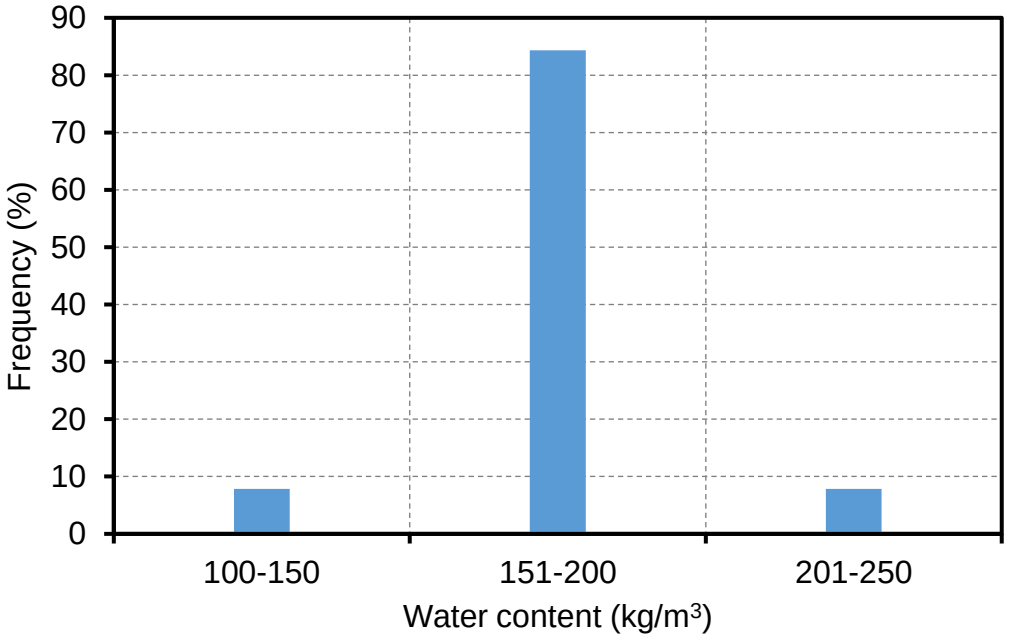

Figure 5-13 Distribution of water content of SCCs included in database

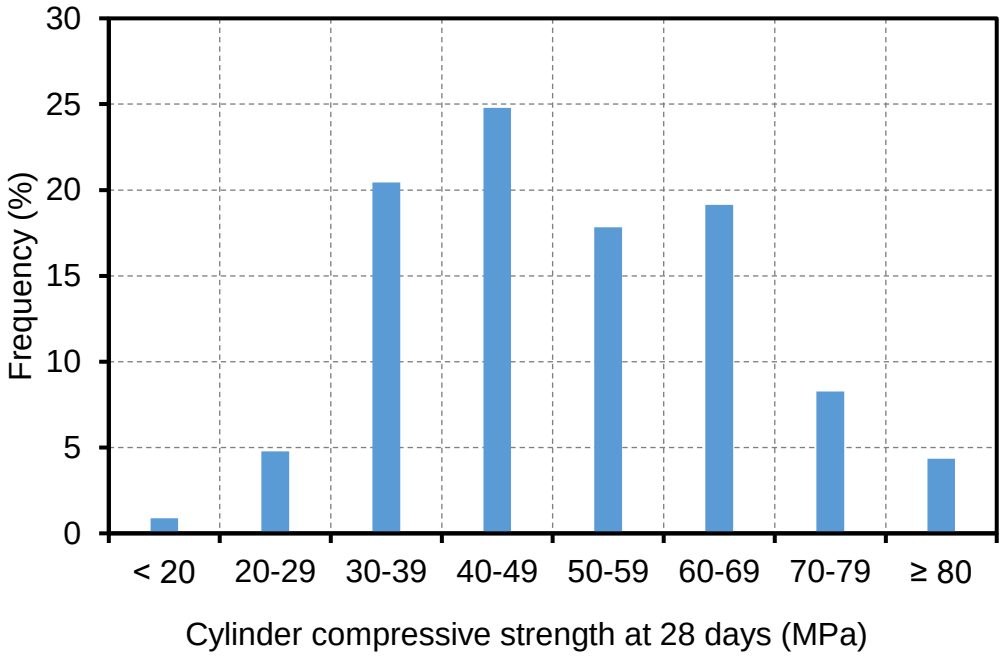

Figure 5-14 Distribution of 28 days cylinder compressive strength of SCCs included in database

Table 5-3 Summary of experimental database

Reference	No. of mixes	t_c (days)	t (days)	RH (%)	Cement type	Filler type
(Bouzoubaa and Lachemi, 2001)	8	1	200	50		
(Proust and Pons, 2001)	5	1	300	55	CEM I, II	Limestone, silica fume
(Collepardi et al., 2002)	9	1	60	50	CEM III	Fly ash, ground limestone
(Chopin et al., 2003)	5	1	500	50		
(Vieira and Bettencourt, 2003)	1	1	180	50	CEM I	
(Assié et al., 2003)	1	1	200	50	CEM I	Calcareous filler
(Horta, 2005)	6	1	200	50	CEM I, CEM II	Fly ash, GGBS
(Poppe and De Schutter, 2005)	6	1	100	60	CEM I	Fly ash, limestone
Turcry et al. (2006)	3	1	210	50	CEM I, CEM II	Limestone
(Rozière et al., 2007)	9	1	120	50	CEM I	Limestone
(Heirman et al., 2008)	7	1	98	60	CEM I, CEMIII	Limestone
(Khatib, 2008)	7	1	56	60	OPC assume Type I	Fly ash
(Loser and Leemann, 2009)	13	1	91	70	OPC, CEM II	Fly ash, limestone
(Loser and Leemann, 2009)	16					
(Gesoğlu et al., 2009)	65	1	50	50	ASTM Type I	Fly ash, silica fume, GGBS, metakaolin,
(Hwang and Khayat, 2010)	10	1	56	50	CEM I	Fly ash, silica fume, limestone
(Khayat and Long, 2010)	16				MS and HE (similar to ASTM C150 Type I/II/III and Type III)	Fly ash
(Gao et al., 2012)	3	1	100	50	OPC Type I	Fly as, clay
(Valcuende et al., 2012)	4	2	365	50		
(Aslani and Maia, 2013)	3	1,2,3	600	50	CEM I	limestone
(Valcuende et al., 2015)	7	1	365	50	CEM II	Limestone, fly ash
Current study (2016)	8	1	1000	50	CEM I	Fly ash
(Bhirud and Sangle, 2017)	2	1	112	50	OPC assume Type I	Fly ash
(Oliveira et al., 2017)	3	1	270	55	CEM I, CEM II	Fly ash
(Huynh et al., 2018)	3	1	120	60	OPC Type I	Fly ash, silica fume, GGBS
(Esquinas et al., 2018)	4	28	196	50	CEM I	Siliceous nature
(Atmaca et al., 2018)	6	1	60	50	CEM I	Fly ash, PVC
Total of mixes	230	GGBS = ground granulated blast slag, PVC= polyvinyl chloride dust				

5.5 Results and analysis

5.5.1 Comparison between experimental database and predicted drying shrinkage strain.

A comparison between measured values of drying shrinkage strains obtained from the database together with the experimental results obtained from current study and predicted values calculated by ACI 209R-92, BSEN-92, ACI 209R-92(Huo), B3 and GL2000 models are presented in **Figure 5.15** to **Figure 5.19**.

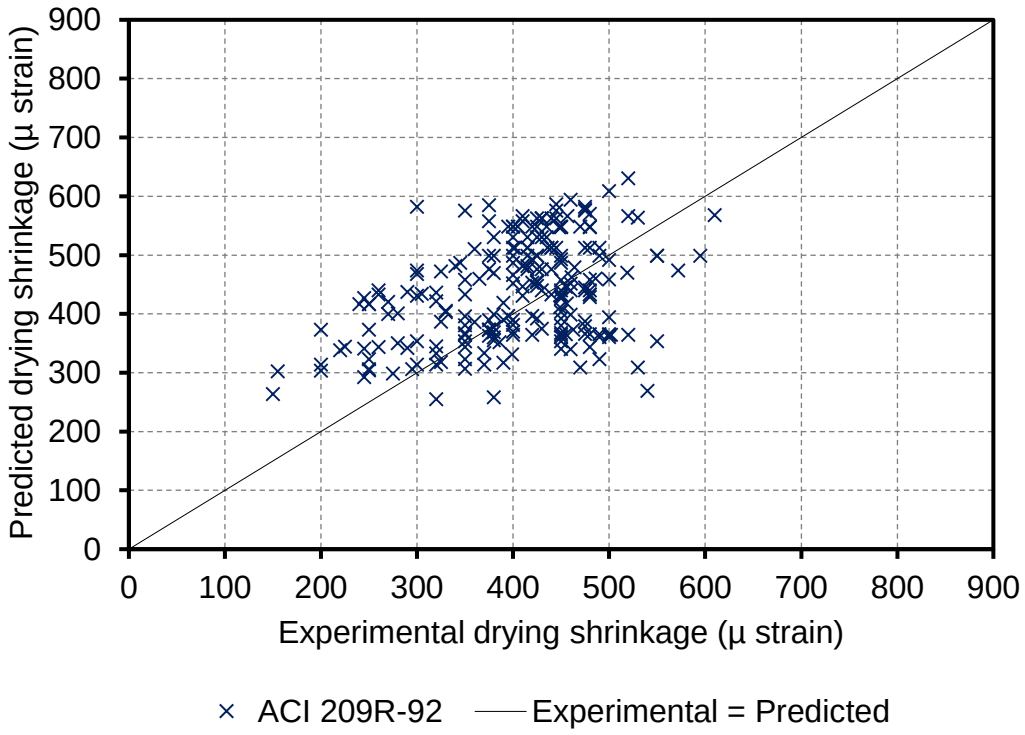

Figure 5-15 Comparison between experimental and predicted drying shrinkage strains of SCCs using ACI 209R-92 model

The diagonal lines in these figures represent where measured and predicted values are equal. For each model four statistical observations; mean, standard deviation, coefficient of variation (COV%) and mean absolute error (MAE%) of $\varepsilon_{Exp}/\varepsilon_{pred}$ were used to compare predictions with experimentally observed

drying shrinkage values as summarized in **Table 5.5**. The mean is an indication of how well the data is grouped about the regression line whereas COV is used to evaluate which model estimates the drying shrinkage strains with the least error. It was observed that the GL2000, ACI 209R-92 and ACI 209R-92(Huo) models had a tendency to overestimate the drying shrinkage values. The BSEN-92 had a slight tendency to overestimate as well. The B3 model appeared to underestimate drying shrinkage values and resulted in a large scattering compared to the other models with the highest mean of 1.53 and standard deviation, COV % and MAE% of 0.55, 35.90 and 55.40, respectively. The ACI 209R-92, ACI 209R-92 (Huo), and BSEN-92 models had mean predicted-to-calculated drying shrinkage ratios of 0.942, 0.869 and 1.171, respectively. However, GL2000 provided a better prediction of drying shrinkage compared to ACI 209R-92 and BSEN-92 with mean of 0.979.

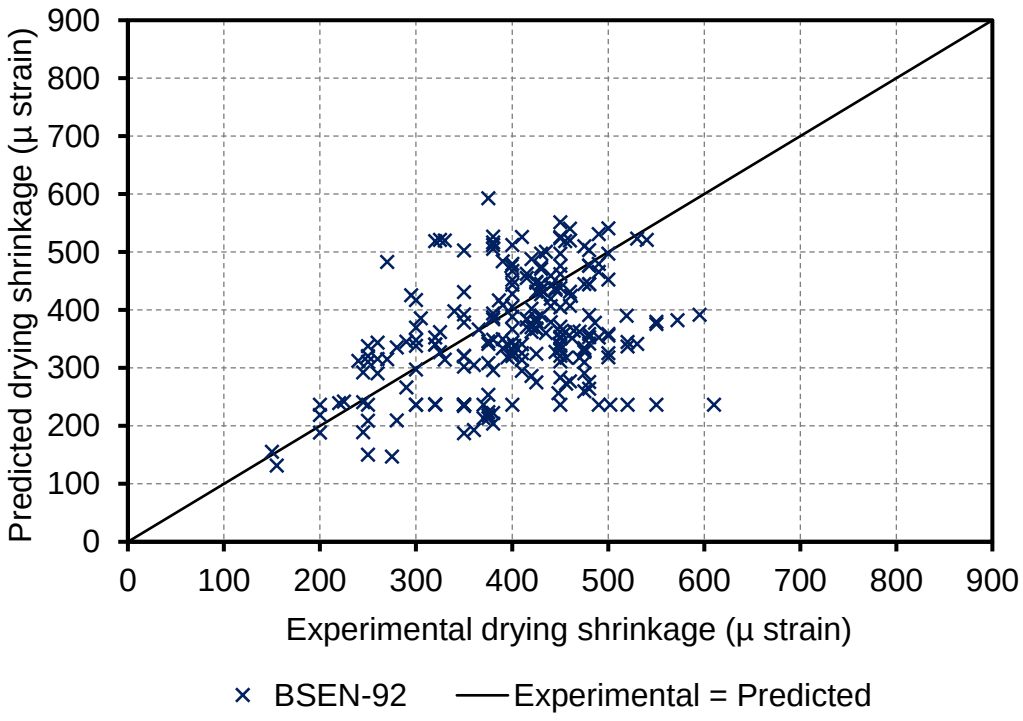

Figure 5-16 Comparison between experimental and predicted drying shrinkage strains of SCCs using BSEN-92 model

.

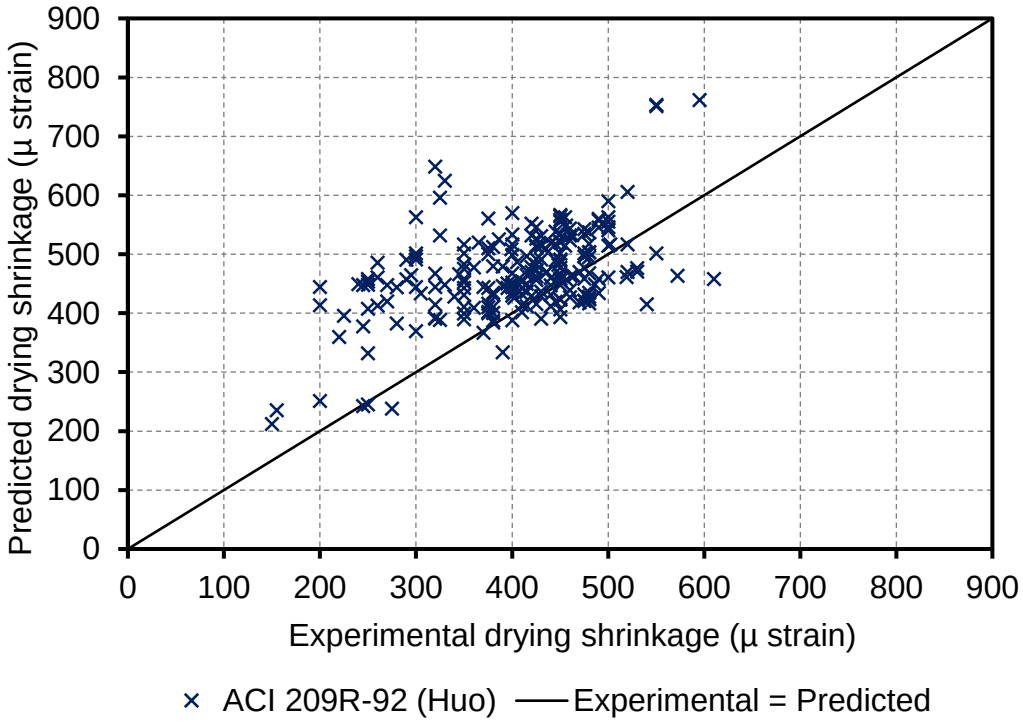

Figure 5-17 Comparison between experimental and predicted drying shrinkage strains of SCCs using ACI 209R-92 (Huo) model

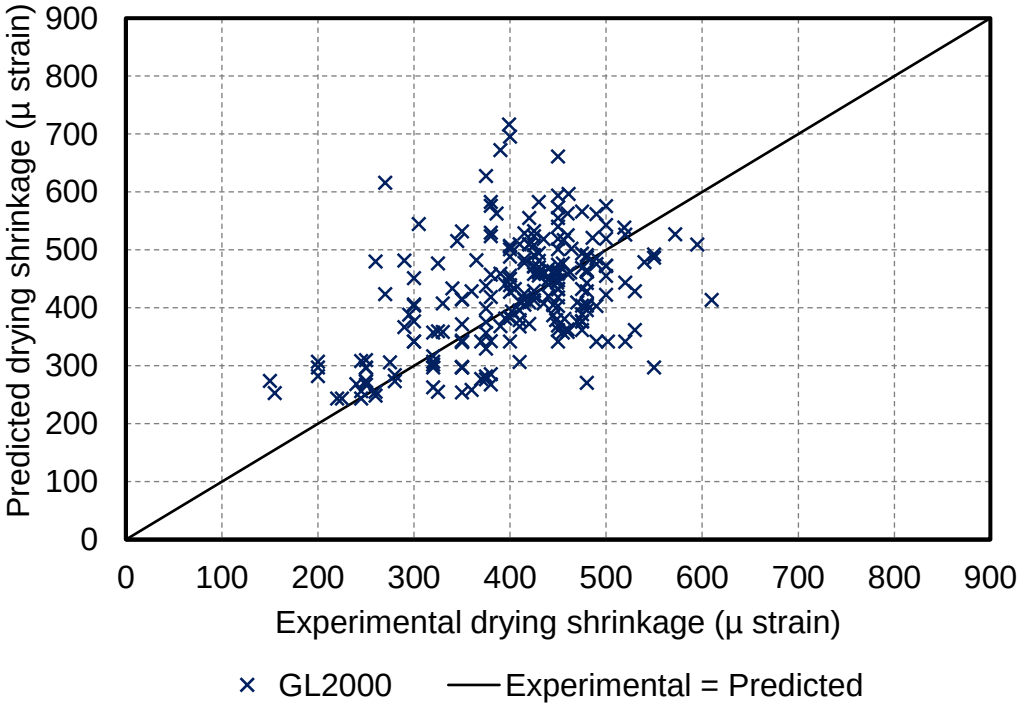

Figure 5-18 Comparison between experimental and predicted drying shrinkage strains of SCCs using GL2000 model

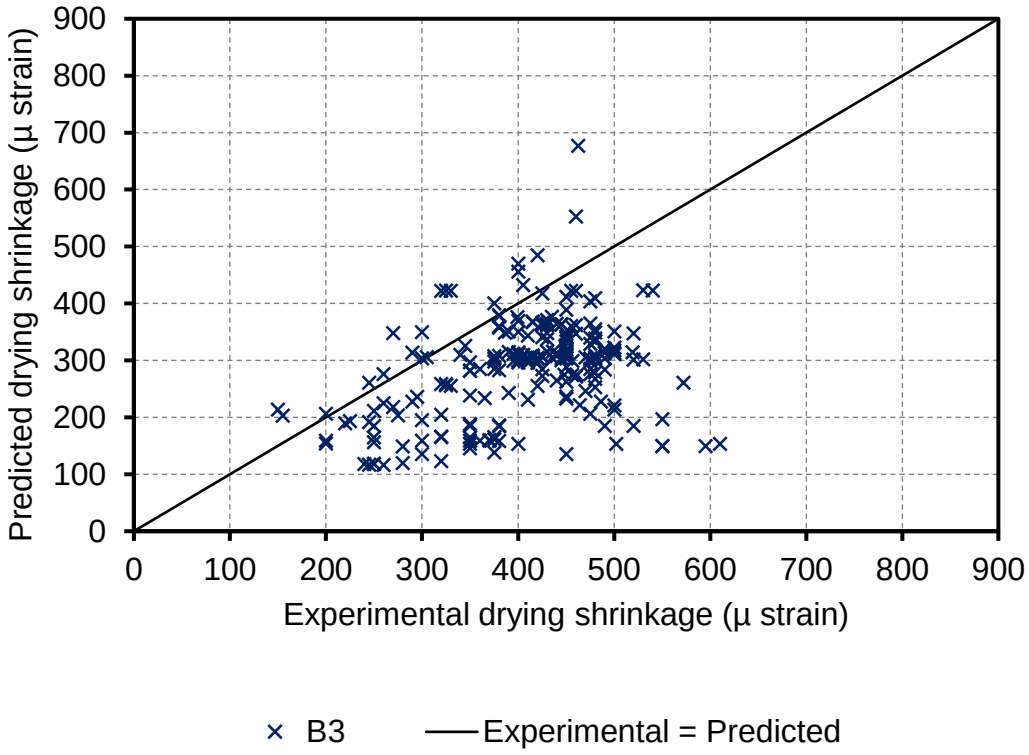

Figure 5-19 Comparison between experimental and predicted drying shrinkage strains of SCCs using B3 model

The variation values in statistical analysis results (mean, COV and MSE (%)) for all models could be related to the influence of various parameters on the drying shrinkage strain considered for each model.

As mentioned earlier in this study, the main parameters affecting drying shrinkage strain of SCC are compressive strength, cement content and water to binder ratio. However, each model has different parameters to calculate drying shrinkage strain. For example, compressive strength was considered as the main parameter to calculate drying shrinkage strain using the ACI 209R-92 (Huo) and GL2000 models while the ACI 209R-92 model considers cement content value to calculate drying shrinkage strain. The BSEN-92 and B3 models also consider compressive strength as one of main parameters to

calculate drying shrinkage strain. However, both models have taken into account two parameters as coefficients according to the cement type to calculate drying shrinkage strain.

Most of the experimental database used in this investigation has one type of cement, with different cement contents and compressive strengths. This could explain the difference in statistical results for the models.

Table 5-4 Summary of statistical results for drying shrinkage predicted by existing models

Predictive models	Mean	Standard deviation	COV (%)	MAE (%)
ACI-209	0.942	0.23	24.3	19.1
BSEN-92	1.171	0.34	28.5	271
ACI-209(Huo)	0.869	0.16	18.8	120
GL2000	0.979	0.14	16.5	16.7
B3	1.530	0.55	35.9	55.4

5.5.2 Evaluation of existing models for predicting drying shrinkage strain

The ratios of drying shrinkage strain experimental results obtained in this investigation to values predicted by ACI 209R-92, BSEN-92, ACI 209R-92(Huo), B3 and GL2000 models ($\eta = \varepsilon_{Exp} / \varepsilon_{Pred}$) at different ages are plotted in **Figure 5.20** to **5.24.** $\eta = \varepsilon_{Exp} / \varepsilon_{Pred}$, where; ε_{Exp} is the experimental value and ε_{Pred} is the predicted value.

η values under 1 indicate that a particular model overestimates the drying shrinkage strains and residual values above 1 indicate that the model underestimates them. The best model predictions for drying shrinkage occur when values of η are closely centred about the one axis and equally distributed under and above one axis. In this study, the η values are plotted against the

log time from 4 to 1000 days and the distribution of the η for all SCCs as percentages (%) are illustrated in the same figures. From **Figure 5.20** to **5.24** it can be observed that the ACI-209R-92, BSEN-92, ACI-209R-92 (Huo) and GL2000 models overestimated most of the drying shrinkage values while the B3 model significantly underestimated the values and resulted in a larger scattering compared to the other models. **Figures 5.20** to **5.23** show that the ACI-209, BSEN-92, ACI-209(Huo) and GL2000 models provided overestimations with η distributions of 72%, 59%, 80% and 84% respectively. The B3 model produced the lowest predicted drying shrinkage values compared to the experimental results with underestimations of η distributions of 80% as illustrated in **Figure 5.24.**

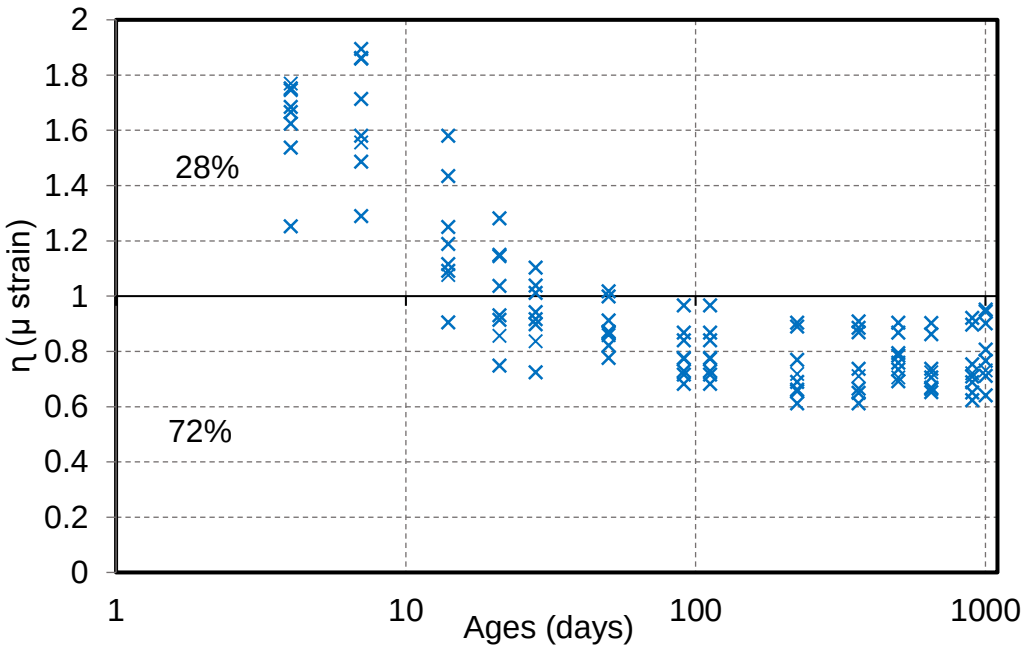

Figure 5-20 Experimental- to- Predicted values of SCC mixes against ages for ACI 209R-92 model

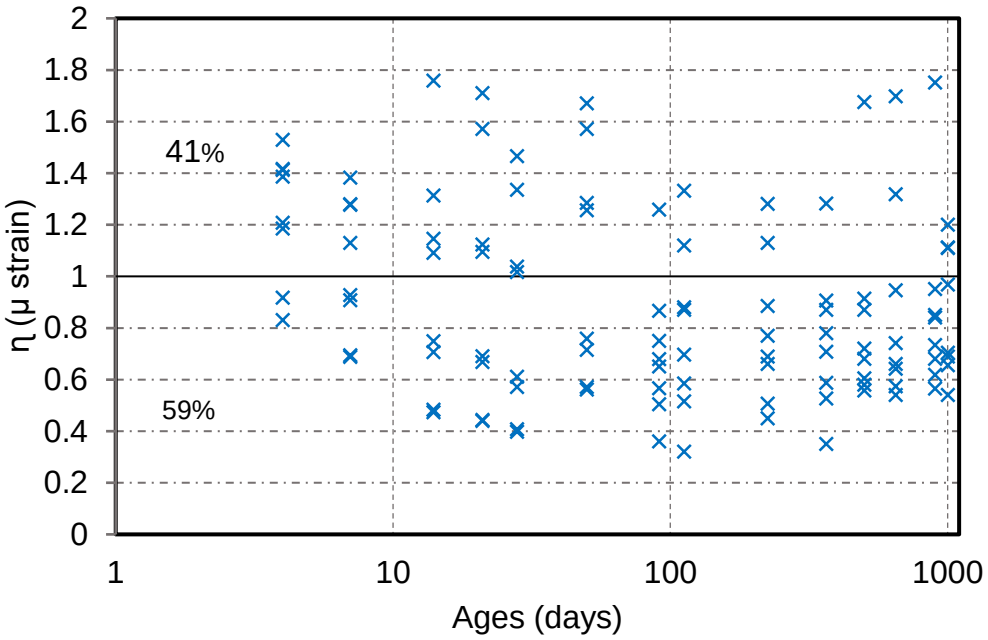

Figure 5-21 Experimental- to- Predicted values of SCC mixes against ages for BSEN-92 model

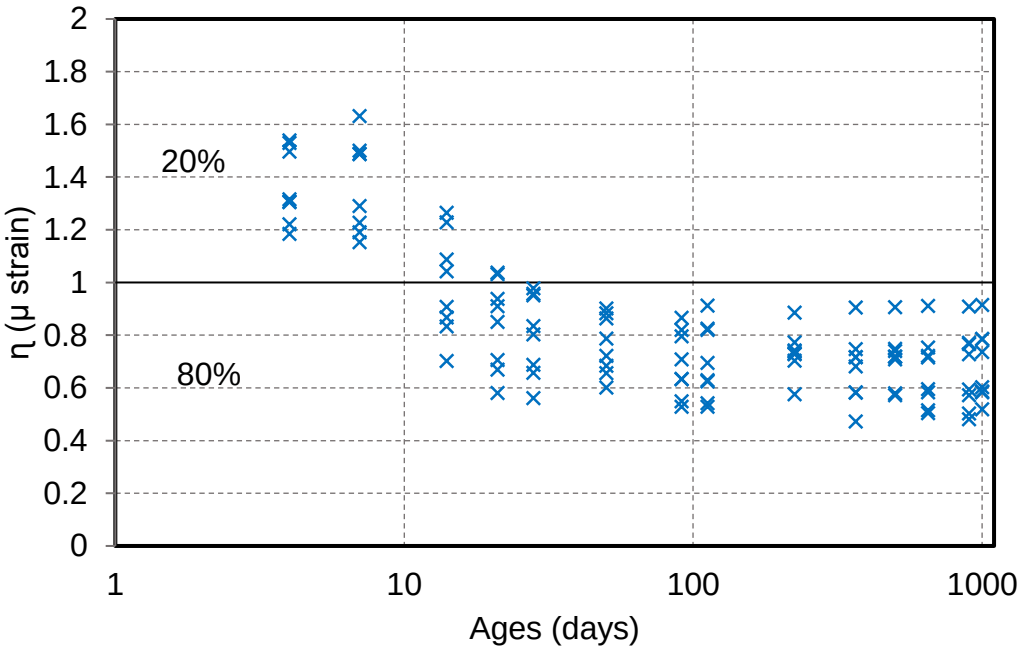

Figure 5-22 Experimental- to- Predicted values of SCC mixes against ages for ACI 209R-92(Huo) model

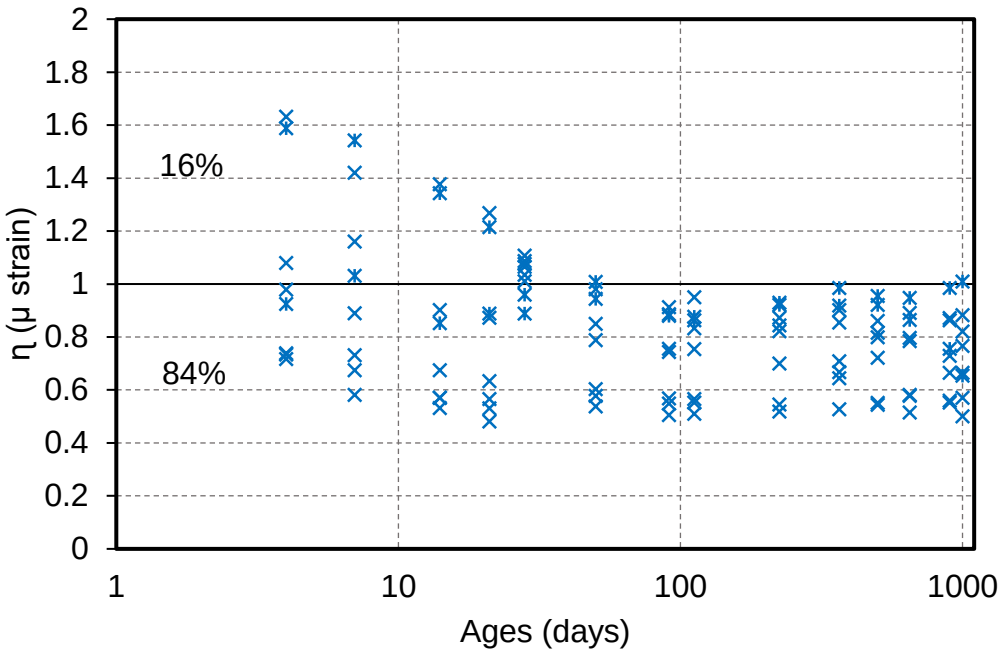

Figure 5-23 Experimental- to- Predicted values of SCC mixes against ages for GL2000 model

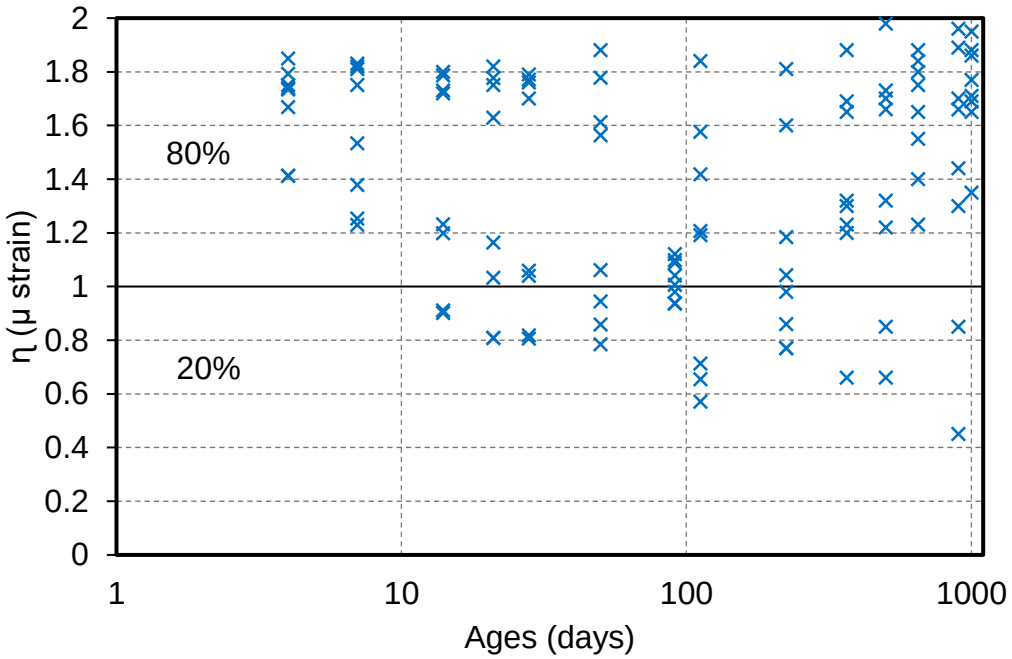

Figure 5-24 Experimental- to- Predicted values of SCC mixes against ages for B3 model

.

It could be concluded that most of the models that were shown, overestimated the values but provided good predictions. However, it is clearly that at early ages up to 21 days most of the models showed underestimated characteristics.

5.6 Concluding remarks

Based on the computational work for comparison between five drying shrinkage models in this investigation, the following conclusions can be highlighted:

1. Most of the models used in this study tend to have overestimating characteristics providing good predictions.
2. GL2000 provided a better prediction of drying shrinkage compared to the other models with the lowest coefficient of variation and mean absolute errors of 16.5% and 13.7%, respectively. Moreover, the ACI 209R-92 and ACI 209R-92-(Huo) model exhibited a good drying shrinkage prediction compared to BSEN-92 and B3 models with mean of 0.942 and 0.869 respectively and lower mean absolute errors of 19.1% and 16.7%, respectively.
3. The B3 model strongly appeared to underestimate the drying shrinkage strain and resulted in a larger scattering compared to the other models with the highest mean of 1.33.
4. Considering experimental-to-predicated values (η) of drying shrinkage strains against different ages using experimental results obtained in this investigation, it is clearly seen that the GL2000, ACI 209R-92 and ACI

209R-92(Huo) models provide good prediction of the drying shrinkage stains of SCCs among other models.

5. The existing models used in this investigation have considered different parameters to calculate the drying shrinkage strain of SCC. This could explain the difference in the models accuracy and statistical result for each model.
6. Selection of the database for studying the applicability of drying shrinkage strain prediction models can influence the conclusions on the performance of the models.
7. SCC mixtures are usually designed with large quantities of mineral fillers which mainly affecting drying shrinkage of SCC. Therefore, new prediction model considering cement replacement materials as one of the main parameters to calculate drying shrinkage of SCC could provide a good prediction of SCC drying shrinkage strain with higher accuracy.

CHAPTER SIX - PREDICTION OF DRYING SHRINKAGE OF SCC USING ARTIFICIAL NEURAL NETWORK

6.1 Introduction

The aim of this chapter is to develop a model which predicts the drying shrinkage strain of self-compacting concrete (DSSCC). As mentioned in the previous chapter all the existing models used to predict DSSCC have considered different parameters for calculating shrinkage which vary from one model to another, thus affecting the models accuracy. The same database that was used in the previous chapter to study the applicability of the existing models is used as well to achieve the aims of this chapter. The chapter will cover applications of artificial neural networks (ANNs), background and principles of artificial neural networks (ANNs), training process of artificial neural networks, experimental data, construction of the ANN model, parametric study, comparison between the prediction given by artificial neural network models (ANNMs) and different existing models and concluding remarks.

6.2 Applications of Artificial neural network

Many researchers have developed different modelling methodologies to predict the strength of SCC and some of its properties. Artificial neural networks (ANNs) have been widely utilized in many applications of civil engineering to model and estimate concrete properties such as compressive strength of concrete (Prasad et al., 2009, Duan et al., 2013, Öztaş et al., 2006, Uysal and Tanyildizi, 2011, Bilim et al., 2009, Sobhani et al., 2010, Ni and

Wang, 2000), drying shrinkage of normal concrete (Bal and Buyle-Bodin, 2013), concrete durability (Jepsen, 2002), concrete workability (Bai et al., 2003), mechanical performance of SCC (Nehdi et al., 2001), chloride penetration and permeability in concrete (Ghafoori et al., 2013, Song and Kwon, 2009), carbonation behaviour in concrete (Kwon and Song, 2010), lifetime period of novel materials in civil engineering (Freitag et al., 2009), damage assessment of prestressed concrete beams (Jeyasehar and Sumangala, 2006). ANNs are also successfully applied in the modelling of shear strength of concrete with fibre reinforced polymer (Bashir and Ashour, 2012). All of the previous studies concluded that ANN is a suitable model used for prediction of fresh and hardened concrete properties.

According to Gonzalez (2000) there are some advantages of using ANN techniques over other regression techniques such as;

- ✓ High tolerance to noisy data.
- ✓ Ability to classify untrained patterns.
- ✓ Well-suited to continuous valued inputs and outputs.
- ✓ Adaptive learning: Ability to adapt its weights to changing environments.
- ✓ Ability to successfully model nonlinear relationships.
- ✓ Do not require prior information on the functional form of a relationship.
- ✓ The same architecture is very flexible.

Despite their wide applications, ANNs also have some drawbacks such as;

- ➢ Long training time.
- ➢ They usually require large samples.

- It is difficult to interpret the estimated network weights, ANN applications are frequently viewed as black boxes.

The use of the ANN approach to describe and predict the properties of fresh and hardened SCC is not new. However, this study is the first attempt to predict the drying shrinkage strain of SCC using ANN modelling.

6.3 Artificial neural network background

In recent years, there has been a growing interest in computational models that operate in a similar way to that of the biological neural system of the human brain. Soft computing techniques called artificial neural networks (ANNs) have been increasingly applied in different fields of civil engineering (Flood and Kartam, 1994, Adeli, 2001). The first computational, trainable neural networks were developed by Rosenblatt (1962) as well as by Rumelhart et al. (1986). This section will describe the basic concepts of ANNs and topology of the ANN concept of neural networks.

The ANNs consist of a number of interconnected groups of artificial neurons. The basic model of an artificial neuron is shown in **Figure 6.1.** Each of neuron is fully connected to the others through connection weights and receive input signals from neurons linked to it. Each neuron also has a single threshold value (bias). The weights are adjusted to minimize the error between the network output and experimental target results after that the neuron activates and passes the signal through a transfer function and sends it to neighbouring neuron (Livingstone, 2008). This process can be expressed as a mathematical model in **Eq.6.1.**

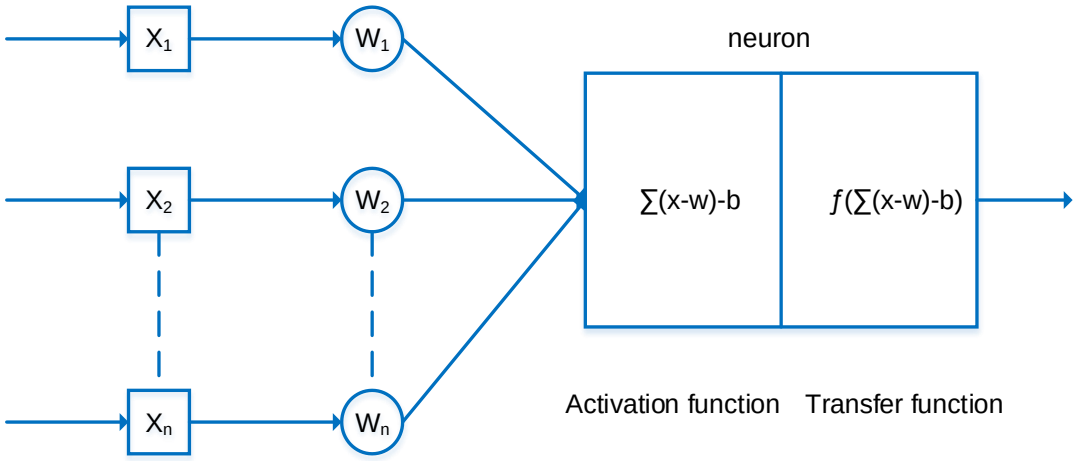

Figure 6-1 Artificial neuron model

$$y = f\sum_{i=0}^{n} w_i\ x_i\ - b \tag{6.1}$$

where; y is the output, f is the transfer function, w_i (w_1, w_2, … w_n) is the weight of input xi (x_1,x_2, … x_n) and b is a bias.

Different activation functions have been used in ANN models. The most common activation function used in the construction of ANNs is the sigmoid transfer function presented in Equation 6.2. This function produces an output in the range from 0 to 1. Thus, the input values are usually linearly scaled to this range before being fed to the network for processing (Fausett, 1994).

$$f_{(y)} = \frac{1}{1+e^{-y}} \tag{6.2}$$

6.3.1 Topology of neural networks

ANNs can be used to model any complex relationships between inputs and outputs in data (Prasad et al., 2009, Bal and Buyle-Bodin, 2013). Three important steps must be considered in constructing a successful artificial neural network; network architecture, training, and testing. The basic aspects

of network architecture consist of the number of hidden layers between the input and output layers, the number of processing units in each hidden layer, the pattern of connectivity among the processing units, and the activation (transfer) function employed for each processing unit. These aspects change from one network to another, leading to a wide variety of network types.

To date, there are no fixed guidelines in selecting the number of hidden layers and neurons in each layer. Boger and Guterman (1997) mentioned that the number of hidden layer neurons are 2/3 (or 70% to 90%) of the size of the input layer. Karsoliya (2012) reported that the number of neurons in the first and second hidden layers should be kept nearly equal so that the network can be trained easily. Also Blum and Rivest (1989) suggested that the size of the hidden layer neurons is between the input layer size and the output layer size. However, no study succeeds in finding the optimal formula for calculating the number of neurons that should be kept in the hidden layer. A starting point, as suggested by (Hill et al., 2006), is one hidden layer with the number of neurons equal to the half of the sum of input and output neurons.

6.4 Training process of neural networks

The training process can occur in a supervised or unsupervised manner. Supervised training means that the network is provided with sets of training data that include the expected output for each set of input and the network is told what to learn. There are no target outputs available in unsupervised training and the network must modify its weights and biases in response to the inputs only by categorizing the input patterns into a finite number of classes (Nehdi et al., 2001).There are several methods and techniques to train a

network. The choice of learning algorithm has a significant impact on the performance of the ANN models (ANNMs). The most applicable network in modelling the performance of concrete is the multi-layer back propagation (MBP). MBP is frequently used because of its efficient generalization capabilities. Many variations of the back propagation logarithm training are provided in the MATLAB Toolbox including;

- **Scaled conjugate gradient (trainscg);** this algorithm takes less memory training and automatically stops when generalization stops improving, as indicated by an increase in the mean square error of the validation samples.
- **Bayesian regularization (trainbr);** this algorithm typically takes more time, but can result in good generalization for difficult, small or noisy datasets. Training stops according to adaptive weight minimization (regularization).
- **Levenberg- Marquardt (trainlm);** this algorithm typically takes more memory but less time. Training automatically stops when generalization stops improving, as indicated by an increase in the mean square error of the validation samples.

The most important issues in ANNMs learning is the adjustment of weights. The number of training iterations (epochs) is a core parameter in weight adjustment. An epoch is defined as one weight update or training iteration. For each epoch, the learning algorithm builds a different mode. If an ANN is trained up to 1000 epochs for example, that means that the learning algorithm has to move through 1000 different models to reach an optimal solution. If the number of training iterations is set too low the ANNMs may not reach a sufficient level

of learning, resulting in underfitting, whilst too many iterations can lead to overfitting the data. Overfitting and underfitting of ANNMs cause reduced generalization ability (Paola and Schowengerdt, 1997). Therefore, the number of iteration is important for ANNM training. It is difficult to identify the value of the maximum number of training iterations required for optimal generalization ability. However, Moyo and Sibanda (2014) suggested that a maximum value of training epochs between 85 and 5000 could be used for generalization of ANNMs. Moreover, Wan et al. (2009) reported that the degree to which a model overfits or underfits the data is related to important factors such as; size of the network architecture, size of the training set, the learning algorithm, the choice of training schedule and the size of the learning rate.

The optimization of the ANNM model is conducted by using the minimization of mean absolute error (MAE %), MAE% measures the average of the squares of errors.

6.5 Experimental database

A database of SCC for training and testing of ANNMs is produced by collecting data from different experimental investigations available in the literature together with experimental results obtained from this investigation. To develop ANNMs for drying shrinkage strains, 230 various mixes with different material proportions were collected (Bouzoubaa and Lachemi, 2001, Proust and Pons, 2001, Collepardi et al., 2002, Chopin et al., 2003, Vieira and Bettencourt, 2003, Assié et al., 2003, Horta, 2005, Poppe and De Schutter, 2005, Turcry et al., 2006, Rozière et al., 2007, Heirman et al., 2008, Khatib, 2008, Loser and Leemann, 2009, Gesoğlu et al., 2009, Hwang and Khayat, 2010, Khayat and

Long, 2010, Gao et al., 2012, Valcuende et al., 2012, Aslani and Maia, 2013, Valcuende et al., 2015, Bhirud and Sangle, 2017, Oliveira et al., 2017, Huynh et al., 2018, Esquinas et al., 2018, Atmaca et al., 2018). The range of different input parameters used to train the ANNMs is given in **Table 6.1.**

The back propagation algorithm in MATLAB (R2016b) recommends to divide the database into three phases; training, validation and testing phases (Beale et al., 2016). In this study the input data are divided into three parts, namely 75% for the training phase, 5% for the validation phase and 20% for the testing phase.

Table 6-1 Range of components of data sets for drying shrinkage prediction (230 mixtures)

Artificial neural networks input parameters	Range	
	minimum	maximum
Water to binder ratio,(W/B)	0.21	0.61
Cylinder 28-days compressive strength, f'_c (MPa)	9	92
Binder content, B (kg/m^3)	350	840
Cement content , C (kg/m^3)	100	665
Fly ash, FA (%)	6	80
Relative humidity, RH (%)	50	70
Fine aggregate to total aggregates ration, F/T$_a$	0.32	1

The testing phase for checking the network employs test specimens from the database, which have not used in the training process. The main purpose of the validation phase is to arrest training when generalization stops improving. The frequencies of each of the input parameters used across the range of 230 test results for training, testing and validation are presented graphically as histograms in **Figure 6.2** to **Figure 6.8.**

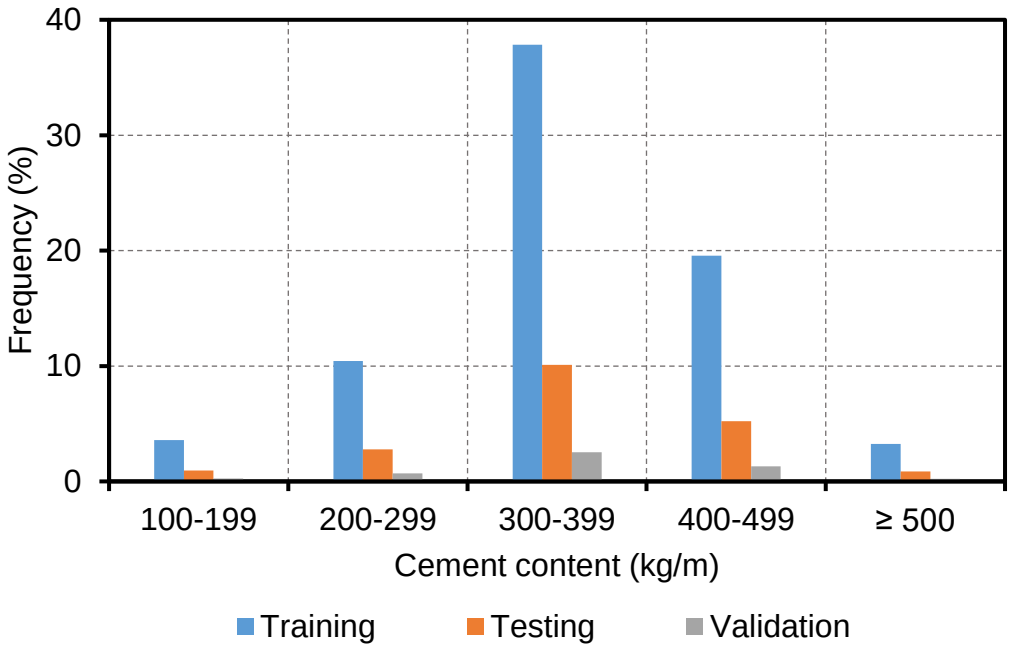

Figure 6-2 Frequency distribution of cement content across the range of 230 tests

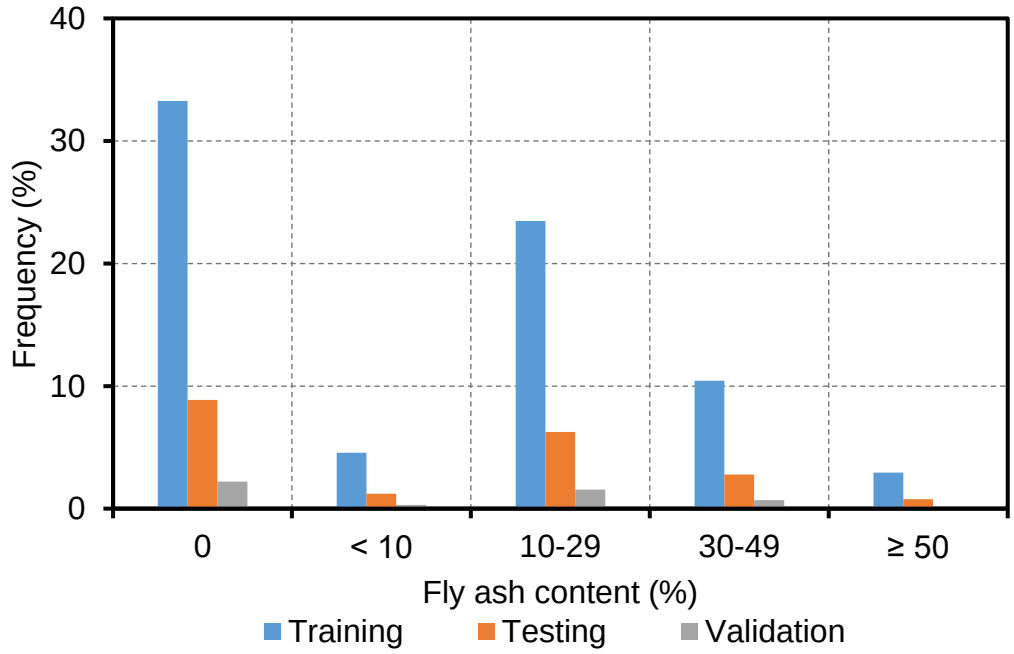

Figure 6-3 Frequency distribution of fly ash % across the range of 230 tests

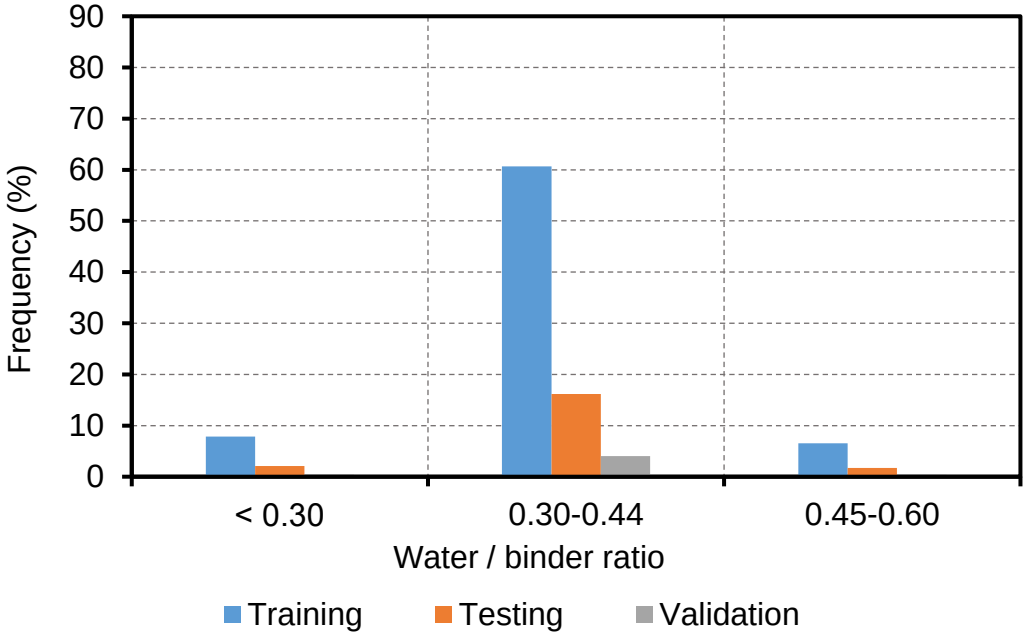

Figure 6-4 Frequency distribution of W/B ratio across the range of 230 tests

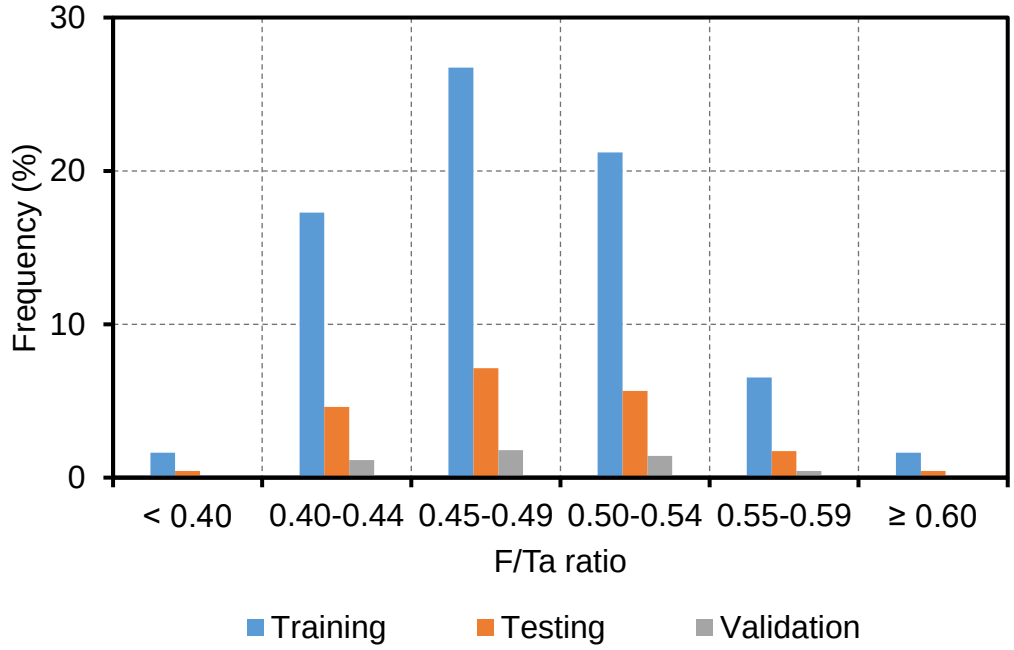

Figure 6-5 Frequency distribution of F/Ta ratio across the range of 230 tests

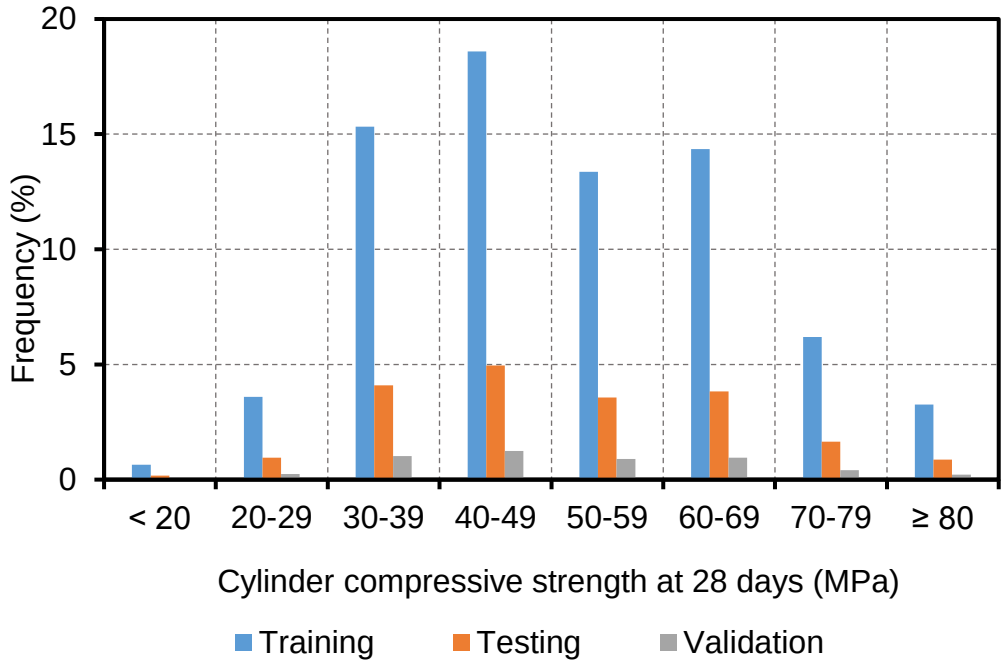

Figure 6-6 Frequency distribution of 28-day compressive strength across the range of 230 tests

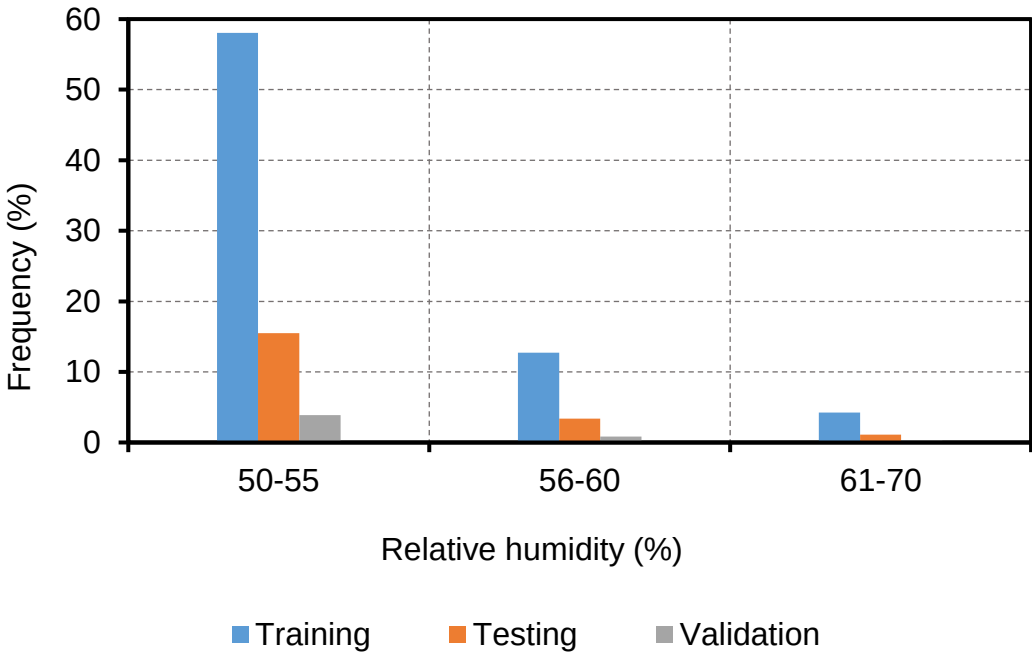

Figure 6-7 Frequency distribution of RH across the range of 230 tests

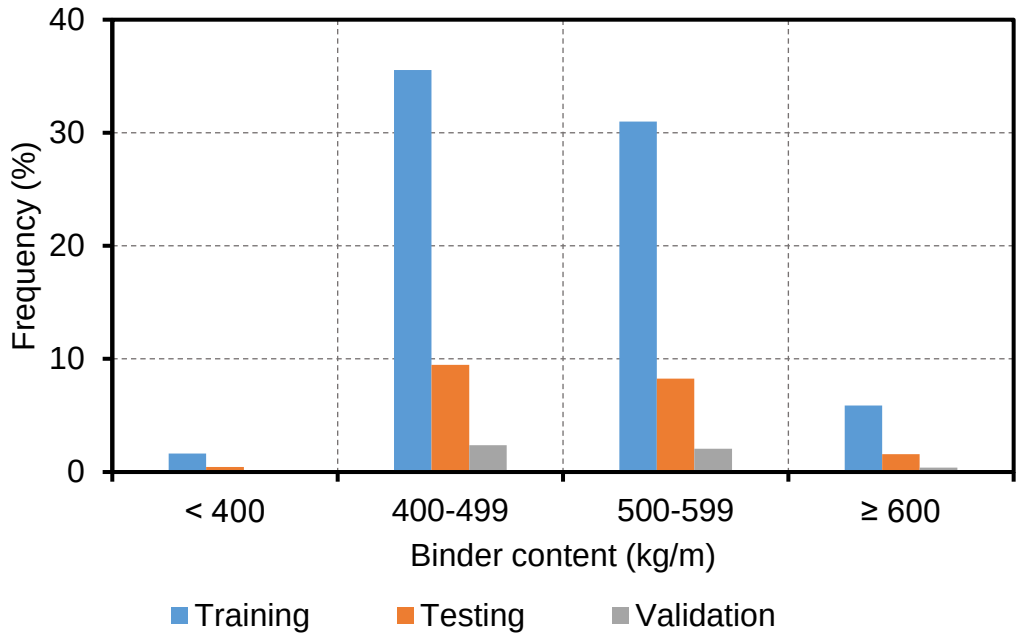

Figure 6-8 Frequency distribution of binder content across the range of 230 tests

6.5.1 Data normalisation

As mentioned early in Section 6.3 the most common activation function used in the construction of ANNs is the sigmoid transfer function. The sigmoid function is nonlinear with upper and lower limits of output between 1 and 0, respectively, therefore, the database must be normalised before training the network between the upper and lower bounds of the activation transfer function. In this model all of the database were normalised to the range between -1 and +1 to improve the learning speed of the ANNM. As reported by Kaastra and Boyd (1996) normalising the input and output parameters before they are used in training the ANNM is important for many reasons, for example ANN training can be made more efficient, giving rise to faster training times, it is difficult to work with high dimensional data and a reduction of data dimensions leads to an efficient pruning of the data space. Another advantage

of normalising the data is reduction of noise that prevents a good approximation of a function by the ANN model. In this investigation, the normalisation of the training database was carried out using the following equation;

$$I_n = \frac{2\times(I-I_{min})}{I_{max}-I_{min}} - 1 \quad (6.2)$$

where; I_n and I are the normalised and non-normalized input values, respectively, I_{max} and I_{min} are the maximum and minimum input values, respectively.

6.6 Construction of ANN model

In this study the neural network toolbox available in MATLAB (R2016b) was constructed to build the current artificial neural network model (ANNM) (Natic, 2016). A multi-layered neural network back-propagation (MBP) with a Levenberg-Marquardt training algorithm (trainlm) was adopted. The sigmoid transfer function and the maximum number of iterations (epochs) was set at 1000. A trial-and-error approach was adopted to create a neural network model with hidden layers. Training, testing and validation of the model were performed using 230 sets of experimental results, and then the predicted results were compared with the experimental results. Two ANNM sets with different numbers of hidden layer neurones were constructed, the input parameters affecting drying shrinkage strain of SCC (DSSCC) for each set are presented as follows;

ANNM1 set: The input layer of this network model to predict DSSCC consists of 5 neurons as; water to binder ratio (W/B), cylinder compressive strength of

concrete (f'_c), binder content (B), relative humidity (RH) and fine to total aggregates ratio (F/Ta). The output neural network layer is drying shrinkage strain (ε).

ANNM2 set: The input layer of this network model to predict DSSCC consists of 5 neurons as; water to binder ratio (W/B), fly ash content (FA), cylinder compressive strength of concrete (f'_c), relative humidity (RH) and ratio of fine to total aggregate (F/T_a). The output neural network layer was the drying shrinkage strain (ε). Only 128 databases that contenting fly ash as cement replacement were used in this model (ANNM2).

The number of hidden layers was one for all ANNM sets with different numbers of neurons and one output. The network architecture for each set is shown in **Figures 6.9** and **Figure 6.10**. I_1 to I_5 represent the input layer one to input layer five.

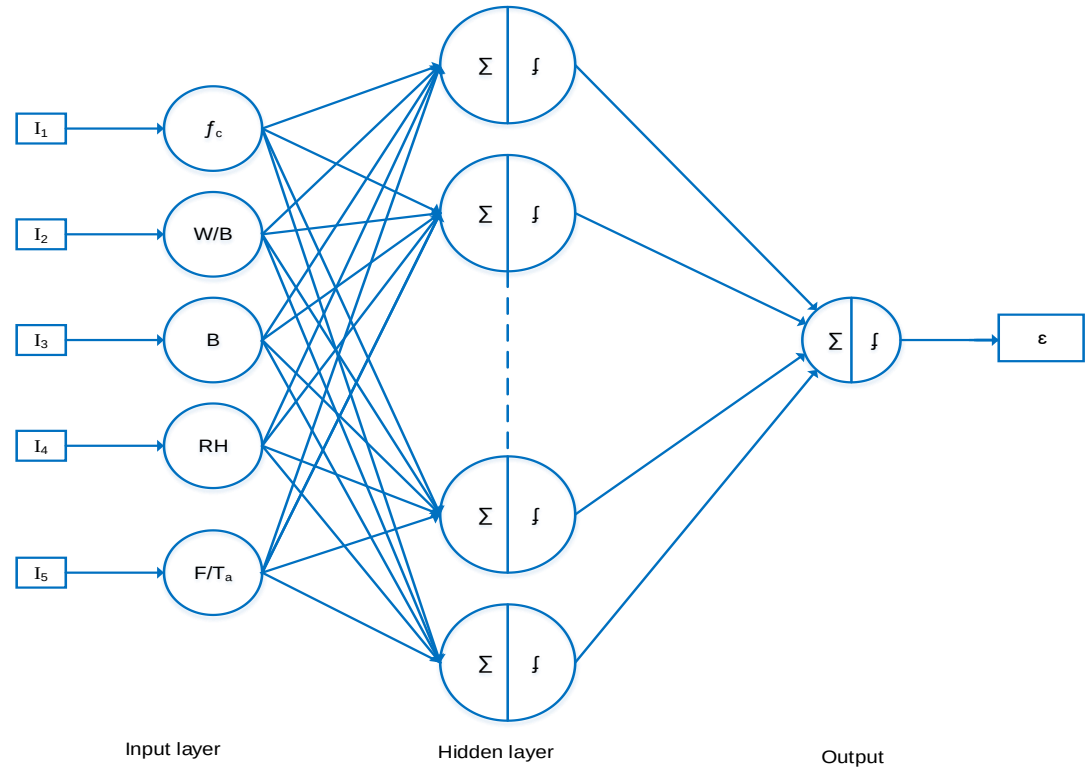

Figure 6-9 ANNM1 model architecture

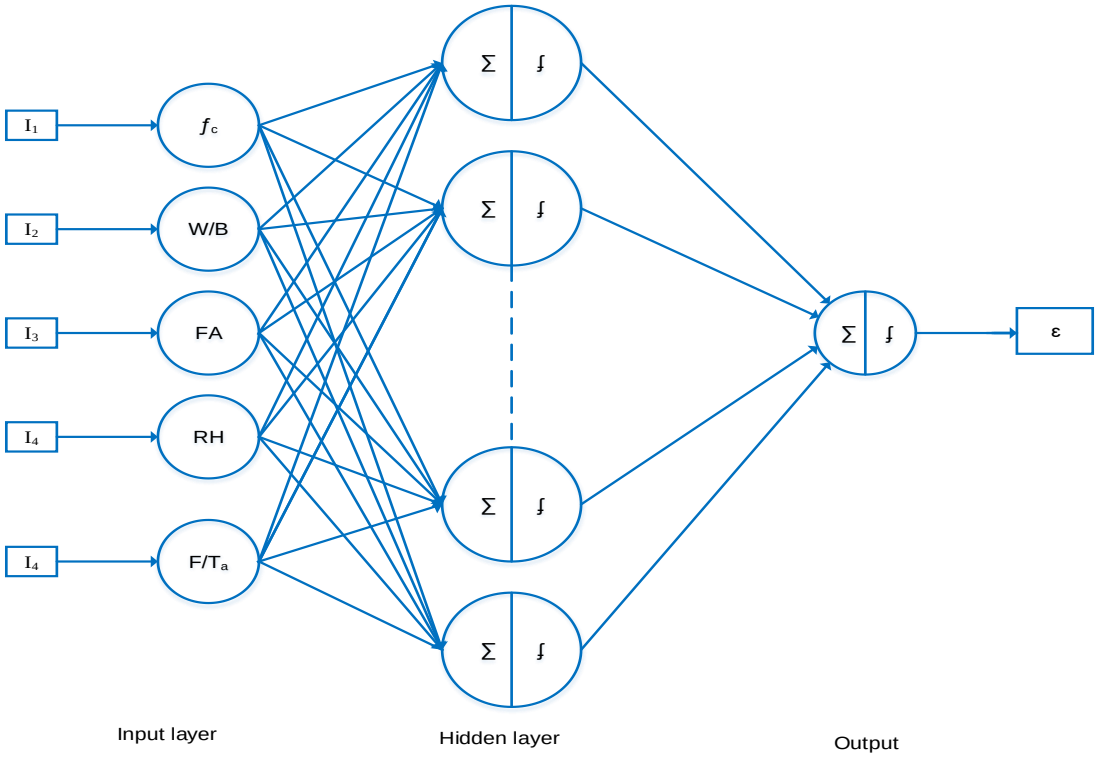

Figure 6-10 ANNM2 model architecture

6.6.1 Performance of developed ANNMs models

In this study many numbers of architecture of the ANNs with different training algorithms and transfer functions were tested as given in **Table 6.2**. The Levenberg- Marquardt training algorithm (trainlm) was chosen at the end for both models (ANNM1 and ANNM2). Four different statistical performance measures were used in order to evaluate effectiveness and accuracy prediction of different neural networks with different hidden layers of neurones; mean, standard deviation, coefficient of variation (COV %) and mean absolute error (MAE %) of $\boldsymbol{\varepsilon}_{Exp}/\boldsymbol{\varepsilon}_{pred}$. The results of the statistical observations for each model are presented in **Table 6.3**. The performance of the ANNM1 5-12-1 was the best for all 230 results in the database and ANNM2 5-10-1 was the best for the 128 results in the database using fly ash. These networks were selected for the prediction model for drying shrinkage strain of SCC. More details of statistical results are illustrated graphically and given in **Appendix C**.

Table 6-2 Comparison of different training algorithms

Training algorithm	ANNM1 model		ANNM2 model	
	Number of iteration	Performance	Number of iteration	Performance
Bayesian regularization (trainbr)	73	0.023	210	0.0146
Levenberg-Marquardt (trainlm)	37	0.005	24	0.0001
Scaled conjugate gradient (trainscg)	19	0.0345	13	0.0232

Table 6-3 Performance of ANNMs models for different hidden layers neurones created

ANNMs models architecture [a]	Mean	Standard deviation	COV (%)	MAE (%)
ANNM1 5-4-1	1.031	0.351	10.25	12.36
ANNM1 5-8-1	1.021	0.231	8.36	14.67
ANNM1 5-10-1	1.009	0.189	7.98	7.36
ANNM1 5-12-1	1.004	0.093	9.29	5.37
ANNM1 5-15-1	1.008	0.147	7.65	11.25
ANNM2 5-5-1	1.041	0.321	9.68	10.02
ANNM2 5-4-1	1.061	0.214	12.02	7.06
ANNM2 5-6-1	1.007	0.164	6.55	6.32
ANNM2 5-10-1	1.002	0.087	7.83	4.91
ANNM2 5-15-1	1.012	0.106	9.21	8.36

The performance of the developed models was observed during the training process. The training process was stopped when any of the following conditions was archived:

- The maximum number of iterations (epochs) was reached.
- The Performance gradient of the Levenberg–Marquardt algorithm was minimized to the required target.
- The validation set error starts to increase for a specified number of epochs.

Comparisons between experimental and predicted drying shrinkage strains of SCCs using ANNM1and ANNM2 for the three sets (training, testing and validation) are illustrated in **Figure 6.11** and **Figure 6.12**, respectively.

The figures clearly show that the ANNM1 and ANNM2 were successful in learning the relationship between the input and output parameters. The average ratio of experimental drying shrinkage to predicted drying shrinkage of SCC (Mean) of ANNM1 and ANNM2 were 1.004 and 1.002, respectively. The mean absolute errors (MAE %) were low for both models with values of 5.37% and 4.91% for ANNM1 and ANNM2, respectively. Both models produced similar predictions for the drying shrinkage strain of SCC. However, the ANNM2 model was more accurate with the lowest MAE. The statistical values show small perceptible deviations between the prediction and experimental values, it indicated that both ANNM1 and ANNM2 models are suitable and can be used to predict the drying shrinkage of SCC with reasonable accuracy. Overall, it could be concluded that the trained neural networks were successful in learning the relationship between the input and output data.

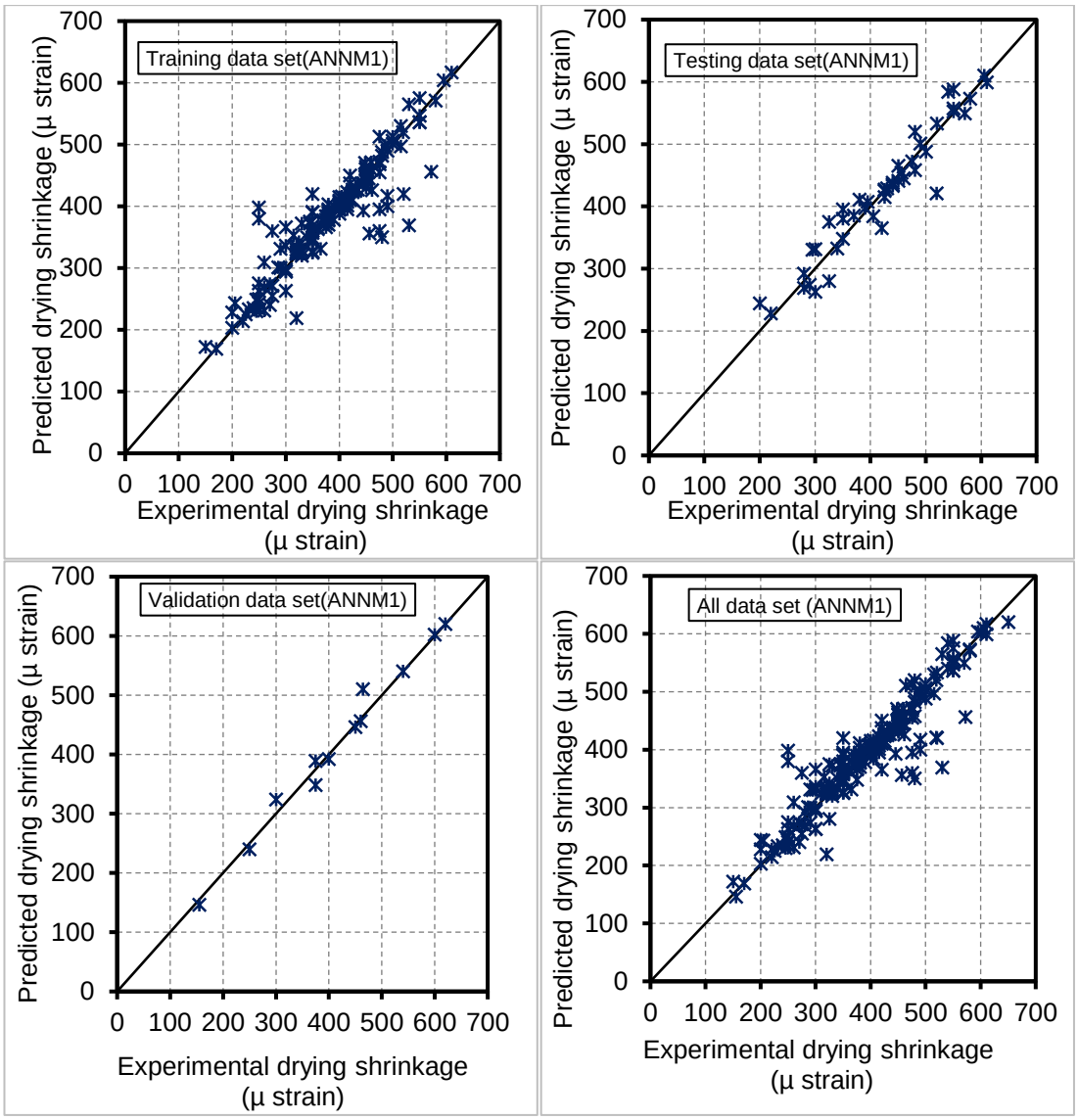

Figure 6-11 Performance of ANNM1 model

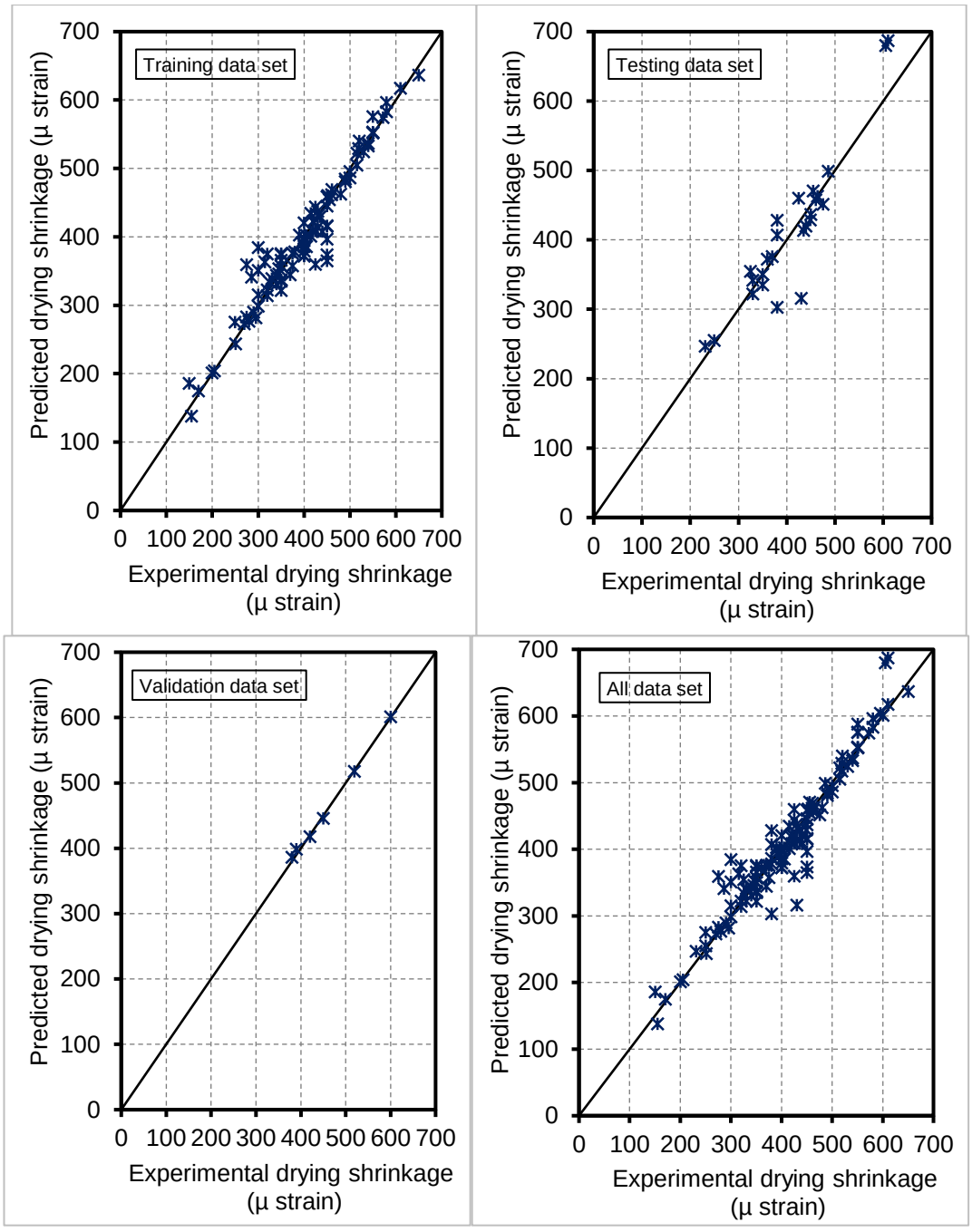

Figure 6-12 . Performance of ANNM2 model

6.7 Parametric study

The parameters affecting the drying shrinkage strain of SCC are varied. Some of these were concrete components while others were environmental conditions. A parametric study could allow quantification of the effect of one

parameter on drying shrinkage of SCC when all of the others are fixed by using the models of neural networks. The trained neural network models (ANNM1 and ANNM2) were applied to conduct a parametric study to investigate the effect of different input parameters on the drying shrinkage of SCC.

6.7.1 Effect of compressive strength on drying shrinkage strain

The relations between compressive strength and drying shrinkage strain predicted by ANNM1 and ANNM2 models are presented in **Figure 6.13**. Compressive strength values were changed from 10 to 70 MPa while all other input parameters values were held constant according to their frequency of occurrence in the database.

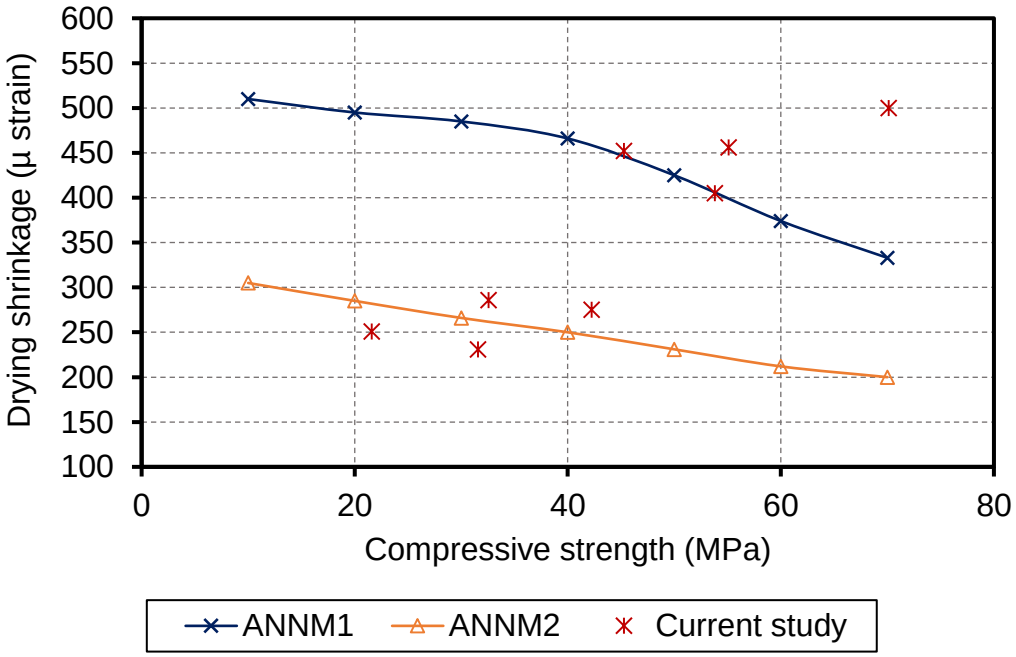

Figure 6-13 Effect of compressive strength on drying shrinkage strain using ANNMs

It is clear that the more the compressive strength increases, the more the drying shrinkage strain predicted decreases for both models (ANNM1 and

ANNM2). From the figure it can be observed that DSSCC predicted by ANNM2 was lower than the DSSCC predicted by ANNM1 due to the presence of fly ash for all databases used in the ANNM2 model. Experimental results of DSSCC obtained from the current study were plotted to compare with the prediction results as shown in the same graph.

6.7.2 Effect of water to binder ratio on drying shrinkage strain.

The influence water to binder ratio (W/B) on drying shrinkage is illustrated in **Figure 6.14**. W/B ratios were changed from 0.30 to 0.60 according to the databases used to train the models. There is an increase in drying shrinkage strain predicted with the increase in water to binder ratio using ANNM1 and ANNM2 models. Some of the experimental results of DSSCC obtained from the current study were plotted in the same figure for comparing with predicted values.

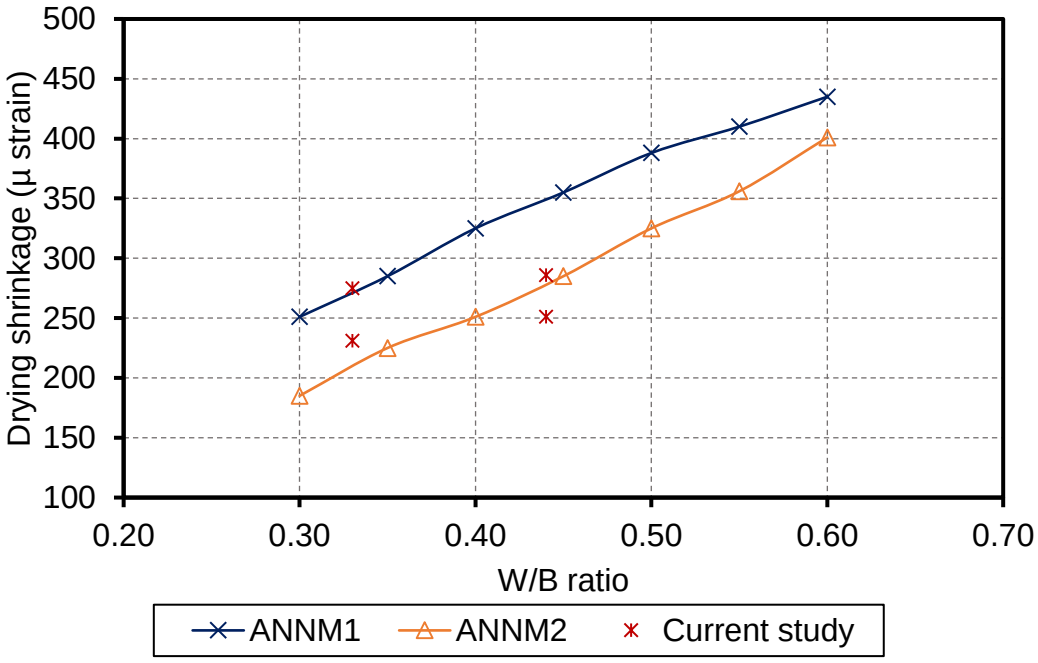

Figure 6-14 Effect of water- binder ratio on drying shrinkage strain using ANNMs

6.7.3 Effect of binder content on drying shrinkage strain.

Figure 6.15 shows the effect of binder content on drying shrinkage strain of SCC using ANNM1 model. Figure 6.15 indicates that the increase of binder content induces an increase of the drying shrinkage strain. Experimental data of DSSCC obtained from the current investigation were plotted as shown in the same graph.

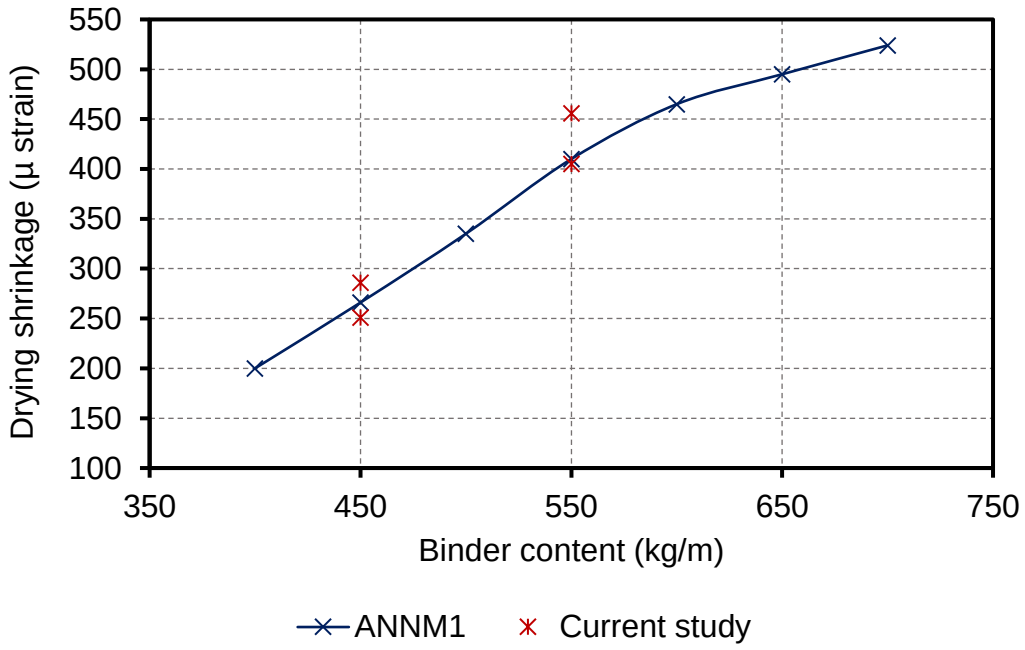

Figure 6-15 Effect of binder content on drying shrinkage strain using ANNM1

6.7.4 Effect of fly ash percentage on drying shrinkage strain.

Figure 6.16 presents the effect of increasing the fly ash percentage on the drying shrinkage strain of SCC using ANNM2. Fly ash was changed from 10 to 70 %. It is observed that as the fly ash percentage increases, the DSSCC clearly decreases for both models. Experimental results that contained fly ash as cement replacement obtained from the current study were plotted in the same figure.

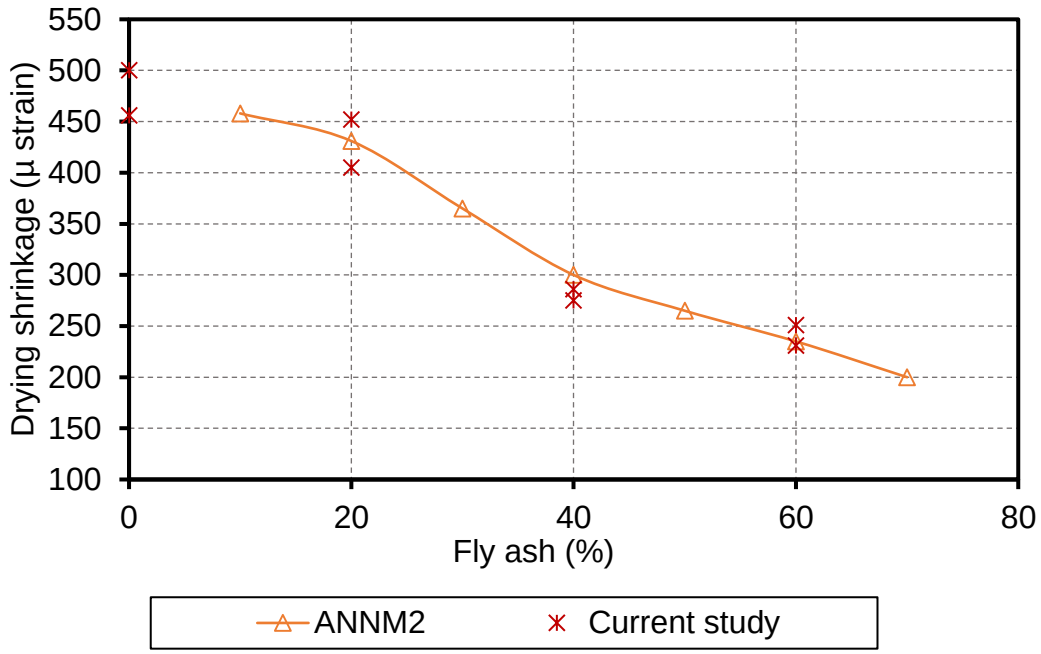

Figure 6-16 Effect of fly ash content on drying shrinkage strain using ANNM2.

6.7.5 Effect of relative humidity on drying shrinkage strain

Figure 6.17 shows the effect of changing the relative humidity percentage of SCC on the drying shrinkage strain using two the models (ANNM1 and ANNM2). The relative humidity was varied from 50 to 70 % in increments of 5 %. The figure indicated that the increase of relative humidity caused a clear reduction in the drying shrinkage strain for ANNM1 and ANNM2 models. Experimental data of DSSCC obtained from the current investigation were plotted as shown in the same graph

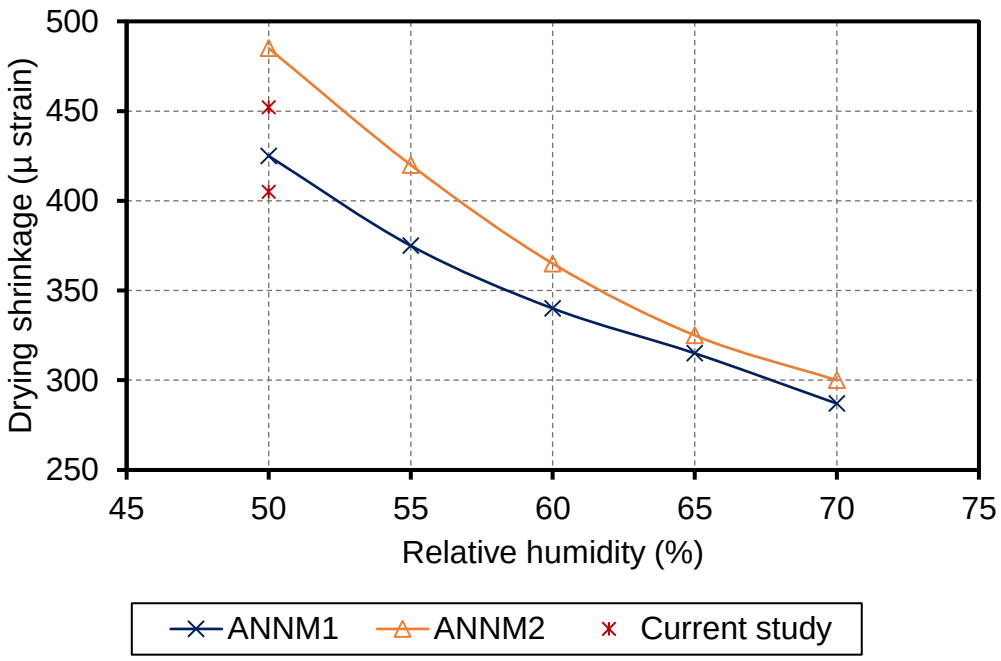

Figure 6-17 Effect of relative humidity on drying shrinkage strain using ANNMs

6.8 Comparison between the prediction given by ANNM1 model and different existing models

The results given by the ANNM1 model in this chapter were compared with the results obtained by the five existing predicted models presented in Chapter five of this investigation. Table 6.4 presents the statistical results of the drying shrinkage strain of SCC predicted by ANNM1, ACI 209-92, BSEN-92, ACI 209-92 (Huo), GL2000 and B3 models. Comparisons between experimental and predicted results of DSSCC using the ANNM1 model and the existing models are presented in Figure 6.18.

Table 6-4 Statistical results of drying shrinkage predicted by ANMM1 and existing models.

Predictive models	Mean	Standard deviation	COV (%)	MAE (%)
ANNM1 model	1.004	0.093	9.29	5.37
ACI-209	0.942	0.23	24.3	19.1
BSEN-92	1.171	0.34	28.5	27.1
ACI-209(Huo)	0.869	0.16	18.8	16.7
GL2000	0.979	0.14	16.5	13.7
B3	1.530	0.55	35.9	55.4

It can be conclude from Table 6.4 that a very high predictability was achieved with the ANNM1 model with a mean of 1.004 and it had the lowest error with an MAE% of 5.37%. The figures clearly show that the prediction of drying shrinkage of SCC using the ANNM1 model is in good agreement with the experimental results among all of the models used. As mentioned previously in this research, the drying shrinkage strain of SCC affected by various parameters including cement replacement and other parameters was considered. None of the existing models that have been developed for conventional concrete have considered fillers, admixtures or additives to calculate drying shrinkage strain. However, it is easy to add any parameters that affect DSSCC using a prediction model such as ANNM1.

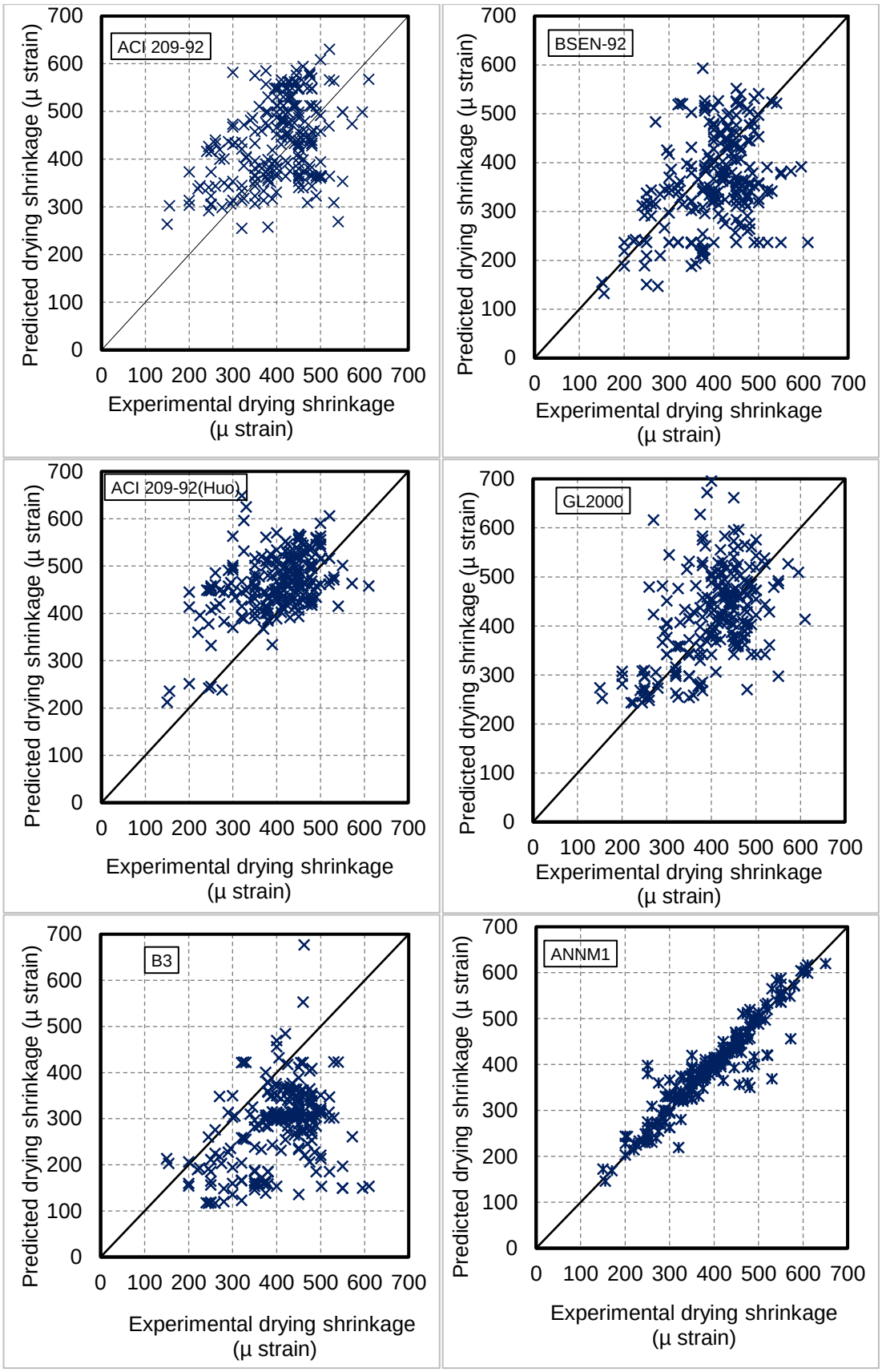

Figure 6-18 Comparison between experimental and predicted drying shrinkage strains of SCCs using ANNM1model and the existing models

6.9 Concluding remarks

This chapter demonstrated the possibilities of adapting ANNs to model the drying shrinkage strain of SCC. Two different databases were used in training and testing the two models. ANNM1 was built using a database of 230 tests and ANNM2 is built using a database of 128 tests, all of which contained fly ash. Both models were constructed to predicted drying shrinkage strain of SCC. A comprehensive comparison of ANNM1 models with various empirical models was presented. The developed ANN and observations from the parametric study given in this paper are valid for the limits of the database shown in **Table 6.1.**

Based on the above investigation, the following conclusions may be drawn:

- A multi-layered neural network back-propagation (MBP) with a Levenberg- Marquardt training algorithm (trainlm) was successfully trained to predict the drying shrinkage strain of SCC.
- The training of the ANNM1 and ANNM2 was achieved using experimental data collected from the comprehensive experimental investigations available in the literature together with experimental results obtained from this investigation.
- At the beginning, the most significant effect on neural network generalisation would be that resulting from the size of the architecture and the training set. After extensive training, it is clear that the choice of training algorithm, the size of the training rate and the schedule of training have as much effect on the ability of the ANNMs generalisation.
- Compared to the existing models used in this study to predict the drying shrinkage strain of SCC (See Chapter five), ANNM1 models were more

accurate with mean, standard deviation, coefficient of variation and mean absolute error values of 1.004, 0.093, 9.29 % and 5.37%.

- There is a reduction in drying shrinkage strain predicted with the increase in compressive strength using ANNM1 and ANNM2 models. Experimental results of DSSCC obtained from this study were close to the predicted results.
- It is clear that the predicted drying shrinkage increases with increasing binder content and W/B ratio, agreeing with DSSCC experimental results.
- The influence of FA content results on drying shrinkage obtained from ANNM2 was close to that of the DSSCC experimental results.
- The drying shrinkage strain of SCC was predicted with high degree of accuracy using ANNM1 and ANNM2 models and the trained neural networks were successful in learning the relationship between the input and output data. Moreover, the ANNM1 model required a lower computation time than the existing models.
- This study has contributed to the understanding of the role of ANNs in predicting drying shrinkage of self-compacting concrete. As well as, to study the main parameters effecting drying shrinkage of SCC.
- SCC mixtures are usually designed with large quantities of mineral fillers such as finely crushed limestone, fly ash or any other cement replacement that effect drying shrinkage strain. By using ANNM1 model, it is easy to insert any of those parameters to the input parameters to predict drying shrinkage strain of SCC.

- One of the greatest disadvantages of using ANNs is that it is difficult to interpret the estimated neural network weights; ANNM applications are frequently viewed as black boxes. However, by evaluating the impact of the choices of network architecture, size of the training set, training algorithm, training schedule and learning rate, it could be that users of ANNs will have a clearer idea of the way in which networks function, so that ANNs are no longer considered to be black-boxes.

CHAPTER SEVEN – CONCLUSIONS AND RECOMMENDATIONS FOR FUTURE WORK

7.1 Summary

The behaviour of free and confined drying shrinkage of SCC was investigated in this thesis. The research includes three phases. Firstly, experimental investigations were presented in chapters three and four including properties of SCC materials used on this work as well as the behaviour of free and confined drying shrinkage of SCC compared to NC. Secondly, the reliability of existing models for the prediction of drying shrinkage was evaluated against a large experimental data base collected from the literature together with the experimental results obtained from the current investigation as presented in chapter four. Finally, a soft computing technique called ANN was developed to predict the drying shrinkage strain of SCC using the same database that was used in the previous chapter four to study the applicability of the existing models as conducted in chapter six.

The experimental phase included preparing, casting and testing of eight SCC mixes and two NC mixes. All specimens were designed with two different water-cement ratios and various percentages of fly ash replacement by cement under different curing conditions. The main experimental measurements in this study were free and confined drying shrinkage of SCCs and NCs. In addition, fresh and hardened properties of SCCs compared to NCs were tested.

The theoretical part of this thesis was to assess the quality of drying shrinkage predictive empirical models (ACI 209-92, BSEN-92, ACI 209-92 (Hou), B3 and GL200) using a range of parameters considered in each model. Furthermore, drying shrinkage strains obtained in the experimental phase of this investigation together with some data collected from previous studies were compared with the values calculated by the existing models.

The final part of this research was to develop an ANNM model to predict drying shrinkage of SCC using the same data collected. A parametric study was conducted to investigate the effect of different input parameters on the drying shrinkage of SCC. Moreover, a comprehensive comparison was conducted on the ANNM models with the five empirical models to evaluate the predictability of the models.

7.2 Conclusions

Findings of each section of the work have been drawn and reported in full detail at the end of each chapter. A summary of the major overall view of the findings and conclusions of this research is drawn briefly in the following sections.

7.2.1 Experimental investigations

- All of the SCC mixes satisfied the fresh properties criteria and achieved the requirements of SCC properties suggested by EFNARC guidelines.
- The use of fly ash was found to have a significant influence on the fresh properties of SCC. The higher the percentage of fly ash, the higher the workability of SCC.
- The compressive strength and flexural strength of SCCs decreased with an increase in the percentage of FA. This reduction is normally

anticipated and is mostly due to the lack of lime content. A long-term compressive strength of above 30 Mpa was achieved at 91 days for SCC mixes containing up to 60% FA as cement replacement. Moreover, using up to 60% of FA as cement replacement can produce SCC with a flexural strength up to 4 Mpa at 91 days.

- For the same water – binder ratio SCCs have higher compressive strength and flexural strength than NCs. This is mainly attributed to the improved interface transition zone between the aggregate and hardened paste due to the absence of vibration of SCCs.
- The water absorption of SCCs increased considerably when FA was used. SCC mixes showed lower absorption compared to NC mixes. This is an indicator of good compaction achieved by the concrete self-weight. Due to the increase of workability of SCCs containing fly ash, the compaction is expected to be better. All concrete mixes had low absorption characteristics (less than 10%).
- For the same w/b ratio, the density of SCC showed a systematic reduction as FA increased due to the lower density of FA compared with ordinary Portland cement (OPC). Even though SCC proportions are different to NCs, a slight difference in density of SCCs compared to NCs has been observed in this study, indicating the good self-compaction of SCCs.
- The drying shrinkage strains of NCs were slightly similar at the very early ages, whereas there was a considerable change in the long-term. A higher magnitude of DSSCC than DSNC was observed.

- Fly ash has a positive effect on the drying shrinkage and reduces the drying shrinkage of SCC. Incorporating increasing amounts of FA in SCC reduces the drying shrinkage at all ages of SCC. The drying shrinkage strain of SCCs containing FA was considerably lower than that of the control concrete with the similar w/b ratio. This is attributed to the reduction of lime content which reduces the rate of hydration of concrete resulting in a lower degree of drying shrinkage strain.
- At the high FA content used in this study (60%), the long term free drying shrinkage strain (at 1000 days age) for SCCs was reduced to 49% compared with the SCCs without FA.
- For both SCCs and NCs, the drying shrinkage strain increased with the increase of w/b ratio.
- Unconfined drying shrinkage specimens exhibited higher values than the confined ones for the same mixes and this could be attributed to the evaporation of water from the exposed sample sides for the unconfined concrete samples.
- Compare to SCCs without FA, confined drying shrinkage strain was reduced by up to 46 % for SCCs using 60% FA.
- The confined drying shrinkage could be very detrimental to the bond between concrete and steel tube which may affect their composite action. In this investigation, using FA up to 60% is recommended in CFET filled with self-compacting concrete to prevent confined drying strain.

7.2.2 Analytical investigations

- Despite differences between parameters considered in the existing models used in this investigation, most of those models tend to have overestimating characteristics providing good prediction of drying shrinkage of SCC.
- Considering statistical analysis results of drying shrinkage prediction models using experimental results collected from previous studies and the results obtained in this investigation, it is evident that the GL2000, ACI 209R-92 and ACI 209R-92(Huo) models are provided good prediction of the drying shrinkage stains of SCCs among other models.
- The existing models used in this investigation have considered different parameters to calculate the drying shrinkage strain of SCC. This could explain the difference in the model's accuracy and statistical result for each model.
- The developed model based on the artificial neural network gives the best prediction of the drying shrinkage strain of SCC compared to the existing models. It requires less computing time and it is not limited by the number and the nature of the input parameters.
- Compared to the existing models used in this study to predict the drying shrinkage strain of SCC, artificial neural network models (ANNM1 and ANNM2) were more accurate. ANNM1 was the best model compared to the five existing models with mean, standard deviation, coefficient of variation and mean absolute error values of 1.004, 0.093, 9.29 % and 5.37%, respectively.

- A parametric study could allow quantification of the effect of some of these parameters by using the ANNM model. In this study the influence of the main factors effecting drying shrinkage such as compressive strength, FA content, w/p ratio, RH% and B content were studied and the relation between drying shrinkage and those parameters agreed with the experimental results.
- In all existing models available in the literature, it seems difficult to add any parameters to extend the models to any type of concrete such as SCC, with any additions or admixtures which usually used in SCC mix. However, by using the ANNM1 model, it is easy to add any of those parameters to predict drying shrinkage strain of any formulation of concrete.

7.3 Recommendations for future work

Based on the work carried out for this investigation and the conclusions made in the previous section, the following potential future investigation areas are recommended:

- Different types of aggregates should be examined to see the influence of the elastic modulus between the aggregates and the matrix on free and confined drying shrinkage behaviour of concrete.
- In order to check effect of matrix on drying shrinkage of SCC behaviour, higher matrix quality (with w/p < 0.44) should be studied.
- It is highly recommended to do more investigation and experimental work on confined drying shrinkage of NC and SCC.

- Investigations similar to this research can be done also for tubes of different shapes and sizes to measure confined drying shrinkage of CFT filled SCC and NC.
- It would be recommended to propose a new prediction model depended on the five existing models used in this research as well as the ANN models developed (ANNM1 and ANNM2) considering cement replacement materials as one of the main parameters to calculate drying shrinkage of SCC. This could provide a good prediction of SCC drying shrinkage strain with higher accuracy.
- New mix design method of SCC can be developed using ANNMs.

REFERENCES

ACI237R 2007. Self-consolidating concrete. *American Concrete Institute-ACI* Farmington Hills, Michigan.

ACI Committee 209 1992. Prediction of creep, shrinkage and temperature effects in concrete structures. Farmington Hills, Michigan: *ACI 209R-92, American Concrete Institute,*.

Adeli, H. 2001. Neural networks in civil engineering: 1989–2000. *Computer-Aided Civil and Infrastructure Engineering,* 16**,** 126-142.

Almusallam, A. A., Maslehuddin, M., Abdul-Waris, M. and Khan, M. M. 1998. Effect of mix proportions on plastic shrinkage cracking of concrete in hot environments. *Construction and Building Materials,* 12**,** 353-358.

Alrifai, A., Aggoun, S., Kadri, A., Kenai, S. and Kadri, E.-h. 2013. Paste and mortar studies on the influence of mix design parameters on autogenous shrinkage of self-compacting concrete. *Construction and Building Materials,* 47**,** 969-976.

Alyhya, W. S. S. 2016. *Self-compacting concrete: mix proportioning, properties and its flow simulation in the V-funnel.* PhD thesis, Cardiff University.

Aslani, F. and Maia, L. 2013. Creep and shrinkage of high-strength self-compacting concrete: experimental and analytical analysis. *Magazine of Concrete Research*.

Assié, S., Escadeillas, G. and Marchese, G. Durability of self-compacting concrete. Proceedings of 3rd International RILEM Symposium on Self-Compacting Concrete, Ed. O. Wallevik and I. Nielsson, France, 2003. 655-662.

Assié, S., Escadeillas, G. and Waller, V. 2007. Estimates of self-compacting concrete 'potential' durability. *Construction and Building Materials,* 21**,** 1909-1917.

ASTM/C29/C29M 2009. Standard Test Method for Bulk Density (Unit Weight) and Voids in Aggregate. *American Society for Testing and Materials*.

ASTM/C33M 2013. Standard Specification for Concrete Aggregates. *American Society for Testing and Materials*

ASTM/C78/C78M 2015. Standard Test Method for Flexural Strength of Concrete (Using Simple Beam with Third-Point Loading). *American Society for Testing and Materials*

ASTM/C127 2015. Standard Test Method for Relative Density (Specific Gravity) and Absorption of Coarse Aggregate. *American Society for Testing and Materials*.

ASTM/C143/C143M 2015. Standard Test Method for Slump of Hydraulic-Cement Concrete. *American Society for Testing and Materials*

ASTM/C157 2008. Standard Test Method for Length Change of Hardened Hydraulic-Cement Mortar and Concrete. *American Society for Testing and Materials*.

ASTM/C192/C192M 2015. Standard Practice for Making and Curing Concrete Test Specimens in the Laboratory. *American Society for Testing and Materials*.

ASTM/C494/494M 2017. Standard Specification for Chemical Admixtures for Concrete. *American Society for Testing and Materials*.

ASTM/C566 2013. Standard Test Method for Total Evaporable Moisture Content of Aggregate by Drying. *American Society for Testing and Materials*

Atmaca, N., Atmaca.Adem, Aljumaili, M. and Özçetin, A. İ. 2018. Strength and shrinkage properties of self-compacting concretes incorporating waste PVC dust. *The International Journal of Energy & Engineering Sciences,* 3**,** 47-57.

Bai, J., Wild, S., Ware, J. A. and Sabir, B. B. 2003. Using neural networks to predict workability of concrete incorporating metakaolin and fly ash. *Advances in Engineering Software,* 34**,** 663-669.

Bailey, J. 2005a. An evaluation of the use of self-consolidating concrete (SCC) for drilled shaft applications.

Bailey, J. D. 2005b. *An Evaluation of the Use of Self-Consolidating Concrete (SCC) for Drilled Shaft Applications.* Master thesis, Auburn University

Bal, L. and Buyle-Bodin, F. 2013. Artificial neural network for predicting drying shrinkage of concrete. *Construction and Building Materials,* 38**,** 248-254.

Bashir, R. and Ashour, A. 2012. Neural network modelling for shear strength of concrete members reinforced with FRP bars. *Composites Part B: Engineering,* 43**,** 3198-3207.

Bazant, Z. P. and Baweja, S. 2000. Creep and shrinkage prediction model for analysis and design of concrete structures: Model B3. *ACI Special Publications,* 194**,** 1-84.

Beale, M., Hagan, M. and Demuth, H. 2016. Neural Network ToolboxTM, User Guide, MATLAB, R2016b.

Bentz, D. P., Geiker, M. R. and Hansen, K. K. 2001. Shrinkage-reducing admixtures and early-age desiccation in cement pastes and mortars. *Cement and Concrete Research,* 31**,** 1075-1085.

Berke, N., Li, L., Hicks, M. and Bae, J. 2003. Improving concrete performance with shrinkage-reducing admixtures. *ACI Special Publication,* 217.

Bhirud, Y. L. and Sangle, K. K. 2017. Comparison of Shrinkage, Creep and Elastic Shortening of VMA and Powder Type Self-Compacting Concrete and Normal Vibrated Concrete. *Open Journal of Civil Engineering,* 7**,** 130.

BIBM, C. and ERMCO, E. 2005. EFNARC (2005) The European guidelines for self-compacting concrete.

Bilim, C., Atiş, C. D., Tanyildizi, H. and Karahan, O. 2009. Predicting the compressive strength of ground granulated blast furnace slag concrete using artificial neural network. *Advances in Engineering Software,* 40**,** 334-340.

Billberg, P. 1999. *Self-compacting concrete for civil engineering structures.: The Swedish experience*, *Cement- och betonginstitutet.*

Bissonnette, B. t., Pierre, P. and Pigeon, M. 1999. Influence of key parameters on drying shrinkage of cementitious materials. *Cement and Concrete Research,* 29**,** 1655-1662.

Blum, A. and Rivest, R. L. Training a 3-node neural network is NP-complete. Advances in neural information processing systems, 1989. 494-501.

Boger, Z. and Guterman, H. Knowledge extraction from artificial neural networks models. IEEE International Conference On Systems Man And

Cybernetics, 1997. INSTITUTE OF ELECTRICAL ENGINEERS INC (IEEE), 3030-3035.
Bonen, D. and Sarkar, S. L. 1995. The superplasticizer adsorption capacity of cement pastes, pore solution composition, and parameters affecting flow loss. *Cement and Concrete Research,* 25**,** 1423-1434.
Bouzoubaa, N. and Lachemi, M. 2001. Self-compacting concrete incorporating high volumes of class F fly ash: Preliminary results. *Cement and concrete research,* 31**,** 413-420.
Bouzoubaâ, N. and Lachemi, M. 2001. Self-compacting concrete incorporating high volumes of class F fly ash: Preliminary results. *Cement and Concrete Research,* 31**,** 413-420.
BS1881-114 1983. Testing concrete: Methods for determination of density of hardened concrete.
BS1881-122 1983. Testing concrete: Method for determination of water absorption. British Standards Institution

BS-12390-3 2009. Testing hardened concrete: compressive strength of test specimens. *British Standards Institution*.
BS-EN/206 2010. Additional Rules for Self-Compacting Concrete (SCC)- Part 9. *British Standards publication*.
Bui, V. K., Akkaya, Y. and Shah, S. P. 2002. Rheological model for self-consolidating concrete. *ACI Materials Journal,* 99.
Burlion, N., Bourgeois, F. and Shao, J.-F. 2005. Effects of desiccation on mechanical behaviour of concrete. *Cement and concrete composites,* 27**,** 367-379.
Bury, M. A. and Christensen, B. J. The role of innovative chemical admixtures in producing selfconsolidating concrete. First North American Conference on the Design and Use of Self-Consolidating Concrete, 2002. 137-140.
Carlswärd, J., Emborg, M., Utsi, S., Öberg, P., Wallevik, O. and Nielsson, I. Effect of constituents on the workability and rheology of self-compacting concrete. Proceeding of the Third international RILEM conference on SCC, Island, Proceedings PRO, 2003. 143-153.
Chai, H.-W. 1998. *Design and testing of self-compacting concrete.* PhD thesis, University of London.
Chan, Y.-W., Chen, Y.-G. and Liu, Y.-S. 2003. Effect of consolidation on bond of reinforcement in concrete of different workabilities. *ACI Materials Journal,* 100**,** 294-301.
Chopin, D., Francy, O., Lebourgeois, S. and Rougeau, P. Creep and shrinkage of heat-cured self-compacting concrete (SCC). 3rd International Symposium on Self-Compacting Concrete, Reykjavik, Iceland, 2003. 672-683.
Collepardi, M., Borsoi, A., Collepardi, S. and Troli, R. Strength, shrinkage and creep of SCC and flowing concrete. Second North American Conference on the Design and Use of Self-Consolidating Concrete and the Fourth International RILEM Symposium on Self-Compacting Concrete, 2005. 911-920.
Collepardi, M., Olagot, J. O., Skarp, U. and Troli, R. Influence of amorphous colloidal silica on the properties of self-compacting concretes. Proceedings of the International Conference" Challenges in Concrete

Construction-Innovations and Developments in Concrete Materials and Construction", Dundee, Scotland, UK, 2002. 473-483.
Craeye, B., De Schutter, G., Desmet, B., Vantomme, J., Heirman, G., Vandewalle, L., Cizer, Ö., Aggoun, S. and Kadri, E. H. 2010. Effect of mineral filler type on autogenous shrinkage of self-compacting concrete. *Cement and Concrete Research,* 40**,** 908-913.
de Larrard, F. and Sedran, T. 2002. Mixture-proportioning of high-performance concrete. *Cement and Concrete Research,* 32**,** 1699-1704.
Dhir, R. K. and Jackson, N. 1996. *Civil engineering materials*, Macmillan Education.
Domone, P. 2006. Mortar tests for material selection and mix design of SCC. *Concrete International,* 28**,** 39-45.
Domone, P. L. 2007. A review of the hardened mechanical properties of self-compacting concrete. *Cement and Concrete Composites,* 29**,** 1-12.
Duan, Z. H., Kou, S. C. and Poon, C. S. 2013. Prediction of compressive strength of recycled aggregate concrete using artificial neural networks. *Construction and Building Materials,* 40**,** 1200-1206.
Engstrand, J. 1997. Shrinkage reducing admixture for cementitious composition. *Con. Chem. J,* 4**,** 149-151.
Esquinas, A., Motos-Pérez, D., Jiménez, M., Ramos, C., Jiménez, J. and Fernández, J. 2018. Mechanical and durability behaviour of self-compacting concretes for application in the manufacture of hazardous waste containers. *Construction and Building Materials,* 168**,** 442-458.
Eurocode2 2004. BS EN 1992-1; Eurocode 2: Design of concrete structures–Part 1-1: General rules and Rules for Buildings. UK: British Standards (BSI).
Fausett, L. V. 1994. *Fundamentals of neural networks: architectures, algorithms, and applications*, Prentice-Hall Englewood Cliffs.
Felekoglu, B. 2007. Utilisation of high volumes of limestone quarry wastes in concrete industry (self-compacting concrete case). *Resources, Conservation and Recycling,* 51**,** 770-791.
Felekoğlu, B., Türkel, S. and Baradan, B. 2007. Effect of water/cement ratio on the fresh and hardened properties of self-compacting concrete. *Building and Environment,* 42**,** 1795-1802.
Fernandez-Gomez, J. and Landsberger, G. A. 2007. Evaluation of shrinkage prediction models for self-consolidating concrete. *ACI Materials Journal,* 104.
Flood, I. and Kartam, N. 1994. Neural networks in civil engineering. I: Principles and understanding. *Journal of computing in civil engineering,* 8**,** 131-148.
Freitag, S., Beer, M., Graf, W. and Kaliske, M. 2009. Lifetime prediction using accelerated test data and neural networks. *Computers & Structures,* 87**,** 1187-1194.
Gambhir, M. L. 2004. *Concrete technology*, Tata McGraw-Hill Education.
Gambhir, M. L. 2013. *Concrete Technology: Theory and Practice*, Tata McGraw-Hill Education.
Gao, X., Kawashima, S., Liu, X. and Shah, S. P. 2012. Influence of clays on the shrinkage and cracking tendency of SCC. *Cement and Concrete Composites,* 34**,** 478-485.

Gardner, N. 2004. Comparison of prediction provisions for drying shrinkage and creep of normal-strength concretes. *Canadian Journal of Civil Engineering,* 31**,** 767-775.

Gesoğlu, M., Güneyisi, E. and Özbay, E. 2009. Properties of self-compacting concretes made with binary, ternary, and quaternary cementitious blends of fly ash, blast furnace slag, and silica fume. *Construction and Building Materials,* 23**,** 1847-1854.

Ghafoori, N., Najimi, M., Sobhani, J. and Aqel, M. A. 2013. Predicting rapid chloride permeability of self-consolidating concrete: A comparative study on statistical and neural network models. *Construction and Building Materials,* 44**,** 381-390.

Ghazi, F. K. and Al Jadiri, R. S. 2010. New method for proportioning self-consolidating concrete based on compressive strength requirements. *ACI Materials Journal,* 107.

Gonzalez, S. 2000. *Neural networks for macroeconomic forecasting: a complementary approach to linear regression models*, Department of Finance Canada.

Güneyisi, E., Gesoğlu, M. and Özbay, E. 2010. Strength and drying shrinkage properties of self-compacting concretes incorporating multi-system blended mineral admixtures. *Construction and Building Materials,* 24**,** 1878-1887.

Halstead, W. J. 1986. Use of fly ash in concrete. *NCHRP Synthesis of Highway Practice.* Washington.

Heirman, G. and Vandewalle, L. The influence of fillers on the properties of self-compacting concrete in fresh and hardened state. Proc. of the 3rd Int. Symp. on Self-Compacting Concrete (SCC2003), 2003. RILEM Publications SARL, 606-618.

Heirman, G., Vandewalle, L. and Van Gemert, D. Influence of mineral additions and chemical admixtures on setting and volumetric autogenous shrinkage of SCC-equivalent mortars. Proc. of the 5th Int. RILEM Symp. on Self-Compacting Concrete (SCC2007), 2007. 553-558.

Heirman, G., Vandewalle, L., Van Gemert, D., Boel, V., Audenaert, K., De Schutter, G., Desmet, B. and Vantomme, J. 2008. Time-dependent deformations of limestone powder type self-compacting concrete. *Engineering Structures,* 30**,** 2945-2956.

Hill, T., Lewicki, P. and Lewicki, P. 2006. *Statistics: methods and applications: a comprehensive reference for science, industry, and data mining*, StatSoft, Inc.

Holt, E. and Leivo, M. 2004. Cracking risks associated with early age shrinkage. *Cement and Concrete Composites,* 26**,** 521-530.

Horta, A. 2005. *Evaluation of Self-Consolidating Concrete for Bridge Structure Applications.* Georgia Institute of Technology.

Hoseini, M., Bindiganavile, V. and Banthia, N. 2009. The effect of mechanical stress on permeability of concrete: A review. *Cement and Concrete Composites,* 31**,** 213-220.

Hossain, K. and Lachemi, M. Thermal conductivity and acoustic performance of volcanic pumice based composites. Materials Science Forum, 2005. Trans Tech Publ, 611-616.

Huo, X. S., Al-Omaishi, N. and Tadros, M. K. 2001. Creep, shrinkage, and modulus of elasticity of high-performance concrete. *ACI Materials Journal,* 98**,** 440-449.

Huynh, T.-P., Hwang, C.-L. and Limongan, A. H. 2018. The long-term creep and shrinkage behaviors of green concrete designed for bridge girder using a densified mixture design algorithm. *Cement and Concrete Composites,* 87**,** 79-88.

Hwang, C.-L. and Hung, M.-F. 2005. Durability design and performance of self-consolidating lightweight concrete. *Construction and building materials,* 19**,** 619-626.

Hwang, S.-D. and Khayat, K. H. 2008a. Effect of mixture composition on restrained shrinkage cracking of self-consolidating concrete used in repair. *ACI Materials journal,* 105.

Hwang, S.-D. and Khayat, K. H. 2008b. Effect of mixture composition on restrained shrinkage cracking of self-consolidating concrete used in repair. *ACI Materials journal,* 105**,** 499.

Hwang, S.-D. and Khayat, K. H. 2010. Effect of mix design on restrained shrinkage of self-consolidating concrete. *Materials and structures,* 43**,** 367-380.

Hwang, S.-D., Khayat, K. H. and Bonneau, O. 2006. Performance-based specifications of self-consolidating concrete used in structural applications. *ACI Materials Journal,* 103.

Iqbal, S., Ahsan, A., Holschemacher, K., Ribakov, Y. and Bier, T. A. 2017. Effect of Fly Ash on Properties of Self-Compacting High Strength Lightweight Concrete. *Periodica Polytechnica. Civil Engineering,* 61**,** 81.

Ismail, I., Bernal, S. A., Provis, J. L., San Nicolas, R., Hamdan, S. and van Deventer, J. S. 2014. Modification of phase evolution in alkali-activated blast furnace slag by the incorporation of fly ash. *Cement and Concrete Composites,* 45**,** 125-135.

Jepsen, M. T. 2002. Predicting concrete durability by using artificial neural network. *Published in a special NCR-publication*.

Jeyasehar, C. A. and Sumangala, K. 2006. Damage assessment of prestressed concrete beams using artificial neural network (ANN) approach. *Computers & Structures,* 84**,** 1709-1718.

Jolicoeur, C. and Simard, M.-A. 1998. Chemical admixture-cement interactions: phenomenology and physico-chemical concepts. *Cement and Concrete Composites,* 20**,** 87-101.

Kaastra, I. and Boyd, M. 1996. Designing a neural network for forecasting financial and economic time series. *Neurocomputing,* 10**,** 215-236.

Karsoliya, S. 2012. Approximating number of hidden layer neurons in multiple hidden layer BPNN architecture. *International Journal of Engineering Trends and Technology,* 3**,** 714-717.

Kasemchaisiri, R. and Tangtermsirikul, S. 2008. Deformability prediction model for self-compacting concrete. *Magazine of Concrete Research.* Thomas Telford Ltd

Khatib, J. 2008. Performance of self-compacting concrete containing fly ash. *Construction and Building Materials,* 22**,** 1963-1971.

Khatib, J. M. 2005. Properties of concrete incorporating fine recycled aggregate. *Cement and concrete research,* 35**,** 763-769.

Khayat, K. 2000. Optimization and performance of air-entrained, self-consolidating concrete. *ACI Materials Journal,* 97.
Khayat, K. and Yahia, A. 1997. Effect of welan gum-high-range water reducer combinations on rheology of cement grout. *ACI Materials Journal,* 94.
Khayat, K. H. 1995. Effects of antiwashout admixtures on fresh concrete properties. *ACI Materials Journal,* 92.
Khayat, K. H. 1998. Viscosity-enhancing admixtures for cement-based materials—an overview. *Cement and Concrete Composites,* 20**,** 171-188.
Khayat, K. H. 1999. Workability, testing, and performance of self-consolidating concrete. *ACI Materials Journal,* 96.
Khayat, K. H. and Assaad, J. 2002. Air-void stability in self-consolidating concrete. *ACI Materials Journal,* 99.
Khayat, K. H., Assaad, J. and Daczko, J. 2004. Comparison of field-oriented test methods to assess dynamic stability of self-consolidating concrete. *ACI Materials Journal,* 101**,** 207-215.
Khayat, K. H. and Guizani, Z. 1997. Use of viscosity-modifying admixture to enhance stability of fluid concrete. *ACI Materials Journal,* 94.
Khayat, K. H. and Long, W. J. 2010. Shrinkage of precast, prestressed self-consolidating concrete. *Materials Journal,* 107**,** 231-238.
Kim, B.-G., Jiang, S., Jolicoeur, C. and Aïtcin, P.-C. 2000. The adsorption behavior of PNS superplasticizer and its relation to fluidity of cement paste. *Cement and Concrete Research,* 30**,** 887-893.
Kim, J.-K., Han, S. H., Park, Y. D. and Noh, J. H. 1998. Material properties of self-flowing concrete. *Journal of Materials in Civil Engineering,* 10**,** 244-249.
Klug, Y. and Holschemacher, K. Comparison of the hardened properties of self-compacting and normal vibrated concrete. 3rd RILEM Symposium on Self Compacting Concrete, Reykjavik, 2003 Bagneux, France. RILEM, 596-605.
Kula, I., Olgun, A., Sevinc, V. and Erdogan, Y. 2002. An investigation on the use of tincal ore waste, fly ash, and coal bottom ash as Portland cement replacement materials. *Cement and Concrete Research,* 32**,** 227-232.
Kuroda, M., Watanabe, T. and Terashi, N. 2000. Increase of bond strength at interfacial transition zone by the use of fly ash. *Cement and concrete research,* 30**,** 253-258.
Kwon, S.-J. and Song, H.-W. 2010. Analysis of carbonation behavior in concrete using neural network algorithm and carbonation modeling. *Cement and Concrete Research,* 40**,** 119-127.
Liu, M. 2009. *Wider application of additions in self-compacting concrete.* PhD thesis, *UCL (University College London)*.
Livingstone, D. J. 2008. *Artificial neural networks: Methods and applications (methods in molecular biology)*, Humana Press.
Loser, R. and Leemann, A. 2009. Shrinkage and restrained shrinkage cracking of self-compacting concrete compared to conventionally vibrated concrete. *Materials and structures,* 42**,** 71-82.
Ma, K., Xie, Y., Long, G. and Luo, Y. Drying shrinkage of medium strength Scc. 2nd Int. Symposium on Design, Performance and Use of Self Consolidating Concrete, 2009. RILEM Publications sarl, 657-663.

Mailvaganam, N. P. and Rixom, M. 2002. *Chemical admixtures for concrete,* London CRC Press.
Malhotra, V. 2002. High-performance high-volume fly ash concrete. *Concrete International, Farmington Hills, USA,* 24.
Mehta, P. K. 1986. *Concrete. Structure, properties and materials,* New Jersey, USA, Prentice-Hall, Incorporated.
Mindess, S., Young, J. F. and Darwin, D. 2003. *Concrete*.
Mörtsell, E. and Rodum, E. Mechanical and durability aspects of SCC for road structures. Proceedings of the 2nd International Symposium on Self-Compacting Concrete, eds. Ozawa K, Ouchi M, Tokyo, Japan, 2001. 459-468.
Moyo, V. and Sibanda, K. 2014. *The Generalization Ability of Artificial Neural Networks in Forecasting TCP/IP Network Traffic Trends.* University of Fort Hare.
Nagataki, S. and Fujiwara, H. 1995. Self-compacting property of highly flowable concrete. *Special Publication,* 154**,** 301-314.
Natic, M. 2016. Matlab User Manual Version R2016b. *Math Works: Natick, MA, USA*.
Nawa, T., Izumi, T. and Edamatsu, Y. State-of-the-art report on materials and design of self-compacting concrete. Proceedings of International Workshop on Self-Compacting Concrete, 1998. 160-190.
Nehdi, M., El Chabib, H. and El Naggar, M. H. 2001. Predicting performance of self-compacting concrete mixtures using artificial neural networks. *ACI Materials Journal,* 98.
Neophytou, M. K., Pourgouri, S., Kanellopoulos, A. D., Petrou, M. F., Ioannou, I., Georgiou, G. and Alexandrou, A. 2010. Determination of the rheological parameters of self-compacting concrete matrix using slump flow test. *Applied Rheology,* 20**,** 62402-1.
Neville, A. M. 1998. *Properties of concrete*, Wiley and Sons, Inc.
Neville, A. M. and Brooks, J. J. 1987. *Concrete technology*, Longman Scientific & Technical Harlow.
Nguyen, T. L. H., Roussel, N. and Coussot, P. 2006. Correlation between L-box test and rheological parameters of a homogeneous yield stress fluid. *Cement and Concrete Research,* 36**,** 1789-1796.
Ni, H.-G. and Wang, J.-Z. 2000. Prediction of compressive strength of concrete by neural networks. *Cement and Concrete Research,* 30**,** 1245-1250.
Nunes, S., Figueiras, H., Milheiro Oliveira, P., Coutinho, J. S. and Figueiras, J. 2006. A methodology to assess robustness of SCC mixtures. *Cement and Concrete Research,* 36**,** 2115-2122.
Okamura, H. and Ouchi, M. 2003. Self-compacting concrete. *Journal of advanced concrete technology,* 1**,** 5-15.
Okamura, H. and Ozawa, K. 1995. Mix design for self-compacting concrete. *Concrete library of JSCE,* 25**,** 107-120.
Okamura, H. and Ozawa, K. 1996. Self-compacting high performance concrete. *Structural engineering international,* 6**,** 269-270.
Oliveira, M. J., Ribeiro, A. B. and Branco, F. G. 2017. Shrinkage of self-compacting concrete. A comparative analysis. *Journal of Building Engineering,* 9**,** 117-124.
Öztaş, A., Pala, M., Özbay, E. a., Kanca, E. a., Çag˘lar, N. and Bhatti, M. A. 2006. Predicting the compressive strength and slump of high strength

concrete using neural network. *Construction and Building Materials,* 20**,** 769-775.

Ozyildirim, C. 2005. Virginia Department of Transportation early experience with self-consolidating concrete. *Transportation Research Record: Journal of the Transportation Research Board,* 1914**,** 81-84.

Pala, M., Özbay, E., Öztaş, A. and Yuce, M. I. 2007. Appraisal of long-term effects of fly ash and silica fume on compressive strength of concrete by neural networks. *Construction and Building Materials,* 21**,** 384-394.

Paola, J. D. and Schowengerdt, R. A. 1997. The effects of neural-network structure on a multispectral land-use/land-cover classification. *Photogrammetric engineering and remote sensing (USA)*.

Park, C. K., Noh, M. H. and Park, T. H. 2005. Rheological properties of cementitious materials containing mineral admixtures. *Cement and Concrete Research,* 35**,** 842-849.

Parra, C., Valcuende, M. and Gómez, F. 2011. Splitting tensile strength and modulus of elasticity of self-compacting concrete. *Construction and Building Materials,* 25**,** 201-207.

Pashias, N., Boger, D., Summers, J. and Glenister, D. 1996. A fifty cent rheometer for yield stress measurement. *Journal of Rheology (1978-present),* 40**,** 1179-1189.

Persson, B. 2001. A comparison between mechanical properties of self-compacting concrete and the corresponding properties of normal concrete. *Cement and concrete Research,* 31**,** 193-198.

Petersson, Ö. Simulation of self-compacting concrete-laboratory experiments and numerical modelling of testing methods, JRING and L-box tests. Proc. of the 3rd Int. Symp. on SCC, 2003 Reykjavik, Iceland. 202-207.

Petersson, O. and Billberg, P. Investigation on blocking of self-compacting concrete with different maximum aggregate size and use of viscosity agent instead of filler. Proceedings of the First International RILEM Symposium Self-Compacting Concrete, Stockholm, Sweden, 1999. 333-344.

Petersson, O., Billberg, P. and Van, B. 2014. A model for self-compacting concrete. *Production methods and workability of concrete.* CRC Press.

Pierard, J., Dieryck, V. and Desmyter, J. Autogeneous Shrinkage of Self-Compacting Concrete. Second North American Conference on the Design and Use of Self-Consolidating Concrete and the Fourth International RILEM Symposium on Self-Compacting Concrete, 2005. 1013-1022.

Pons, G., Proust, E. and Assié, S. Creep and shrinkage of self-compacting concrete: a different behaviour compared with vibrated concrete. Proceedings of the 3rd International RILEM Symposium on Self-Compacting Concrete, 2003. 17-20.

Poppe, A.-M. and De Schutter, G. Creep and shrinkage of self-compacting concrete. First International Symposium on Design, Performance and Use of Self-Consolidating Concrete, China, 2005. 329-336.

Prasad, B. K. R., Eskandari, H. and Reddy, B. V. V. 2009. Prediction of compressive strength of SCC and HPC with high volume fly ash using ANN. *Construction and Building Materials,* 23**,** 117-128.

Proust, E. and Pons, G. 2001. Macroscopic and microscopic behavior of self-compacting concrete creep and shrinkage. *Proc. of Concreep,* 6**,** 569-574.
Raghavan, K., Sarma, S. and Chattopadhyay, D. Creep, Shrinkage and Chloride Permeability Properties of Self-Consolidating Concrete. First North American Conference on the Design and Use of Self-Consolidating Concrete, 2002. 12-13.
Reinhardt, H. W. and Wüstholz, T. 2006. About the influence of the content and composition of the aggregates on the rheological behaviour of self-compacting concrete. *Materials and structures,* 39**,** 683-693.
Roeder, C. W., Cameron, B. and Brown, C. B. 1999. Composite action in concrete filled tubes. *Journal of structural engineering,* 125**,** 477-484.
Rols, S., Ambroise, J. and Pera, J. 1999. Effects of different viscosity agents on the properties of self-leveling concrete. *Cement and Concrete Research,* 29**,** 261-266.
Rongbing, B. and Jian, S. 2005. Synthesis and evaluation of shrinkage-reducing admixture for cementitious materials. *Cement and Concrete Research,* 35**,** 445-448.
Rosenblatt, F. 1962. Principles of neurodynamics.
Rozière, E., Granger, S., Turcry, P. and Loukili, A. 2007. Influence of paste volume on shrinkage cracking and fracture properties of self-compacting concrete. *Cement and concrete composites,* 29**,** 626-636.
Rumelhart, D. E., Hinton, G. E. and Williams, R. J. 1986. Learning Internal Representations by Error Propagation, Parallel Distributed Processing, Explorations in the Microstructure of Cognition, ed. DE Rumelhart and J. McClelland. Vol. 1. 1986. Cambridge, MA: MIT Press.
Saha, A. K. and Sarker, P. K. 2017. Sustainable use of ferronickel slag fine aggregate and fly ash in structural concrete: Mechanical properties and leaching study. *Journal of Cleaner Production,* 162**,** 438-448.
Saliba, J., Rozière, E., Grondin, F. and Loukili, A. 2011. Influence of shrinkage-reducing admixtures on plastic and long-term shrinkage. *Cement and Concrete Composites,* 33**,** 209-217.
Sato, T., Goto, T. and Sakai, K. 1983. Mechanism for reducing drying shrinkage of hardened cement by organic additives. *CAJ Rev,* 5**,** 52-55.
Schindler, A. K., Barnes, R. W., Roberts, J. B. and Rodriguez, S. 2007. Properties of self-consolidating concrete for prestressed members. *ACI Materials Journal,* 104**,** 53.
Schonlin, K. and Hilsorf, H. 1988. Permeability as a Measure of Potential Durability of Concrete--Development of a Suitable Test Apparatus. *ACI Special Publication,* 108.
Schwartzentruber, L. A., Le Roy, R. and Cordin, J. 2006. Rheological behaviour of fresh cement pastes formulated from a Self Compacting Concrete (SCC). *Cement and Concrete Research,* 36**,** 1203-1213.
Sedran, T. and De Larrard, F. Optimization of self-compacting concrete thanks to packing model. Proceedings 1st SCC Symp, CBI Sweden, RILEM PRO7, 13-15 September 1999 Stockholm. 321-332.
Seng, V. and Shima, H. Creep and shrinkage of self-compacting concrete with different limestone powder contents. Second North American Conference on the Design and Use of Self-Consolidating Concrete and

the Fourth International RILEM Symposium on Self-Compacting Concrete, 2005. 981-987.
Siddique, R. 2004. Performance characteristics of high-volume Class F fly ash concrete. *Cement and Concrete Research,* 34**,** 487-493.
Siddique, R. 2013. Compressive strength, water absorption, sorptivity, abrasion resistance and permeability of self-compacting concrete containing coal bottom ash. *Construction and Building Materials,* 47**,** 1444-1450.
Skarendahl, Å. and Petersson, Ö. 2000. *Report 23: Self-Compacting Concrete–State-of-the-Art report of RILEM Technical Committee 174-SCC*, RILEM publications.
Sobhani, J., Najimi, M., Pourkhorshidi, A. R. and Parhizkar, T. 2010. Prediction of the compressive strength of no-slump concrete: A comparative study of regression, neural network and ANFIS models. *Construction and Building Materials,* 24**,** 709-718.
Somayaji, S. 2001. *Civil engineering materials*, Pearson Education India.
Sonebi, M. 2004. Medium strength self-compacting concrete containing fly ash: Modelling using factorial experimental plans. *Cement and Concrete Research,* 34**,** 1199-1208.
Sonebi, M. and Bartos, P. 2002. Filling ability and plastic settlement of self-compacting concrete. *Materials and Structures,* 35**,** 462-469.
Song, H.-W. and Kwon, S.-J. 2009. Evaluation of chloride penetration in high performance concrete using neural network algorithm and micro pore structure. *Cement and Concrete Research,* 39**,** 814-824.
Su, N., Hsu, K.-C. and Chai, H.-W. 2001. A simple mix design method for self-compacting concrete. *Cement and Concrete Research,* 31**,** 1799-1807.
Su, N. and Miao, B. 2003. A new method for the mix design of medium strength flowing concrete with low cement content. *Cement and Concrete Composites,* 25**,** 215-222.
Tam, C., Shein, A., Ong, K. and Chay, C. 2005. Modified J-ring approach for assessing passing ability of SCC. *Hanley Wood.* U.S.A.: The 2nd North American Conference on the Design and Use of Self-consolidating Concrete.
Teychenné, D. C., Franklin, R. E., Erntroy, H. C., Building Research, E., Transport and Road Research, L. 1975. *Design of normal concrete mixes,* London, H.M.S.O. [for the] Building Research Establishment [and the] Transport and Road Research Laboratory.
Tragardh, J. Microstructural features and related properties of self-compacting concrete. Proceedings of the First International RILEM Symposium on Self-Compacting Concrete, 1999. 175-186.
Turcry, P. and Loukili, A. A study of plastic shrinkage of self-compacting concrete. Proceedings of the 3rd international RILEM symposium on self-compacting concrete. Reykjavik: RILEM Publications SARL, 2003. 576-585.
Turcry, P., Loukili, A. and Haidar, K. Mechanical properties, plastic shrinkage, and free deformations of self-consolidating concrete. First North American Conference on the Design and Use of Self-Consolidating Concrete, 2002. 335-340.
Turcry, P., Loukili, A., Haidar, K., Pijaudier-Cabot, G. and Belarbi, A. 2006. Cracking tendency of self-compacting concrete subjected to restrained

shrinkage: experimental study and modeling. *Journal of Materials in Civil Engineering,* 18**,** 46-54.

Uchikawa, H., Hanehara, S. and Sawaki, D. 1997. The role of steric repulsive force in the dispersion of cement particles in fresh paste prepared with organic admixture. *Cement and Concrete Research,* 27**,** 37-50.

Utsi, S., Emborg, M., Carlswärd, J., Wallevik, O. and Nielsson, I. Relation between workability and rheological parameters. Third international RILEM symposium, RILEM Pub. PRO, 2003. 154-164.

Uysal, M. and Tanyildizi, H. 2011. Predicting the core compressive strength of self-compacting concrete (SCC) mixtures with mineral additives using artificial neural network. *Construction and Building Materials,* 25**,** 4105-4111.

Valcuende, M., Benito, F., Parra, C. and Miñano, I. 2015. Shrinkage of self-compacting concrete made with blast furnace slag as fine aggregate. *Construction and Building Materials,* 76**,** 1-9.

Valcuende, M., Marco, E., Parra, C. and Serna, P. 2012. Influence of limestone filler and viscosity-modifying admixture on the shrinkage of self-compacting concrete. *Cement and Concrete Research,* 42**,** 583-592.

Vieira, M. and Bettencourt, A. Deformability of hardened SCC. International RILEM Symposium on Self-Compacting Concrete, 2003. RILEM Publications SARL, 637-644.

Wan, W., Mabu, S., Shimada, K., Hirasawa, K. and Hu, J. 2009. Enhancing the generalization ability of neural networks through controlling the hidden layers. *Applied Soft Computing,* 9**,** 404-414.

Wong, Y. L., Lam, L., Poon, C. S. and Zhou, F. P. 1999. Properties of fly ash-modified cement mortar-aggregate interfaces. *Cement and Concrete Research,* 29**,** 1905-1913.

Yamada, K., Takahashi, T., Hanehara, S. and Matsuhisa, M. 2000. Effects of the chemical structure on the properties of polycarboxylate-type superplasticizer. *Cement and concrete research,* 30**,** 197-207.

Yammamuro, H., lzumi, T. and Mizunuma, T. 1997. Study of non-adsorptive viscosity agents applied to self-compacting concrete. *ACI Special Publication,* 173**,** 427-444.

Zhu, W., Sonebi, M. and Bartos, P. 2004. Bond and interfacial properties of reinforcement in self-compacting concrete. *Materials and structures,* 37**,** 442-448.

APPENDIXE A. PILOT STUDY

Table A-1 Mix proportions of SCC trial mixes

Trail No.	C (kg/m^3)	W (kg/m^3)	F_{agg} (kg/m^3)	C_{agg} (kg/m^3)	SP (%)	FA (%)	W/B ratio
TR1 (Nc)	500	256	870	692	0.5	0	0.44
TR2(NC)	455	205	896	794	0	0	0.44
TR3(NC)	585	205	858	702	0.5	0	0.33
TR4(NC)	585	205	858	702	0	0	0.33
TR5 (SCC)	450	198	890	780	1	0	0.44
TR6(SCC)	270	198	890	780	0.75	40	0.44
TR7(SCC)	550	180	890	780	0.81	0	0.33
TR8(SCC)	180	198	890	780	0.5	60	0.44
TR9(SCC)	180	198	890	780	1	20	0.44
TR10(SCC)	180	198	890	780	0.6	60	0.44
TR11(SCC)	330	180	890	780	1	40	0.44
TR12(SCC)	220	180	890	780	1	60	0.33

Table A-2 Fresh properties and compressive strength of SCC trail mixes

Trial No.	Slump (mm)	Slump flow		J- Ring		V -funnel (sec)	Segregation Index (%)	Compressive strength (MPa)	
		Flow (mm)	T_{500} (sec)	Flow (mm)	T_{500} (sec)			7 days	28 days
TR1 (NC)	collapse	-	-	-	-	-	-	16.16	21.30
TR2 (NC)	168	-	-	-	-	-	-	31.25	41.25
TR3 (NC)	collapse	-	-	-	-	-	-	24.12	29.36
TR4 (NC)	59	-	-	-	-	-	-	45.12	50.36
TR5 (SCC)	0.44	695	1.5	645	5.9	8.10	9.61	26.83	35.67
TR6 (SCC)	0.44	830	1.12	700	1.90	7.50	5.25	22.31	31.08
TR7 (SCC)	0.33	740	1.70	760	2.81	12	8.23	36.15	59.47
TR8 (SCC)	0.44	775	1.60	680	3.7	9.15	6.8	18.13	23.55
TR9 (SCC)	0.44	730	1.56	700	2.81	8.12	7.90	25.43	35.11
TR10 (SCC)	0.44	710	1.6	660	3.2	7.3	14	14.3	21.01
TR11 (SCC)	0.44	770	1.4	560	3.5	6.7	12.3	23.12	29.12
TR12 (SCC)	0.33	600	2.2	790	1.8	11.12	11.8	21	30.6

APPENDIX B. DATABASE OF DRYING SHRINKAGE STRAIN

Table B-1 Details of database

References	ID	C	F_{agg}	C_{agg}	FA	W/B	W	B	t	$f'_c\ (MPa)$	RH (%)
(Güneyisi et al., 2010)	1	550	728	935	0	0.32	176	550	50	69	50
	2	440	714	917	20	0.32	176	550	50	59	50
	3	330	700	899	40	0.32	176	550	50	52	50
	4	220	686	881	60	0.32	176	550	50	40	50
	5	440	725	931	0	0.32	176	550	50	64	50
	6	330	722	928	0	0.32	176	550	50	68	50
	7	220	720	924	0	0.32	176	550	50	66	50
	8	523	724	930	0	0.32	176	550	50	68	50
	9	495	720	925	0	0.32	176	550	50	73	50
	10	468	716	920	0	0.32	176	550	50	72	50
	11	523	725	932	0	0.32	176	550	50	82	50
	12	495	724	929	0	0.32	176	550	50	78	50
	13	468	721	927	0	0.32	176	550	50	84	50
	14	440	713	916	15	0.32	176	550	50	67	50
	15	330	699	898	30	0.32	176	550	50	57	50
	16	220	685	880	45	0.32	176	550	50	51	50
	17	440	715	919	15	0.32	176	550	50	69	50

	18	330	703	903	30	0.32	176	550	50	72	50
	19	220	690	887	45	0.32	176	550	50	57	50
	20	440	721	927	0	0.32	176	550	50	68	50
	21	330	716	920	0	0.32	176	550	50	74	50
	22	220	710	912	0	0.32	176	550	50	72	50
	23	440	724	929	0	0.32	176	550	50	76	50
	24	330	720	924	0	0.32	176	550	50	69	50
	25	220	715	919	0	0.32	176	550	50	71	50
	26	440	720	924	10	0.32	176	550	50	65	50
	27	330	711	913	20	0.32	176	550	50	53	50
	28	220	703	903	30	0.32	176	550	50	59	50
	29	523	724	931	0	0.32	176	550	50	80	50
	30	495	721	927	0	0.32	176	550	50	79	50
	31	468	718	923	0	0.32	176	550	50	80	50
	32	440	714	917	15	0.32	176	550	50	67	50
	33	330	700	900	30	0.32	176	550	50	63	50
	34	220	688	883	45	0.32	176	550	50	52	50
	35	440	722	928	0	0.32	176	550	50	77	50
	36	330	717	922	0	0.32	176	550	50	75	50
	37	220	713	915	0	0.32	176	550	50	63	50
	38	440	717	922	8	0.32	176	550	50	67	50
	39	330	707	909	15	0.32	176	550	50	62	50
	40	220	697	896	23	0.32	176	550	50	55	50
	41	440	720	924	8	0.32	176	550	50	78	50
	42	330	711	913	15	0.32	176	550	50	73	50
	43	220	703	903	23	0.32	176	550	50	65	50

	44	450	826	869	0	0.44	198	450	50	52	50
	45	360	813	855	17	0.44	198	450	50	44	50
	46	270	801	842	33	0.44	198	450	50	38	50
	47	180	788	829	49	0.44	198	450	50	26	50
	48	360	823	866	0	0.44	198	450	50	50	50
	49	270	821	863	0	0.44	198	450	50	49	50
	50	180	819	860	0	0.44	198	450	50	48	50
	51	428	823	865	0	0.44	198	450	50	52	50
	52	405	819	861	0	0.44	198	450	50	50	50
	53	383	816	858	0	0.44	198	450	50	60	50
	54	360	813	855	13	0.44	198	450	50	52	50
	55	270	801	841	25	0.44	198	450	50	40	50
	56	180	788	828	37	0.44	198	450	50	32	50
	57	360	820	863	0	0.44	198	450	50	51	50
	58	270	816	857	0	0.44	198	450	50	50	50
	59	180	810	852	0	0.44	198	450	50	49	50
	60	360	819	927	8	0.44	198	450	50	53	50
	61	270	811	852	17	0.44	198	450	50	46	50
	62	180	803	845	25	0.44	198	450	50	39	50
	63	360	817	859	5	0.44	198	450	50	52	50
	64	270	808	849	12	0.44	198	450	50	46	50
	65	180	799	840	19	0.44	198	450	50	38	50
(Khatib, 2008)	66	500	876	876	0	0.36	180	500	56	43	60
	67	500	876	876	0	0.36	180	500	56	61	60
	68	500	876	876	0	0.36	180	500	56	55	60
	69	400	845	876	20	0.36	180	500	56	47	60

	70	300	813	876	40	0.36	180	500	56	49	60
	71	200	782	876	60	0.36	180	500	56	27	60
	72	100	751	876	80	0.36	180	500	56	9	60
	73	300	1071	866	0	0.60	180	425	400	40	50
	74	350	1073	734	0	0.42	210	350	400	40	50
	75	350	939	884	0	0.60	210	395	400	37	50
(Valcuende et al., 2012)	76	350	997	726	0	0.48	210	440	400	38	50
	77	247	845	846	40	0.45	186	412	224	35	50
	78	238	844	844	40	0.40	159	397	224	38	50
	79	232	846	847	40	0.35	136	357	224	48	50
	80	207	845	843	50	0.45	188	414	224	33	50
	81	200	842	843	50	0.40	161	400	224	35	50
	82	197	856	856	50	0.35	138	394	224	39	50
	83	163	851	851	60	0.40	164	408	224	26	50
(Bouzoubaa and Lachemi, 2001)	84	161	866	864	60	0.35	141	402	224	36	50
	85	256	817	964	0	0.32	139	435	200	47	50
	86	292	768	906	0	0.32	159	496	200	47	50
	87	329	719	848	0	0.32	179	559	200	42	50
	88	365	670	790	0	0.32	199	620	200	45	50
	89	402	621	732	0	0.32	219	683	200	42	50
	90	365	646	762	0	0.35	219	620	200	34	50
	91	365	623	734	0	0.38	239	620	200	33	50
	92	365	719	848	0	0.39	199	508	200	39	50
(Rozière et al., 2007)	93	365	621	732	0	0.27	199	732	200	43	50
	94	386	792	848	30	0.30	166	552	120	37	60
(Ma et al., 2009)	95	359	792	848	30	0.35	180	513	120	36	60

	96	335	792	848	30	0.40	192	479	120	29	60
	97	389	792	848	20	0.40	195	486	120	33	60
	98	335	792	848	30	0.40	192	479	120	30	60
	99	283	792	848	40	0.40	189	472	120	29	60
	100	394	865	689	25	0.40	210	525	120	26	60
	101	382	841	742	25	0.40	204	510	120	28	60
	102	370	818	795	25	0.40	198	495	120	31	60
	103	360	796	848	25	0.40	192	480	120	31	60
	104	348	771	901	25	0.40	186	465	120	33	60
	105	338	748	954	25	0.40	180	450	120	36	60
	106	390	715	848	25	0.40	208	520	120	44	60
	107	375	755	848	25	0.40	200	500	120	46	60
	108	360	796	848	25	0.40	192	480	120	45	60
	109	337	848	848	25	0.40	180	450	120	48	60
	110	427	599	940	9	0.30	182	599	200	73	50
	111	433	700	828	0	0.37	208	567	200	57	50
	112	445	790	870	0	0.38	171	445	200	57	50
	113	463	714	855	18	0.31	177	560	200	87	50
	114	461	790	865	17	0.33	181	550	200	76	50
(Horta, 2005)	115	457	712	850	17	0.32	175	545	200	78	50
	116	360	853	698	0	0.28	165	600	98	49	60
	117	360	853	698	0	0.28	165	600	98	59	60
	118	300	853	698	0	0.28	165	600	98	42	60
	119	360	865	707	0	0.24	144	600	98	58	60
	120	360	835	683	0	0.33	198	600	98	40	60
(Heirman et al., 2008)	121	360	853	698	0	0.28	165	600	98	62	60

	122	360	825	675	0	0.36	216	600	98	34	60
(Hwang and Khayat, 2010)	123	309	814	842	30	0.35	166	475	56	53	50
	124	309	814	842	30	0.35	166	475	56	50	50
	125	309	814	842	30	0.35	166	475	56	46	50
	126	333	774	800	25	0.42	200	475	56	35	50
	127	333	774	800	25	0.42	200	475	56	46	50
	128	333	774	800	25	0.42	200	475	56	40	50
	129	333	785	811	0	0.42	200	475	56	42	50
	130	333	785	811	20	0.42	200	475	56	46	50
	131	357	763	789	20	0.42	200	475	56	37	50
	132	309	774	800	25	0.42	200	475	56	41	50
(Chopin et al., 2003)	133	344	810	843	0	0.25	131	516	500	47	50
	134	396	723	760	0	0.24	154	652	500	46	50
	135	396	815	848	0	0.21	115	557	500	65	50
	136	347	801	833	0	0.27	139	524	500	45	50
	137	348	710	942	0	0.25	132	525	500	59	50
(Poppe and De Schutter, 2005)	138	300	853	698	0	0.28	165	600	100	50	60
	139	360	853	698	0	0.28	165	600	100	54	60
	140	400	853	698	0	0.28	165	600	100	63	60
	141	450	853	698	0	0.28	165	600	100	63	60
	142	360	853	698	0	0.28	165	600	100	57	60
	143	360	853	698	0	0.28	165	600	100	57	60
(Turcry et al., 2006)	144	330	950	825	0	0.41	180	440	160	40	50
	145	350	857	742	0	0.40	198	489	160	42	50
	146	350	860	790	0	0.37	187	500	160	48	50
(Loser and Leemann, 2009)	147	455	867	867	0	0.40	178	455	91	52	70

	148	512	840	840	0	0.36	179	512	91	60	70
	149	407	894	894	0	0.45	181	407	91	50	70
	150	435	866	866	0	0.46	199	435	91	49	70
	151	489	867	867	0	0.35	166	489	91	63	70
	152	452	868	868	0	0.40	178	452	91	48	70
	153	322	869	869	23	0.43	178	420	91	44	70
	154	350	867	867	23	0.37	166	456	91	54	70
	155	327	867	867	27	0.40	178	451	91	43	70
	156	453	956	783	0	0.40	177	453	91	56	70
	157	461	847	891	0	0.39	177	461	91	52	70
	158	454	869	869	0	0.40	174	454	91	54	70
	159	454	869	869	0	0.40	170	454	91	50	70
	160	352	810	690	20	0.34	150	440	300	63	50
	161	352	690	810	20	0.34	150	440	300	63	50
	162	352	690	810	20	0.34	150	440	300	63	50
	163	352	810	690	20	0.34	150	440	300	63	50
	164	352	690	810	20	0.40	176	440	300	63	50
	165	352	810	690	20	0.40	176	440	300	63	50
	166	352	810	690	20	0.40	176	440	300	63	50
	167	352	690	810	20	0.40	176	440	300	63	50
	168	400	690	810	20	0.34	170	500	300	63	50
	169	400	810	690	20	0.34	170	500	300	63	50
	170	400	810	690	20	0.34	170	500	300	63	50
	171	400	690	810	20	0.34	170	500	300	63	50
	172	400	810	690	20	0.40	200	500	300	63	50
(Khayat and Long, 2010)	173	400	690	810	20	0.40	200	500	300	63	50

	174	400	690	810	20	0.40	200	500	300	63	50
	175	400	810	690	20	0.40	200	500	300	63	50
	176	375	1090	657	6	0.55	220	400	365	33	50
	177	375	954	657	6	0.55	220	400	365	33	50
	178	375	818	657	6	0.55	220	400	365	33	50
	179	375	691	657	6	0.55	220	400	365	33	50
	180	375	465	656	6	0.55	220	400	365	33	50
	181	375	438	656	6	0.55	220	400	365	32	50
(Valcuende et al., 2015)	182	375	310	655	6	0.55	220	400	365	33	50
(Assié et al., 2003)	183	350	888	791	0	0.38	187	490	200	34	50
	184	306	964	824	0	0.38	178	463	60	31	50
	185	306	964	824	0	0.38	178	463	60	31	50
	186	306	964	824	0	0.38	178	463	60	29	50
	187	307	965	824	29	0.41	178	435	60	37	50
	188	307	944	806	29	0.41	174	425	60	38	50
	189	307	964	822	29	0.41	176	431	60	37	50
	190	312	981	838	29	0.41	181	442	60	45	50
	191	312	981	838	29	0.41	181	441	60	47	50
(Collepardi et al., 2002)	192	312	981	838	29	0.41	181	442	60	43	50
	193	400	796	852	0	0.24	140	592	600	92	50
	194	400	796	852	0	0.24	140	592	600	92	50
(Aslani and Maia, 2013)	195	400	796	852	0	0.24	140	592	600	92	50
	196	330	863	863	0	0.41	195	470	300	62	55
	197	380	863	863	0	0.37	175	470	300	70	55
	198	380	847	838	0	0.40	190	470	300	58	55
(Proust and Pons, 2001)	199	425	759	1001	0	0.43	195	455	300	66	55

	200	277	793	881	0	0.39	177	456	300	38	55
(Vieira and Bettencourt, 2003)	201	205	786	786	18	0.29	161	563	180	38	50
	202	300	400	642	30	0.50	190	400	100	39	50
	203	300	400	642	30	0.50	190	400	100	36	50
(Gao et al., 2012)	204	300	400	642	30	0.50	190	400	100	40	50
	205	450	890	780	0	0.44	198	450	1000	47	50
	206	360	890	780	20	0.44	198	450	1000	38	50
	207	270	890	780	40	0.44	198	450	1000	24	50
	208	180	890	780	60	0.44	198	450	1000	13	50
	209	550	890	780	0	0.33	180	550	1000	60	50
	210	440	890	780	20	0.33	180	550	1000	45	50
	211	330	890	780	40	0.33	180	550	1000	44	50
Current study (2016)	212	220	890	780	60	0.33	180	550	1000	27	50
	213	665	611	898	0	0.22	163	739	120	70	60
	214	518	660	728	6	0.22	181	840	120	72	60
(Huynh et al., 2018)	215	336	792	904	9	0.22	131	594	120	68	60
	216	410	923	795	0	0.36	186	510	196	47	50
	217	430	946	828	0	0.46	196	430	196	37	50
	218	439	1131	565	0	0.35	185	535	196	51	50
(Esquinas et al., 2018)	219	440	1175	583	0	0.45	199	440	196	37	50
	220	400	1114	573	0	0.33	132	400	112	42	50
(Bhirud and Sangle, 2017)	221	330	1130	458	40	0.33	182	550	112	58	50
	222	440	786	808	20	0.35	193	550	60	51	50
	223	418	776	799	20	0.35	193	550	60	49	50
	224	396	767	1160	20	0.35	193	550	60	48	50
(Atmaca et al., 2018)	225	374	757	1146	20	0.35	193	550	60	47	50

	226	352	748	1131	20	0.35	193	550	60	41	50
	227	330	738	1117	20	0.35	193	550	60	39	50
	228	265	780	768	40	0.46	200	437	270	27	55
	229	283	774	764	38	0.43	194	455	270	45	55
(Oliveira et al., 2017)	230	316	819	804	36	0.31	151	494	270	81	55
	Max	665	1175	1160	80	0.60	239	840	1000	92	70
	Min	100	310	458	0	0.21	115	350	50	9	50

APPENDIX C. STATISTICAL ANALYSIS OF ANN MODELS

Figure C-1 Screenshot of Performance Plot of ANNM1

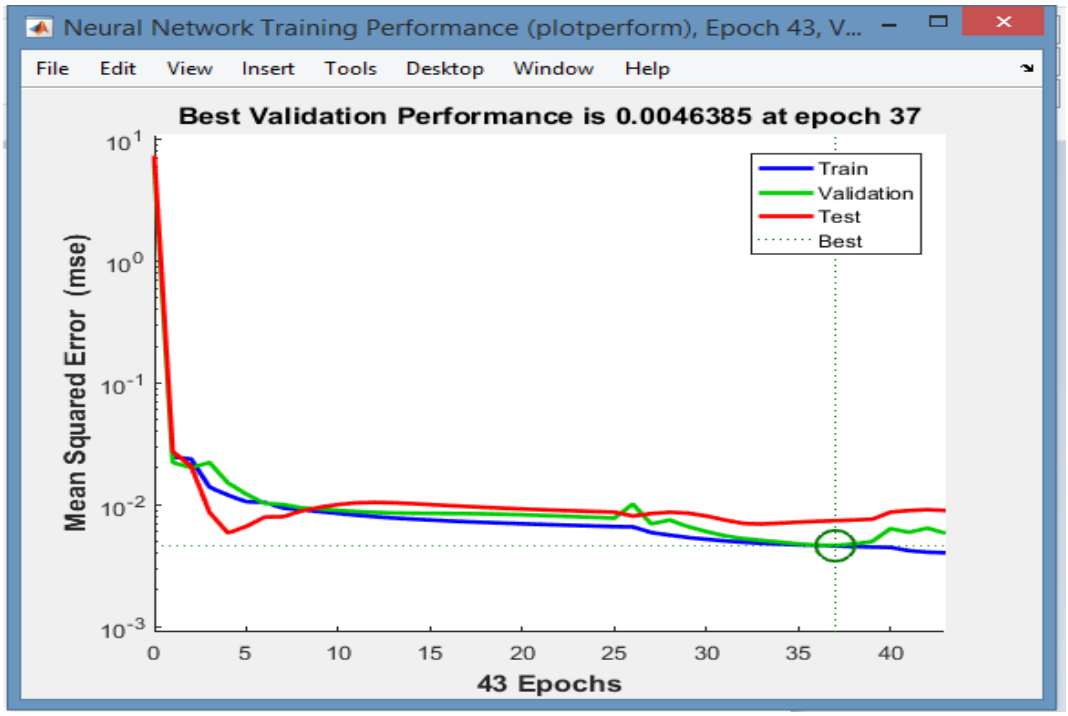

Figure C-2 Screenshot of Performance Plot of ANNM2

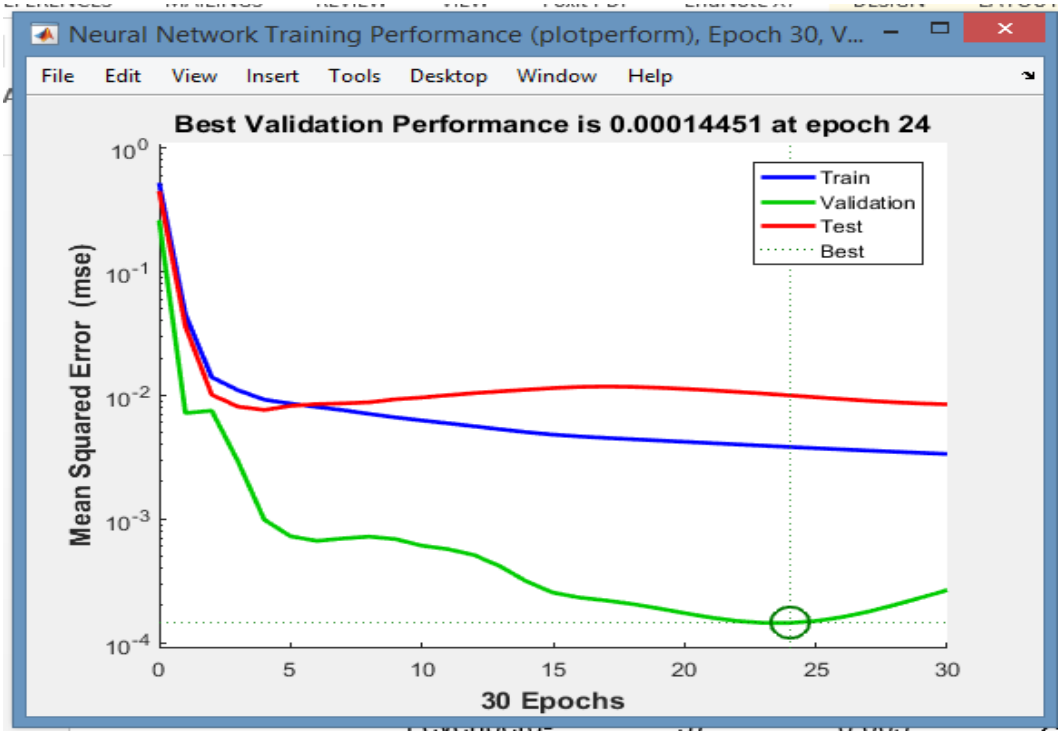

Figure C-3 Screenshot of Training state of ANNM1

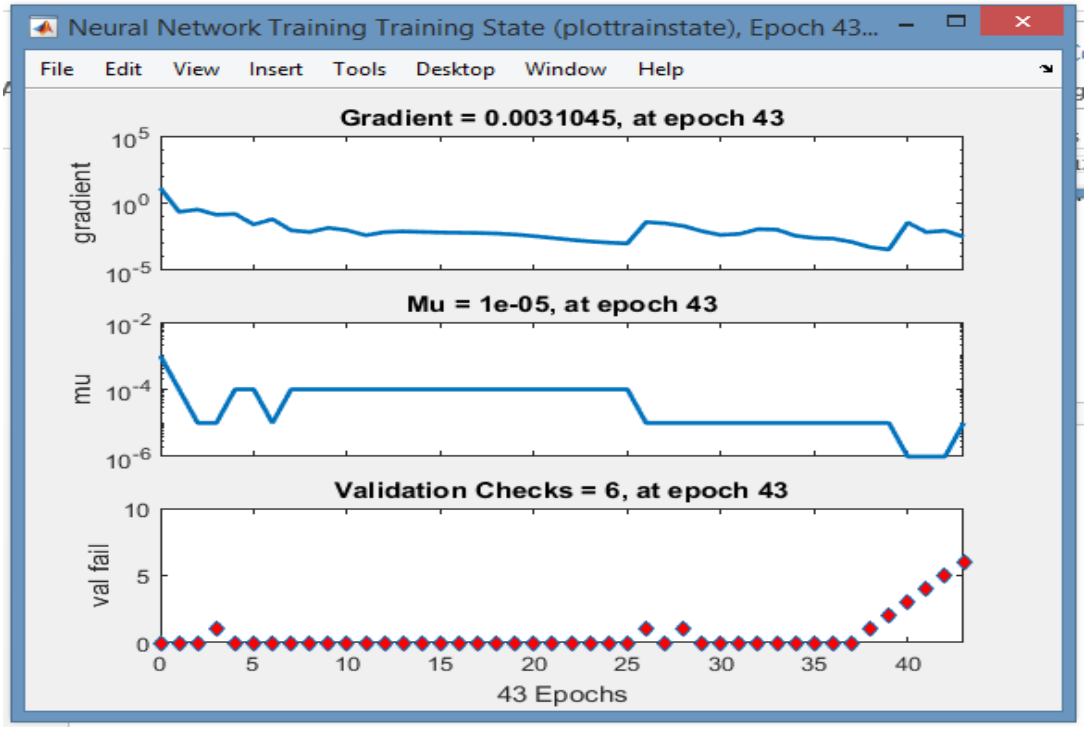

Figure C-4 Screenshot of Training state of ANNM2

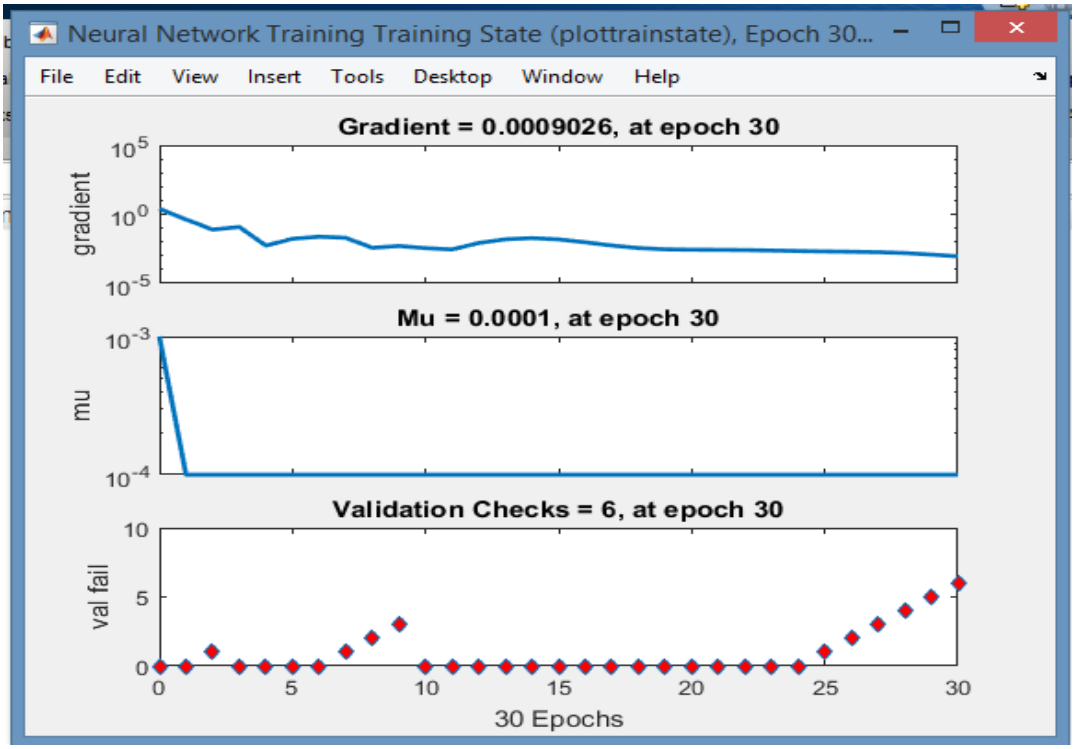

Figure C-5 Screenshot of Training Error Histogram of ANNM1

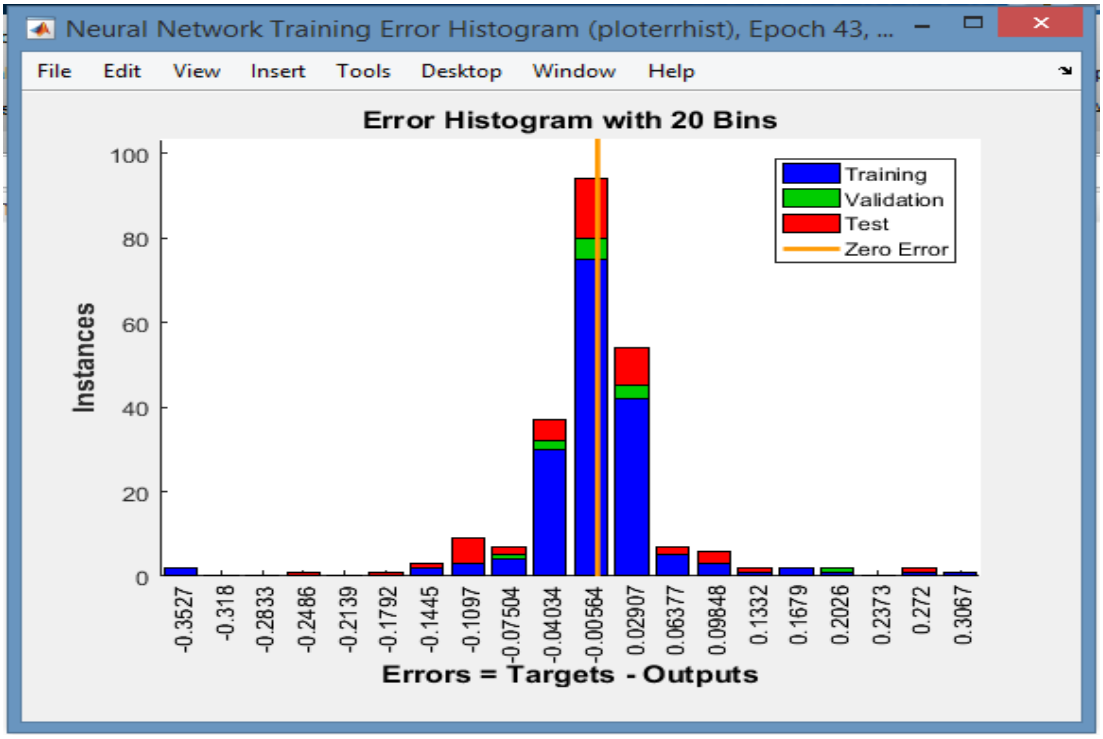

Figure C-6 Screenshot of Training Error Histogram of ANNM2

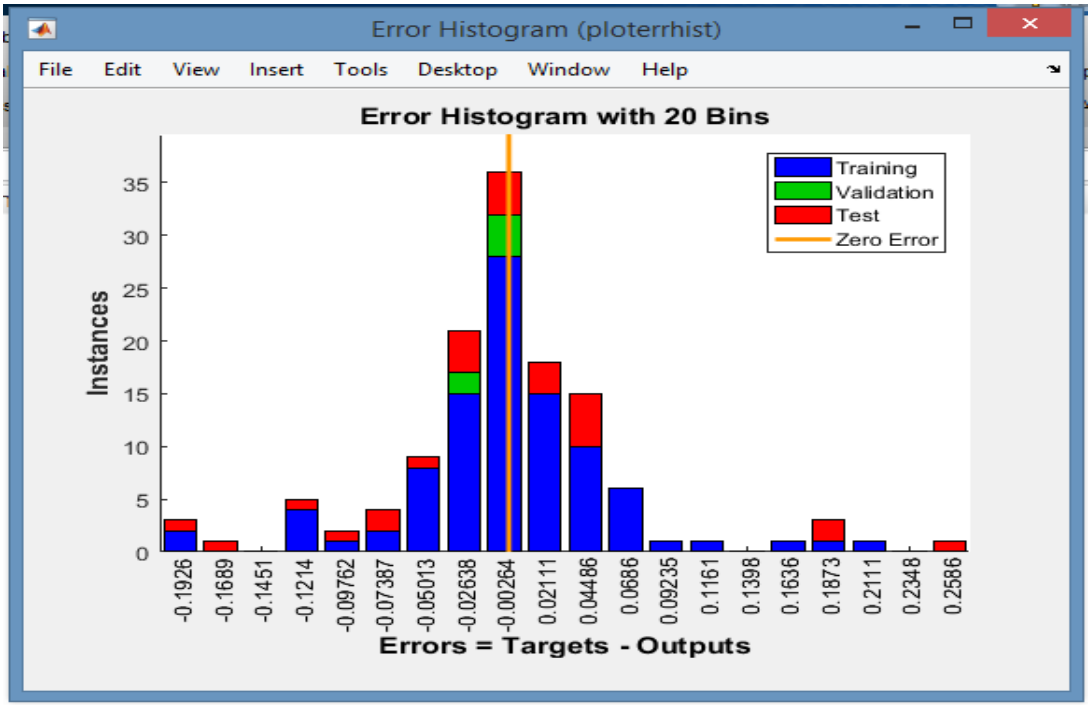

Figure C-7 Screenshot of Training Regression of ANNM1

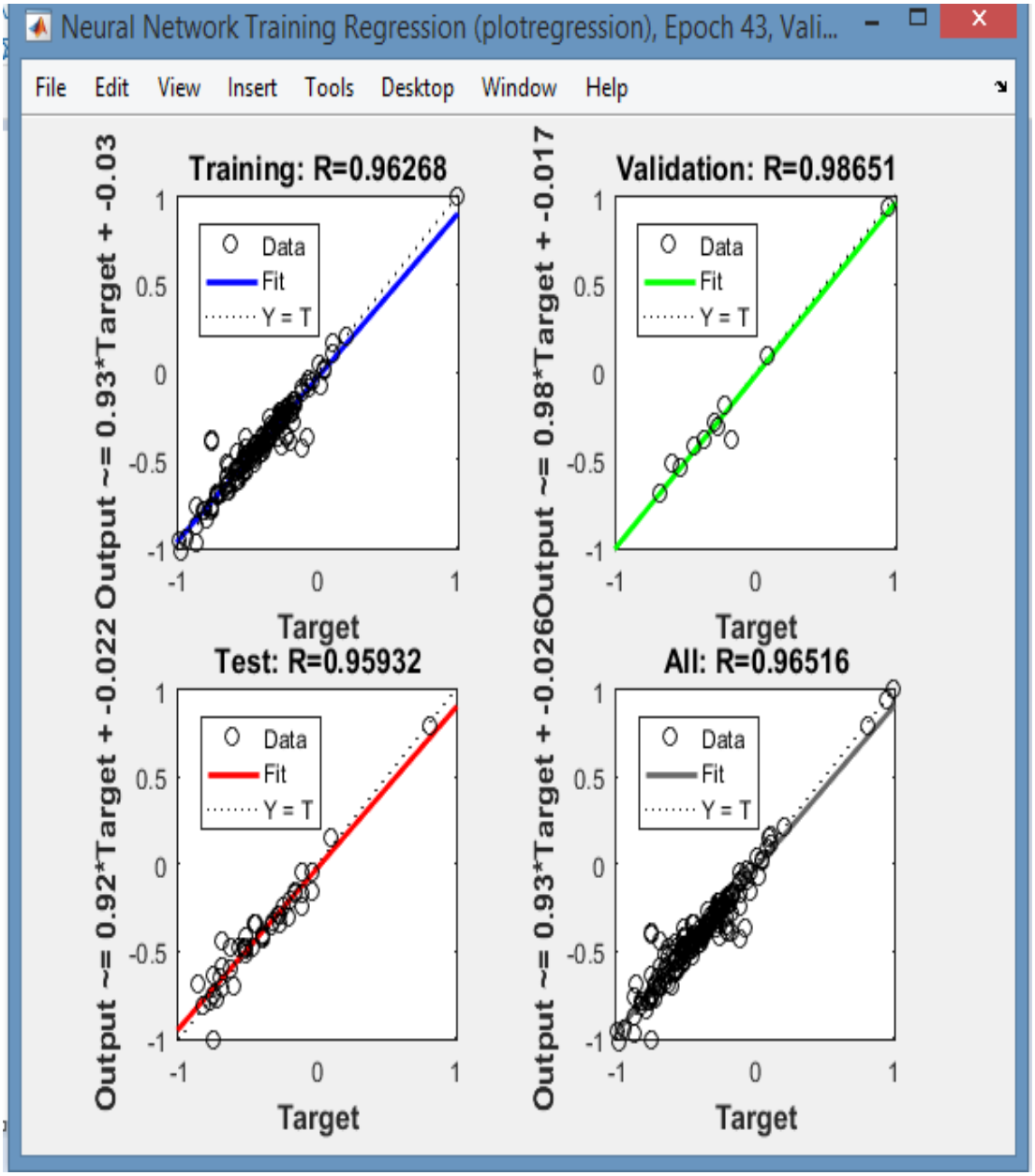

Figure C-8 Screenshot of Training Regression of ANNM2